Abstract

This work leads with the improvement and evaluation of a time-resolved spectroscopy system applied to determine the optical properties at multiple wavelengths in healthy breast tissue of volunteers.

A commonly used analytical model, the diffusion approximation is applied for the evaluation of the *in vivo* measurements of the optical properties of breast tissue, making use of a fitting algorithm implemented by a computer program.

Data resulting from *in vivo* measurements on 30 volunteers is presented and analysed, in an attempt to find differences in the optical properties of breast tissue between individuals and between different locations on the breast. The stability and reliance of the system together with the measuring procedure is evaluated.

1 Introduction and aims

The use of lasers in medicine started around 1960, and since then therapeutic applications of lasers in medicine have been very dominant. Applications of laser to diagnostic techniques are only now emerging, as an alternative to existing diagnostic modalities such as x-ray radiography, NMR imaging or ultrasound imaging.

Special attention is being directed to the possibility of detecting cancer tumors in breasts. X-rays have been proved to have a potential to induce cancer due to them being ionising radiation. Furthermore, conventional x-ray mammography is in some cases worthless due to its poor contrast, which makes it difficult to detect small lesions, especially for young women where the breast is more fibrous.

Laser induced spectroscopy is a non-invasive technique which employs non-ionising radiation, and which may develop better resolution than x-ray in a near future.

Every year about 75.000 women die of breast cancer in central Europe[1]. The RTD Project OPTIMAMM funded by the fifth framework programme (FP5) of the European Community aims at improving detection and clinical evaluation of breast cancer applying time-domain optical mammography.

It has been proven that the optical properties of tissue can provide information on malignancy, due to the structural changes produced as tumors develop. This fact makes it valuable to characterise the optical properties of healthy tissue as a previous step for laser tissue diagnostics of breast cancers.

This thesis is part of the research within the Optimamm project. The aim has been both to improve the time-resolved diffuse spectroscopy system working at the Lund Medical Laser Centre[2] and investigate by *in vivo* measurements using this system how much the optical properties of breast tissue at four different wavelengths vary between individuals and between different locations on the breast.

2 Tissue optics

The breast is a quite heterogeneous part of the body, which can be seen in figure 2.1. This makes *in vivo* measurements more complicated to perform, and there are a lot of things that need to be taken into account in order to obtain good results.

In this chapter the absorption and scattering properties together with the substances of interest for this thesis are going to be described and in the next one, the mathematical basis of light interaction with tissue will be described.

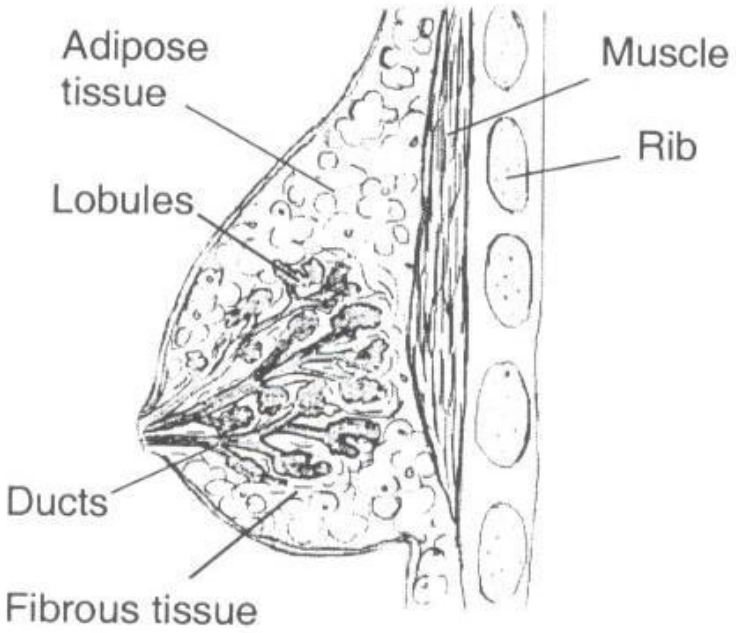

Figure 2.1 A schematic picture of the breast, from C. Eker[3].

2.1 Absorption

The coefficient for absorption is μ_a [cm-^{1}] and is defined as the probability of absorption per unit length for a photon. The absorption of light in tissue is strongly wavelength dependent (see figure 2.2). In NIR the main absorbing chromophores are haemoglobin, lipids and water. For dark skin, melanin has a rather high absorption but only within a thin layer.

Absorption occurs when the energy of a photon is the same as the gap between two electronic level states of a chromophore. The energy can then be released as fluorescence, phosphorescence or as heat[4].

The region approximately between 600-1300 nm is usually referred to as the *optical window* for tissues because the absorption is low so the penetration of light can be deep.

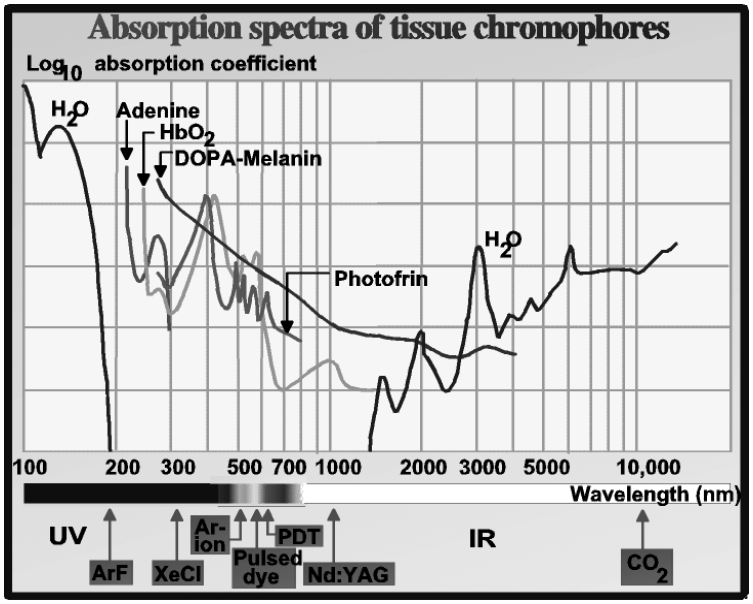

Figure 2.2 Different absorption spectra for chromophores in tissue. From J.-L. Boulnois [5].

2.1.1 Water

Water is one of the most common chromophores in the body. The amount of water is different in different types of tissue e g water contents in muscle can be as high as 75% and in adipose only 20%. Water is the main absorbent in the region under 200 nm and over 900nm for most tissues. The figure 2.3 shows the absorption spectra for pure water and it can be noticed that the first peak is situated around 975 nm.

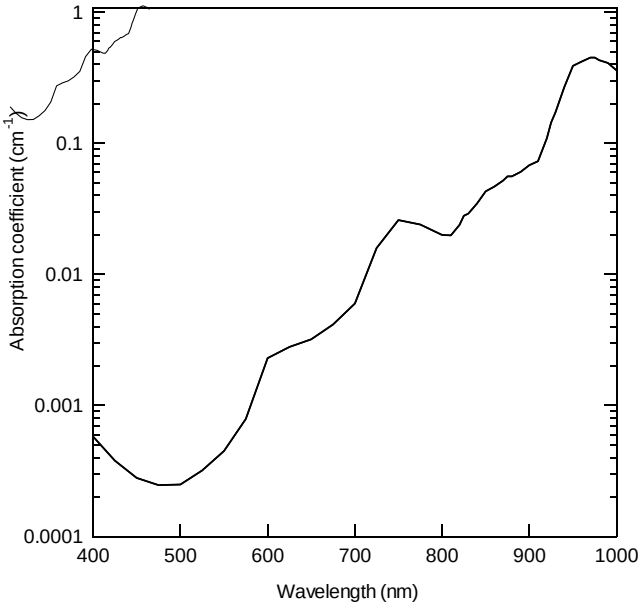

Figure 2.3 Absorption spectra of pure water. From Hale and Querry[6].

2.1.2 Haemoglobin

Haemoglobin is a protein in the blood and the human body's oxygen-carrier in the red blood cells. Four heam groups with an iron-ion (Fe^{2+}) in the middle are attached to the haemoglobin. Oxygen can be carried by means of the iron-ion.

Haemoglobin is the strongest absorber in the human tissue, mainly in the visible wavelength region, but it has a very low concentration of about a few percent of volume. It can be seen in figure 2.4 that there is a difference in the absorption spectra between oxy-heamoglobin (HbO_2) and deoxy-heamoglobin (Hb). Deoxy-haemoglobin has a peak around 760 nm which oxy-heamoglobin does not have. This can be used to measure the oxygenation in tissues.

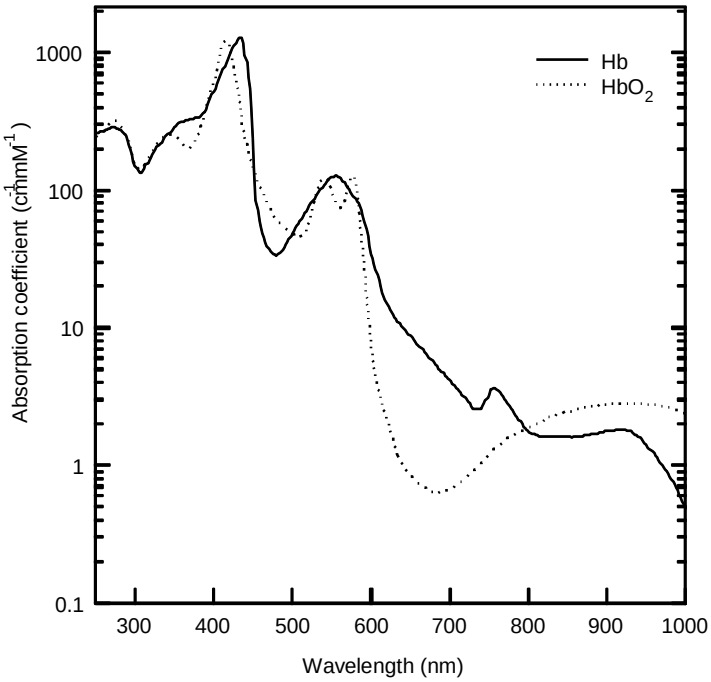

Figure 2.4 Absorption spectra of oxy- and deoxy-haemoglobin. Data compiled by Prahl[7].

2.1.3 Lipids

In the human body, lipids are almost only present in adipose tissue, around 70%. The breasts contain a lot of adipose tissue but the quantity varies largely depending on hormone status, age and constitution of the individual.

Among the different types of lipids that exist all the absorption spectra look similar. Lipids are normally whitish but in humans adipose tissue has a yellowish colour because it consists of β-carotene. Lipids have a low absorption in the visible wavelengths but in the NIR region they have to be taken into account. In figure 2.5 the spectra can be seen together with the absorption for β-carotene; the high absorption peak is situated around 930 nm.

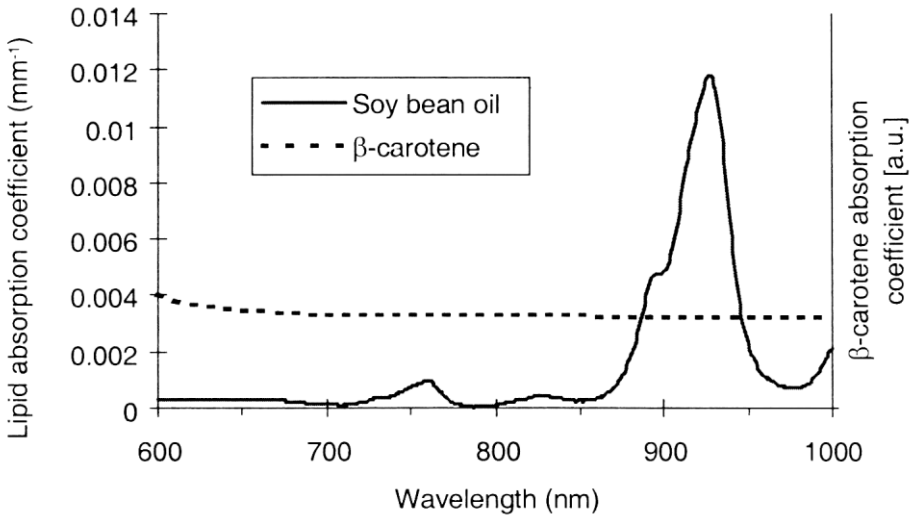

Figure 2.5 Absorption spectra of lipid and β-carotene. From C. Eker[3].

2.1.4 Melanin

Melanin is the pigment that gives the skin, the iris and the hair its colour. Melanin exists only in a thin layer in the skin but can be a problem during measurements because it is such a high absorber, especially if the skin is dark. It can be compared to a grey filter.

The absorption for melanin is highest in the UV region (see figure 2.6) to protect the skin from the harmful effects of UV radiation. A problem is that melanin cannot be extracted from the skin without changing its properties so it is hard to measure the extinction.

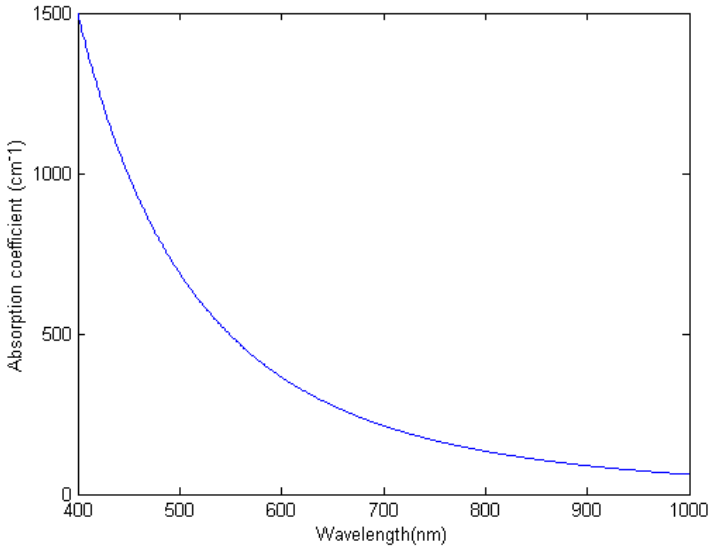

Figure 2.6 Absorption spectrum of melanin in skin. The spectrum is approximated by the formula $\mu_a = 1.70 \cdot 10^{12} \lambda^{-3..48}$ cm^{-1} λ is in nm. Formula given by Jacques[8].

2.2 Scattering

The scattering coefficient is $\boldsymbol{\mu_s}$ [cm^{-1}], which is the probability of scattering per unit length. The properties of scattering are not as wavelength dependent as for absorption. Scattering is caused by random spatial variations in tissue density, refractive index and dielectric constants[9].

The refractive index is for most tissues in the range of 1.38-1.41 at 633 nm and experiences a decrease of approximately 1% per 100 nm. Some types of tissues have higher refractive index e g adipose with n=1.46[10,11].

Scattering in tissue is not isotropic, it is anisotropic, therefore μ_s', the reduced scattering coefficient, is used instead of μ_s. To describe the anisotropy the g-factor is commonly used. The g-factor depends on the average scattering angle:

$$\boldsymbol{\mu_s' = \mu_s(1-g),\ g = \cos\theta}$$

The scattering is strongly forward directed (see figure 2.7) and the g-factor takes values between 0.7-0.95 for *in vitro* and about 0.9 in the optical window[9]. If g had been 0 then the scattering would have been isotropic. A time resolved system, as the one used for this thesis, is only measuring the μ_s'. The g-factor and the scattering coefficient cannot be separated have scattered enough times to be considered diffuse[12].

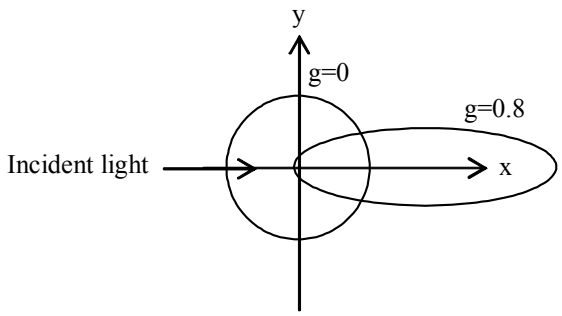

Figure 2.7 Phase function for two different values of the anisotropy factor.

The light can be scattered via different processes. If the wavelength of the incoming light is the same as vibration or rotation levels of molecules then the light will be scattered inelastically, if a transition between the levels occurs. Inelastic scattering means that the emitted wavelength is different from the incoming.

If the incoming light's wavelength is not matching any of the molecules resonant frequencies scattering can still occur. If the molecule is much larger than the wavelength the light will be Mie scattered. The intensity of the scattered light has in this case dependence with λ^{-2}. If the incoming light instead has a wavelength longer than the size of the molecule then the scattering is called Rayleigh. The intensity of the type of scattering has dependence with λ^{-4}. Both of these types of scattering are elastic, which means that the light is only changing direction and not loosing any energy[4].

Another scattering process is Raman scattering. Raman scattering can occur when the wavelength of the incoming light does not match any of the energy levels in the molecule. The molecule will then be excited to a virtual level from which light may be emitted. The emitted light will be three bands (see figure 2.8). Where the Strokes and the Anti-Stokes Raman bands have lower and higher energy respectively than the incoming light and are therefore inelastic scattering. The Raman bands are approximately 1/1000 times weaker than the Rayleigh line.

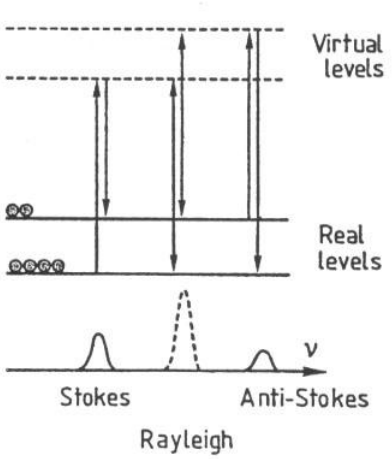

Figure 2.8 Raman scattering. From Svanberg[4].

3 Theoretical Model

Tissue can be considered as turbid media, due to its highly scattering properties, derived from variations of the refractive index on the cellular level. There are two different approaches to the study of the propagation of light through turbid media as tissue.

The first approach is based on considering light as an electromagnetic wave propagating through a dielectric medium. In this case, interaction between light and tissue is described in a rigorous mathematical way by Maxwell's equations. However, in most cases, especially in those related with tissue optics due to the complex molecular distribution of tissue, it is not possible to have a complete knowledge of the dielectric properties for all positions in the medium, microscopically considered. Moreover, it would be impossible to solve the integro-differential equations even if these properties were known, due to the complex structure of tissue. So we are forced to look for an easier approach to the problem.

As a second alternative, the transport theory of radiative transfer considers light as a flow of power through a scattering medium. The transport equation is an equation of conservation of energy, regarding light as photon particles travelling through turbid media, and making a statistical approximation of the process. The transport equation can be formulated as:

$$\int_V \frac{\partial N(\mathbf{r},\mathbf{s},t)}{\partial t} dV = -\int_V c\mathbf{s}\cdot\nabla N(\mathbf{r},\mathbf{s},t)dV - \int_V c\mu_s(\mathbf{r})N(\mathbf{r},\mathbf{s},t)dV - \int_V c\mu_a(\mathbf{r})N(\mathbf{r},\mathbf{s},t)dV + \int_V c\mu_s(\mathbf{r})\int_{4\pi} p(\mathbf{s}'\cdot\mathbf{s})N(\mathbf{r},\mathbf{s}',t)d\omega' dV + \int_V q(\mathbf{r},\mathbf{s},t)dV$$

Equation 3.1

where:

> $N(\mathbf{r},\mathbf{s},t)$ [$m^{-3}sr^{-1}$] represents the number of photons located at **r** per unit volume and solid angle with the direction **s** at time t and is called the **photon distribution function**.

The explanation of the terms follows:

Considering a small volume in the tissue under study, dV , located around **r**, and a certain direction **s**, the conservation of energy yields that photons can only be added to or subtracted from the photon distribution function in certain interactions (see figure 3.1) :

- $\int_V \frac{\partial N(\mathbf{r},\mathbf{s},t)}{\partial t} dV$ represents the change in the photon distribution function in dV over time.

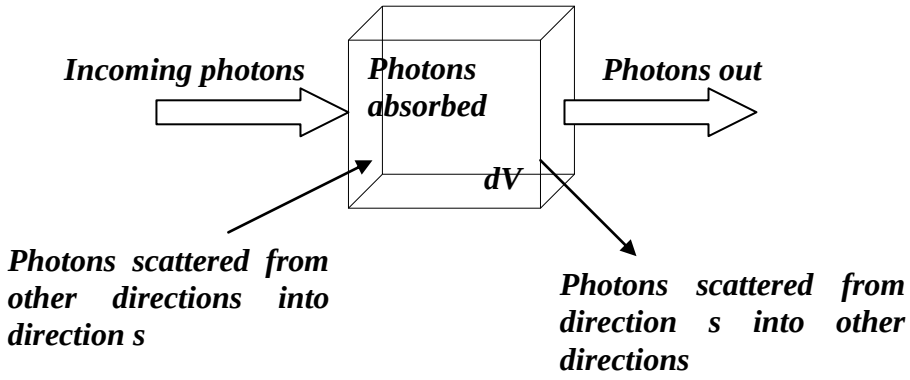

Figure 3. 1 Conservation of energy according to the transport equation in a small volume dV.

- $\int_V c\mathbf{s}\cdot\nabla N(\mathbf{r},\mathbf{s},t)dV$ represents the photons which are lost through the boundaries of dV, considering Gauss theorem to convert the surface integral $\oint_S cN(\mathbf{r},\mathbf{s},t)\mathbf{s}\cdot dS$ into a volume integral.

- $\int_V c\mu_s(\mathbf{r})N(\mathbf{r},\mathbf{s},t)dV$ represents the photons which are scattered from the direction of interest **s** into other directions.

- $\int_V c\mu_a(\mathbf{r})N(\mathbf{r},\mathbf{s},t)dV$ represents the photons which are absorbed inside the volume.

- $\int_V c\mu_s(\mathbf{r})\int_{4\pi} p(\mathbf{s}'\cdot\mathbf{s})N(\mathbf{r},\mathbf{s}',t)d\omega' dV$ represents the photons which are scattered from other directions into direction **s**, where $p(\mathbf{s}'\cdot\mathbf{s})$, called the scattering phase function, gives the probability of scattering from direction **s'** into **s**.

- $\int_V q(\mathbf{r},\mathbf{s},t)dV$ represents the photons which are gained through a light source $q(\mathbf{r},\mathbf{s},t)$.

The transport equation stated above is only valid under the assumption that no energy is gained or lost in the interaction of the non-absorbed photons with the medium, and that the light source considered is monochromatic (one wavelength light).

The equation is more commonly expressed in terms of the **radiance** $L(\mathbf{r},\mathbf{s},t)$ [$Wm^{-2}sr^{-1}$], which is defined as the photon power per unit solid area and angle, and can be easily calculated by multiplying the photon distribution function by the speed and energy of the photons:

$$L(\mathbf{r},\mathbf{s},t) = N(\mathbf{r},\mathbf{s},t)\frac{hc^2}{\lambda}$$

Equation 3.2

Since all terms in the transport equation are integrated over an arbitrary volume V, the balance must also apply for the integrands, so finally the equation can be rewritten as:

$$\frac{1}{c}\frac{\partial L(\mathbf{r},\mathbf{s},t)}{\partial t} + \mathbf{s}\cdot\nabla L(\mathbf{r},\mathbf{s},t) + (\mu_s + \mu_a)L(\mathbf{r},\mathbf{s},t) = \mu_s \int_{4\pi} L(\mathbf{r},\mathbf{s}',t)p(\mathbf{s},\mathbf{s}')d\omega' + Q(\mathbf{r},\mathbf{s},t)$$

Equation 3.3

Due to its complexity, no analytical solution for the transport equation in 3D is available. It is necessary to make use of numerical methods to reach full solutions, by discretizing the equation. A commonly used option is Monte Carlo simulation[13,14], a probabilistic method which can be applied to any geometry no matter how complex it is, but which requires great computational capacity and time.

In this work, the **diffusion approximation** is the method chosen for simplification of the transport equation. By expanding the radiance $L(\mathbf{r},\mathbf{s},t)$, the phase function $p(\mathbf{s},\mathbf{s}')$ and the source function $Q(\mathbf{r},\mathbf{s},t)$ in the transport equation into spherical harmonics and keeping only the zeroth and first terms in the infinite series, we reach the diffusion equation[9], which can be solved analytically for simple geometries:

$$\frac{1}{c}\frac{\partial}{\partial t}\phi(\mathbf{r},t) - D\nabla^2\phi(\mathbf{r},t) + \mu_a\phi(\mathbf{r},t) = Q(\mathbf{r},t)$$

Equation 3.4

where:

$\phi(\mathbf{r},t)$ [Wm^{-2}] is the **fluence rate**, which describes the power incident on a volume element per surface area, and can be expressed in terms of the radiance as:

$$\phi(\mathbf{r},t) = \int_{4\pi} L(\mathbf{r},\mathbf{s},t)d\omega(\mathbf{s})$$

Equation 3.5

D is called the **diffusion coefficient**, and is defined by:

$$D = \frac{1}{3\mu_{tr}} = \frac{1}{3(\mu_a + (1-g)\mu_s)}$$

Equation 3.6

A new parameter is defined, the **reduced scattering coefficient**:

$$\mu_s' = (1-g)\mu_s$$

Equation 3.7

where $1/\mu_S'$ [mm^{-1}] represents the effective mean free path between scattering events if the scattering is regarded as isotropic (diffusive propagation).

The diffusion approximation consists on assuming that the light propagates diffusely, i.e. almost isotropically. Thus, radiance is only slightly anisotropic, and its directional dependence can be expressed only with two terms. Although tissue is very forward scattering (g ~ 0.9), by the use of the reduced scattering coefficient μ_s' instead of μ_s in the equation it is ensured that scattering can be considered isotropic.

The diffusion equation is then valid only under certain circumstances:

- The reduced scattering coefficient must be much larger than the absorption coefficient, $\mu_S' >> \mu_a$.
- The optical mean free path, $1/\mu_t$, must be much smaller than the distance between the light source and the detector. Typically, $r_{s-d} > \frac{2 \sim 3}{\mu_s'}$.

The restrictions above assure that the propagation of light through the medium can be considered as diffusive, and thus the diffusion equation can be applied.

The advantage of using the diffusion equation is that it can be solved for simple geometries, such as semi-infinite homogeneous media, which can be applied to the case under study. Using theory of images, expressions for the fluence rate and for the diffuse reflectance in the semi-infinite geometry are reached:

$$R(\mathbf{r},t) = (4\pi Dc')^{-3/2} z_0 t^{-5/2} \exp(-\mu_a c' t) \exp\left[-\frac{\mathbf{r}^2 + z_0^2}{4Dc't}\right]$$

Equation 3. 8

where $z_0 = \frac{1}{\mu_s'}$.

In this work, the diffuse reflected light coming out of the tissue through the boundary will be measured by means of a time-resolved system, and the expression for the diffuse reflectance R(**r**,t) will be fitted by means of a program to the so called Temporal Point Spread Function (TPSF) thus obtained. A group in the Politecnico di Milano developed this program, called FIT[15].

In this way, the optical parameters μ_a and μ_s' can be estimated, and therefore the characterisation of the tissue under study achieved.

4 Measuring Techniques

Several techniques can be applied for the measurement of the optical properties of a tissue under study. These can be classified into two-parameter techniques or three-parameter techniques, if only μ_a and μ_s' can be determined or also μ_s, respectively. Two-parameter methods are based on measuring the diffuse reflectance or transmittance from the medium. The technique that will be used in this work is a two-parameter one, time-resolved *in vivo* spectroscopy, in which the diffuse reflectance coming out of the tissue is measured. Some of the other techniques will be briefly introduced now, to focus later in the one used for the present study.

4.1 Spatially resolved diffuse reflectance

This technique consists in injecting continuous wave light into the tissue on one point and measuring the diffuse reflectance coming out at different distances from the injection point. By fitting the measured R(r) with the steady state form of the diffusion equation, the optical parameters of interest can be determined.

The main advantage of this kind of measurements is the low cost of the necessary equipment and the possibility to perform *in vivo* measurements. As a drawback, the sensitivity the measurements show to inhomogeneities in the tissue under study.

4.2 Frequency resolved measurements

In this method, a sinusoidally modulated light source is injected in the tissue and the diffuse reflected light is collected by a detection fibre at some distance from the injection fibre. The signal detected will be sinusoidally modulated, but will present a delay in time and a reduction in amplitude with respect to the source signal. Measuring the phase shift between the light detected and the source (or a reference fibre situated very near the source) and the amplitude of the oscillation relative to the DC level in the detected signal, the optical parameters of the tissue can be extracted.[9]

The advantage this method presents in comparison to the spatially resolved technique is its robustness against noise. It can also be used for *in vivo* measurements. As main disadvantage, the difficulty of measuring the interesting parameters of the detected signal can be pointed out.

4.3 Time resolved diffuse reflectance

This technique is based on sending very short laser pulses in the picosecond regime into the tissue. These pulses are broadened in time as a result of their propagation through the highly scattering medium, as photons take paths of different lengths from the source to the detector fibre. For each pulse sent, the time each photon detected takes from the injection fibre to the detection fibre is measured, by means of a reference signal that is generated for each laser pulse delivered into the tissue. If the process is repeated a large number of times and recorded in a histogram, a statistical distribution of the time delay is obtained, the Temporal Point Spread Function (TPSF). The signal to noise ratio is made higher as the acquisition time is increased.

The main advantages this method presents are the fact that it can be performed in *in vivo* measurements, and that the optical parameters of interest do not depend on the amplitude of the TPSF detected, making it more insensitive to inhomogeneities in the tissue.

In the present study, two different distances between the injection and detection fibres were used: 15 mm and 20 mm. As the inter fibre distance increases, so does the depth the light reaches into the tissue, and the information on the tissue structure which can be extracted from the measurement of the diffuse reflectance. On the other hand, the intensity received decreases with the inter fibre distance, and as a consequence, the signal to noise ratio decreases.

In a second stage, the TPSF measured is fitted with the analytical form of the diffuse equation shown in Eq 3.8, using a method based on the Levenberg-Marquardt algorithm[15] and implemented by the FIT program mentioned before. In this way, an estimation of the optical parameters μ_a and μ_s' is obtained.

As has already been said, it is μ_s' and not μ_s the parameter which will be estimated with the measurements performed in this study. In some of the graphs showing the resulting data, μ_s' is referred to as Mus, for the sake of comfort. Let the reader not be confused by this nomenclature.

The following figure, from J. Swartling[13] shows schematically the set-up for the three measuring techniques explained:

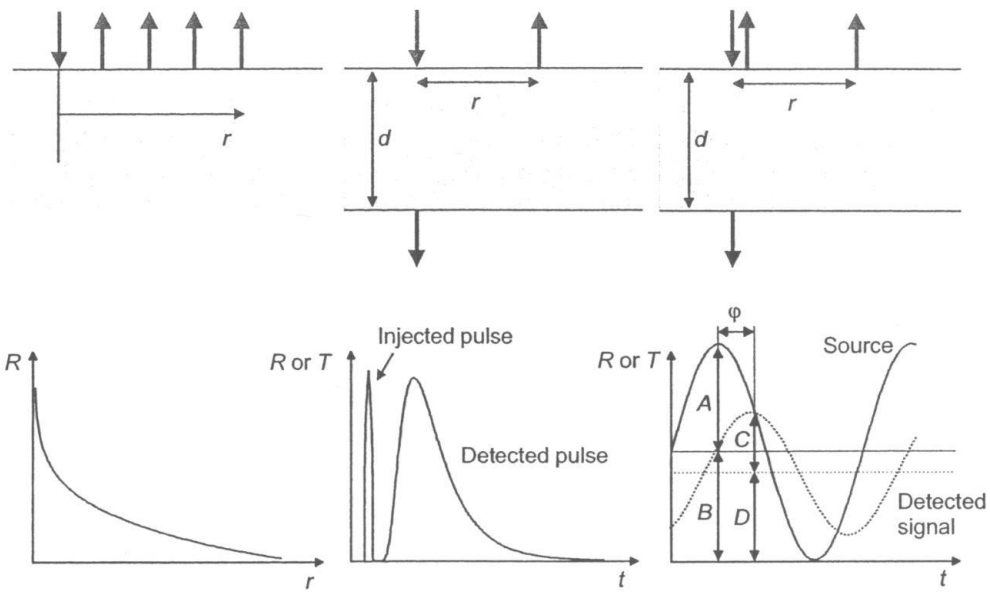

(a) **(b)** **(c)**

Figure 4. 1 (a) Spatially resolved diffuse reflectance measurements, (b) time resolved diffuse reflectance (or transmittance) measurements and (c) frequency modulated measurements.

5 Measuring instrumentation

The instrument that has been used for these time resolved measurements was built by two former diploma workers Magnus Andersson and Anders Nilsson[16] and named MAAN 230. To be able to perform the measurements some changes had to be made during this diploma work. The instrument has two main components, the computer and the apparatus. The computer part consists of an ordinary PC, with a touch-screen, with an installed SPC-program (Single Photon Counter) and an SPC-card. The apparatus has two main parts: the laser driver, with four laser heads, and the detector, which are all mounted into a box. Two graded index fibers are connected to the box. One is used for sending laser light and the other for the light to be detected. Graded index fiber is used to eliminate pulse broadening by mode dispersion. These fibers are 1.5m long due to hospital regulations. The fibers end in a probe made of metal, so a fixed inter-fibre distance of 15 and 20 mm could be maintained during the measurements.

In the box there is also a slightly moveable lens, to collect the incoming photons on the detector, a filter wheel so that the intensity of the light reaching the detector can be controlled and a red filter so the light under 640 nm will not be disturbing the measurements. These components and a new shutter, to protect the detector, were built into the system a few weeks before the measurements began.

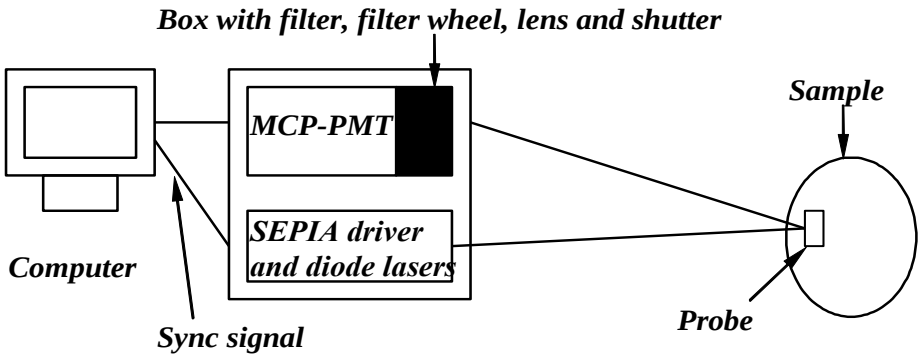

Figure 5.1 A schematic picture of the system, showing the main components.

When performing measurements with a time resolved system like this, it is very important to have a narrow instrument response function with a full width at half maximum (FWHM) of less than 100 ps. The narrowness of the instrument response function determines the resolution of the system. A measured curve can not be narrower than the instrument response function. There are several factors that have an influence on the instrument response function e g signal broadening in the detector, width of the laser pulse and the performance of the electrical parts.

During the measurements for this thesis the instrument response function was between 100 and 150 ps depending on the laser. This was obtained by supressing

some of the photons by changing the level high and level low for the CFD so that only the “main” photons remained.

5.1 The lasers

The laser source consists of four pulsed diode laser heads with different wavelength (660 nm, 785 nm, 910 nm and 974 nm). The name of the laser used is PDL 808 SEPIA.The repetition frequencies for the lasers can be selected between 5, 10, 20, 40 or 80 MHz. These frequencies are derived from a crystal controlled oscillator. The pulse width for the lasers depends on the power but cannot be narrower than 70 ps[17].

For this thesis a power of 1 mW/laser was used. Higher power is not needed and the broadening of the laser was acceptable for this power. To keep the measuring time low but still be able to see all four wavelengths on the screen at the same time, a repetition frequency of 40 MHz was used and the lasers were running synchronously, with a time delay of about 6 ns between each laser. The time delay was created by using four coax cables with different lengths. 20 cm coax cable introduces about 1 ns time delay. This is the same as 160 million pulses/sec.

5.2 The detector

The detector used is a photomultiplicator with a microchannel plate, MCP-PMT (Hamamatsu R3809-59). The difference between this and an ordinary PMT is that this one has a MCP instead of a dynode chain that creates the amplification of the incoming photon (see figure 5.2).

A MCP-PMT is used because it is broader banded than an ordinary PMT. This is needed to be able to measure as high as 974 nm. Inside the channels of the MCP there is a coating, made of Ag-O-Cs, which makes it sensitive up to about 1200 nm[18]. This coating is decreased by the influence of light and therefore it is important to have a shutter that can protect the detector if the intensity is too high.

To keep the dark current down in the detector and minimize the background noise, the detector is cooled to about -30°C.

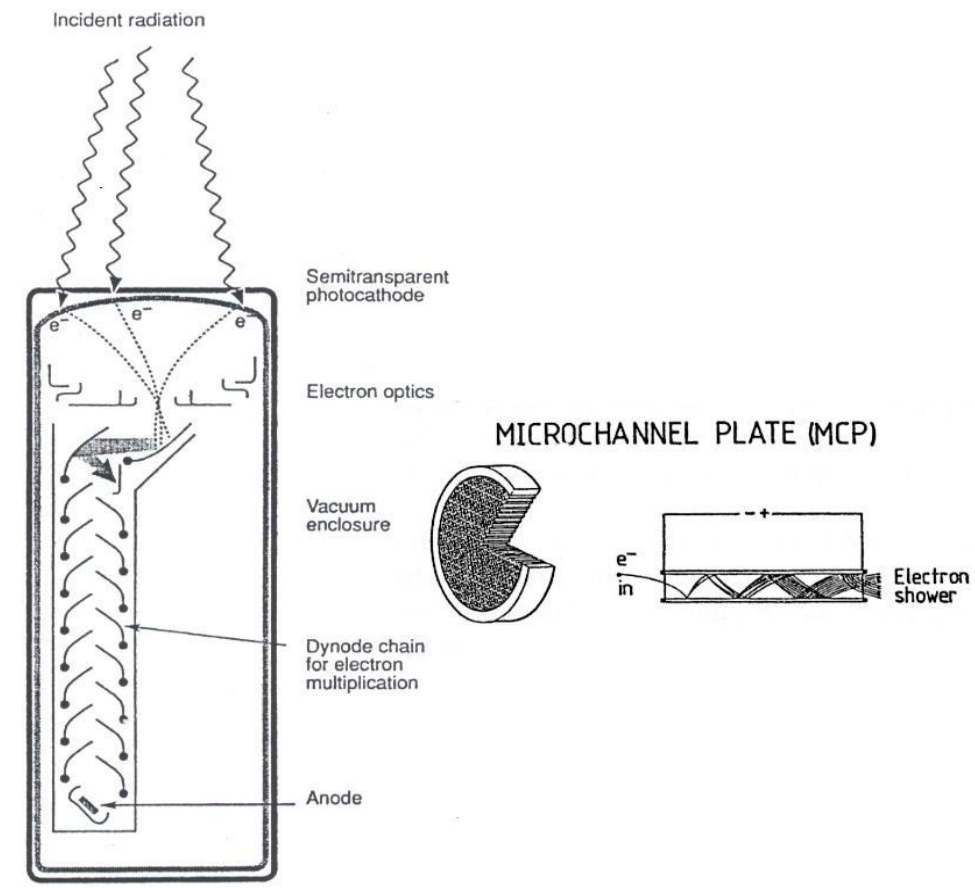

Figure 5.2 The left picture is an ordinary PMT and the right one is a MCP[4].

5.3 TCSPC

The SPC-300 computer card (Beck & Hickl GmbH, Germany) together with the SPC-program installed on the computer is used for detecting the time-correlated single-photon counting (TCSPC) and obtaining a temporal point-spread function (TPSF). The TPSF is in this case the actual measured curve convolved with the instrument response function. The TCSPC method is working with very low intensity levels where individual photons are detected. The advantage of TCSPC is that it increases time resolution, dynamic range and sensitivity[13].

The principle behind TCSPC can be seen in Fig 5.3.

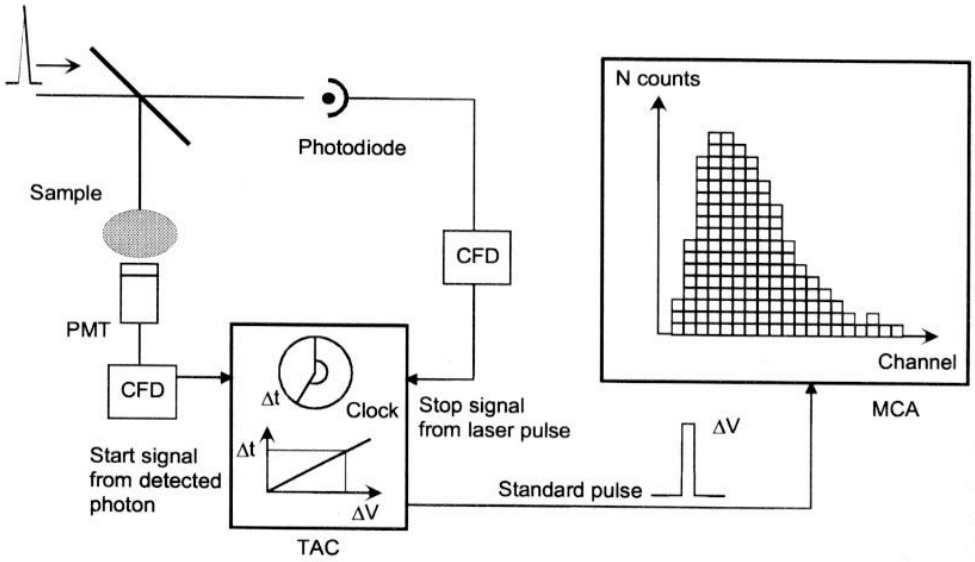

Figure 5.3 The principle of TCSPC. From J. Swartling[13].

When a pulse from the detector, after detecting a photon, reaches the SPC-card the time-to-amplitude converter (TAC) is triggered. At the same time an internal clock is started. This clock stops when the next laser pulse is fired and a sync-signal from the laser driver is set. The time differences between the detection and the sync-signal is converted to amplitude and fed to the multichannel analyzer which converts it to a channel number (between 0 and 1023). This channel number is then stored in the computer memory. This is repeated over and over again and a histogram representing the shape in time of the signal is formed[13,19].

In order to avoid a *pile-up* effect the probability of two photons or more to be detected at the same time must be kept low. If this is not the case the later photon will not be detected and small time delays would be over represented. To avoid this effect the probability to detect one photon per laser shot should be under 1:30[4].

5.4 The probe

The probe used for these measurements was designed for the measurements made by Karin Kolmert[20] (see figure 5.4). For the measurements made during this thesis 15 and 20 mm was used instead of 10 mm inter-fibre distance, so that the light could reach depeer into the tissue. There was another smaller probe designed and made by us, which is supposed to be used for measurements on tumours during surgery (see figure 5.4). This probe needs to be sterilized after every use and is therefore made of stainless steel and two cannulas that can be thrown away after use.

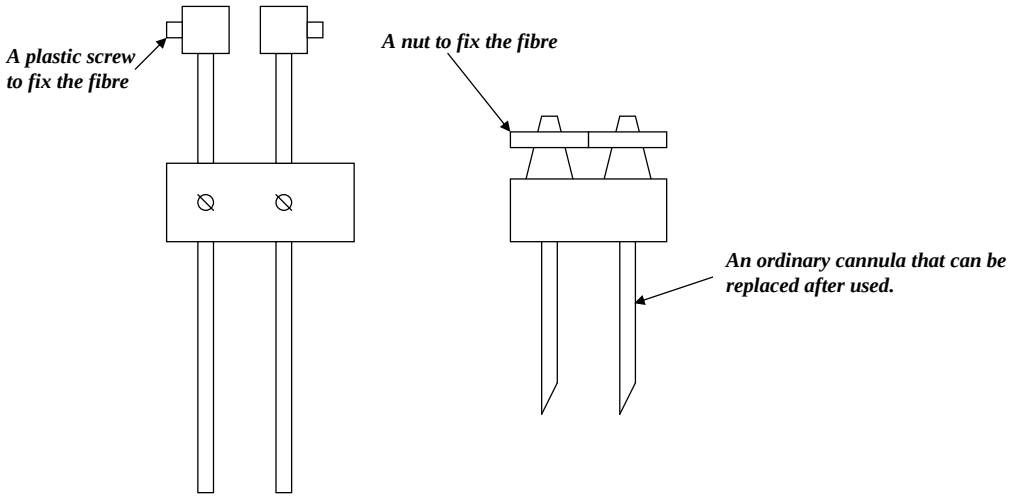

Figure 5.4 A schematic picture of the probe used to the left and the one designed and built to the right.

5.5 Changes performed on the system

There were some changes performed before the measurements started. First of all the electrical engines were removed because it was not a good solution. Therefore, now the power from the lasers is manually controlled. The two last lasers were installed and a new coupling for the four laserheads to the measuring fibre was made from graded index fibre. Some switches were installed on the outside of the box to control laser on/off and the shutter due to the fact that the program written for controlling the instrument was not working in a safe way. A new movable lens solution to make sure that all incoming light was reaching the detector was built in, together with the filter wheel and the new shutter, in a small black box and put in before the detector house.

In the beginning of June 2003 the system was taken to Milan for tests, evaluation and measurements. During this time some changes were made: The offset was adjusted to make the four wavelengths be visualized in an adequate position on the screen. It was moved from the SPC-program and a new offset was created by a different length between the sync and the signal coax cable. The frequency deviator in the program was changed from 8 to 1 and a moderation of detector's amplified signal to the SPC-card was made because the signal was too high the card. After these changes a very large increase in the signal was received. All these changes were made after the measurements had already been performed at the hospital.

6 Description Of The Measuring Procedure

A room at the breast-endocrine department at the hospital was kindly offered to perform the measurements. In order to prevent environmental light from disturbing the measurements by entering the detector, the window was conveniently covered and a yellow light lamp was used instead of the ordinary illumination of the room. Light below 640 nm is filtered by the system and does not interfere with the signal.

The system was always turned on one and a half hours before starting the measurements in order to let the cooling system stabilise the temperature and the lasers warm up. The laser power was measured throughout the day approximately every four hours in order to control its variations.

Before the measurements on each volunteer were started, the instrument function of the system was measured by means of a rigid metal pipe in which the source fibre tip and the detector fibre tip were inserted in both ends in such a way that they faced each other. To avoid the detector being overloaded, there are two narrow points on the pipe which reduce the light power reaching the detector fibre tip. (See figure 6.1, from K. Kolmert[20])

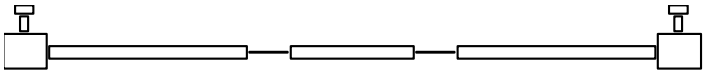

Figure 6.1 Pipe used to measure the instrument function. Each fibre tip was inserted in one end and fastened by means of a plastic bolt.

The distance between the source and detector fibre tips was carefully measured in order to calculate the time shift between the instrument function measured in this way and the data signal recorded later measuring on the volunteer. This parameter was critical for a correct fitting to be achieved, as will be later explained.

The reason for measuring the instrument function before each set of measurements was started was to minimize the risk of there being an uncontrolled time shift between the instrument function used as reference in the FIT program and the data curves from one specific volunteer. In this way, each set of measurements from one volunteer had its corresponding instrument function to be used in the fitting.

The following figure shows both the instrument function and the data recorded for one volunteer and one specific measurement.

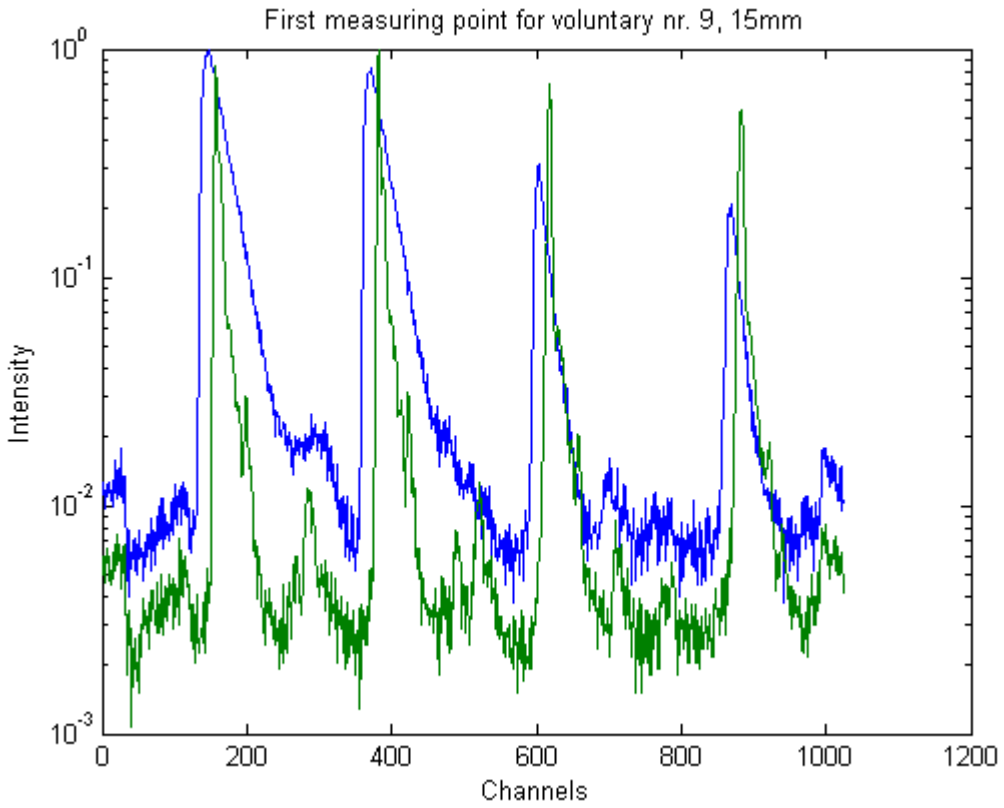

Figure 6.2 Instrument function (narrower peaks) and data corresponding to measurement nr. 1 on volunteer nr.9, for 15 mm.

Before the measurements were started, each volunteer was given a brief explanation on how the system works and the aim of the measurements. They were also instructed on how to hold the probe to perform the measurements and in which points on the breast. Finally, each volunteer signed a form to certify that she had been informed about the procedure and give her consent for the measurements. During the performance of the measurements, relevant information concerning the volunteer was collected, including age, weight, length and other attributes. The complete protocol including the form mentioned before and the set of questions can be found in appendix A.

For each volunteer, a set of 28 measurements was performed, fourteen using 15 mm inter-fibre distance and fourteen using 20 mm. The data collecting time for each measurement was of 60 seconds. If an overload signal was received during the acquisition of data in one measurement, the shutter at the entrance of the detector was closed and the data-collecting phase had to be restarted. For each inter-fibre distance, a total of seven points on each breast were measured, following the pattern shown on figure 6.3:

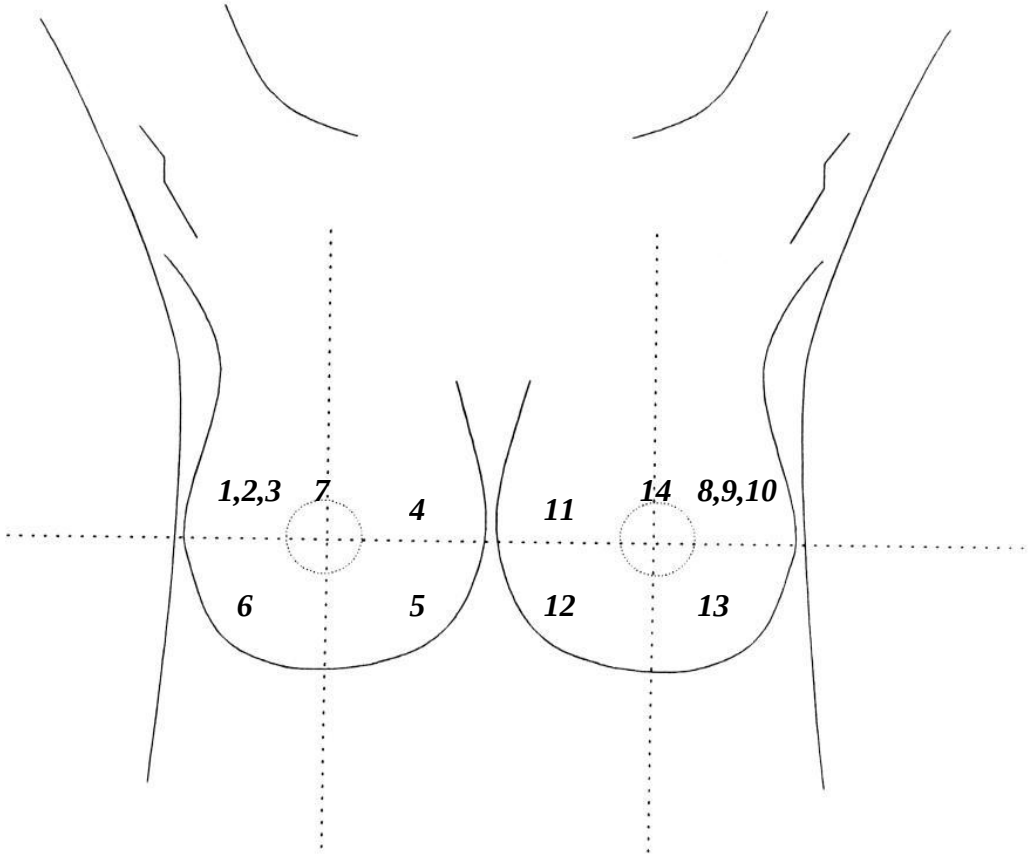

Figure 6.3 Points on which the measurements were performed for each volunteer and each inter-fibre distance.

Measurements 1, 2 and 3 (upper outer quadrant on the right breast) were performed lifting the probe between each measurement so that small variations in the measured position were achieved. The aim was to investigate how much the optical properties varied within a very small region.

Measurements 8, 9 and 10 (upper outer quadrant on the left breast) were performed without varying the position of the probe between them. Therefore, the total time the probe had to be held on the same spot was of three minutes. The stability of the system was susceptible of being evaluated with these measurements.

7 Extraction of μ_a and μ_s' from the curves

In order to estimate the values of the optical properties μ_a and μ_s', the evaluation program FIT was used, as has already been mentioned. This computer program that was developed by a group in the Politecnico di Milano[15] fits the diffusion equation (3.4) to the Temporal Point Spread Function obtained from the measurements. As a result, a data file containing the estimated values of some of the optical properties of the tissue under study is obtained.

The program interface contains different parameters that can be assigned different values by the user in order to configure the fitting execution. Some of these parameters are critical for a fitting to be achieved, as will be explained later. Difficulties were encountered in the evaluation of the measurements until help from the developers of the program was received, since there is no real user´s guide for it.

The main window of the FIT program is showed in the following figure, where the parameters used for the fitting of the curves obtained in this study are shown:

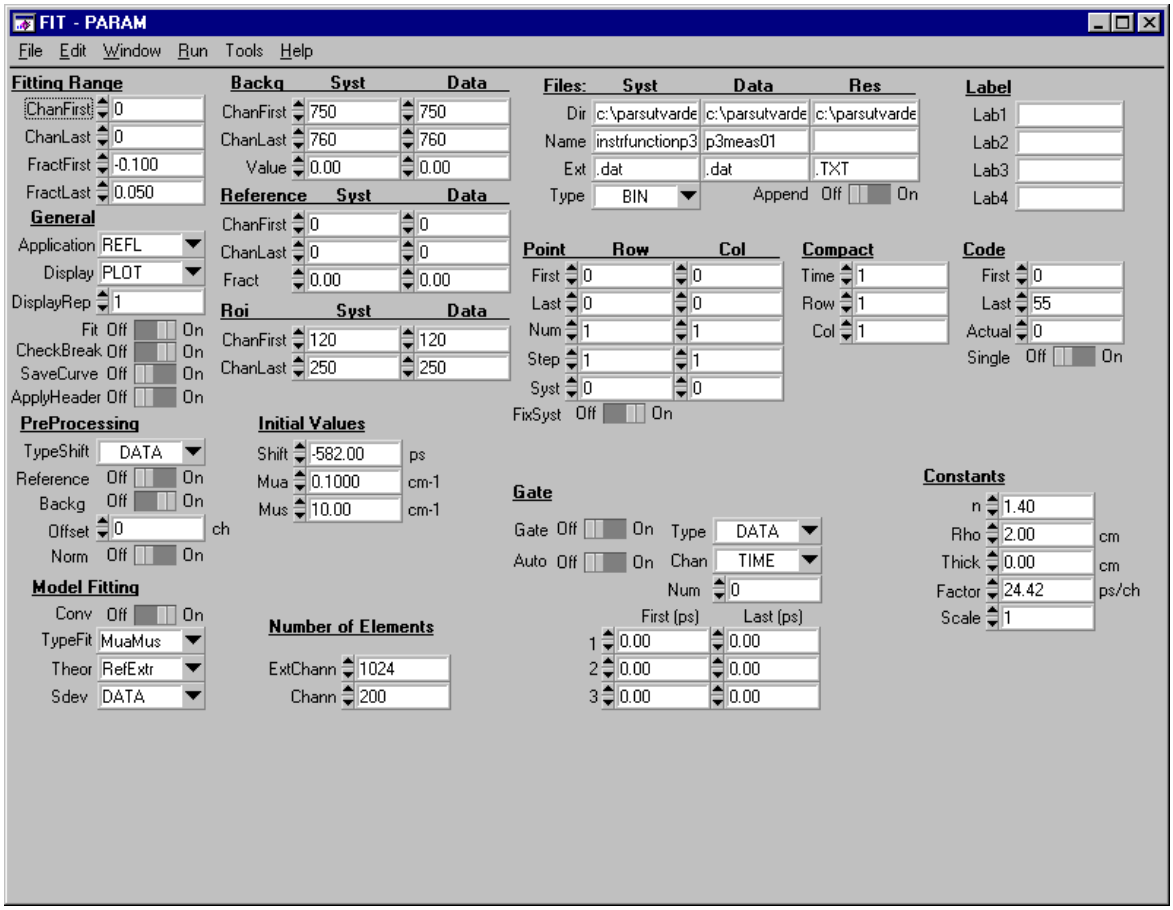

Figure 7.1 Main window of the FIT program, where the parameters must be configured by the user depending on the application.

The main parameters that have been important for this application and the values assigned to them will be briefly explained in the following paragraphs.

Files: under this title, the paths for the files in which the instrument function (**Syst**) and the data curve (**Data**) have been saved should be written. The path for the file in which the results of the fitting should be saved must also be specified (**Res**). The first two files should have .DAT extension, while the result file should have .TXT. The program needs the instrument function in order to deconvolve it with the TPSF and thus obtain the "real" TPSF without the effect the response of the system has on it.

Code: this parameter controls which data curves from the ones contained in the override window which will be explained later will be processed (if the fitting is executed) or visualized in the plot window (if the user wants to monitor the curves before fitting). With **Single = ON**, only one will be visualized at a time.

Constants: the following important parameters were assigned a value here:
n: refractive index for the tissue under study. The value used for this study was 1.40, typical for human tissue.
Rho: distance between the source and the detector fibres in cm. The values used will be 1.5 or 2, depending on the measurement.
Factor: specified the number of picoseconds per channel that had been used during the data acquisition in the SPC program. In this study, the value was 24.42 ps/ch.

Backg: the fitting algorithm uses the information inserted under this headline to find the part of the instrument function and the data curves which can be considered as background noise. This noise level is subracted from the signal during the fitting procedure in order to obtain more accurate values for the optical parameters. The range specified as noise should be the same both for the instrument function and the data.

Model Fitting: under the title **TypeFit** the option **MuaMus** was chosen, since these are the optical parameters searched for. The parameter **Theor** refers to the type of theoretical model used. It will be fixed to **RefExtr** since the diffuse reflectance is the magnitude measured and the mathematical model considered is the extrapolated boundary model.

Initial Values: In **Mua** and **Mus**, the initial values introduced were the ones typical from human tissue (see figure 6.1). The **Shift** parameter refers to the time shift existing between the collected data and its corresponding instrumental function. The value introduced was the time the light took from the source fibre tip to the detector fibre tip in the set-up for the instrumental function measurement (see figure 5.1). The sign used was negative because the data had to be delayed in time with respect to the instrument function. This parameter turned out to be a

critical one: small inaccuracies in its calculated value could produce unstable results in the fitting.

Roi: this title stands for region of interest. The first (**ChanFirst**) and last (**ChanLast**) values of the x-axis (channels) where the fitting algorithm will be performed on the signal should be specified here, both for the instrument function and the data. By the use of these parameters, each peak corresponding to each wavelength was isolated from the rest to perform the fitting, and undesirable effects such as reflections were not taken into account during the fitting.

Fitting Range: the critical parameters **FractFirst** and **FractLast** refer to the fraction of the maximum amplitude of the TPSF that was used for the fitting. In this way, specifying **FractFirst = -0.1** and **FractLast = 0.05**, the fitting started at the point in the rising flank of the TPSF with intensity 90 % of the maximum value and ended at the point in the trailing flank with intensity 5 % of the maximum. The aim was to discard the parts of the TPSF that are more susceptible to noise.

Override window: the override is a very useful function of the FIT program when a large amount of data needs to be processed, as was the case in this study. By specifying in the first column (**Field = FileDataName**) the names of the .SDT files to be processed and **Rep = 4**, the program understands that each file contains four curves to be fitted (corresponding to the four wavelengths). In the next four columns, each row contains the regions of interest at one wavelength to execute the fitting both for instrument function and data. In this way, the 56 fittings to be performed for each set of measurements from one volunteer at one inter-fibre distance (14 points measured and four wavelengths each) were done automatically and in an efficient way.

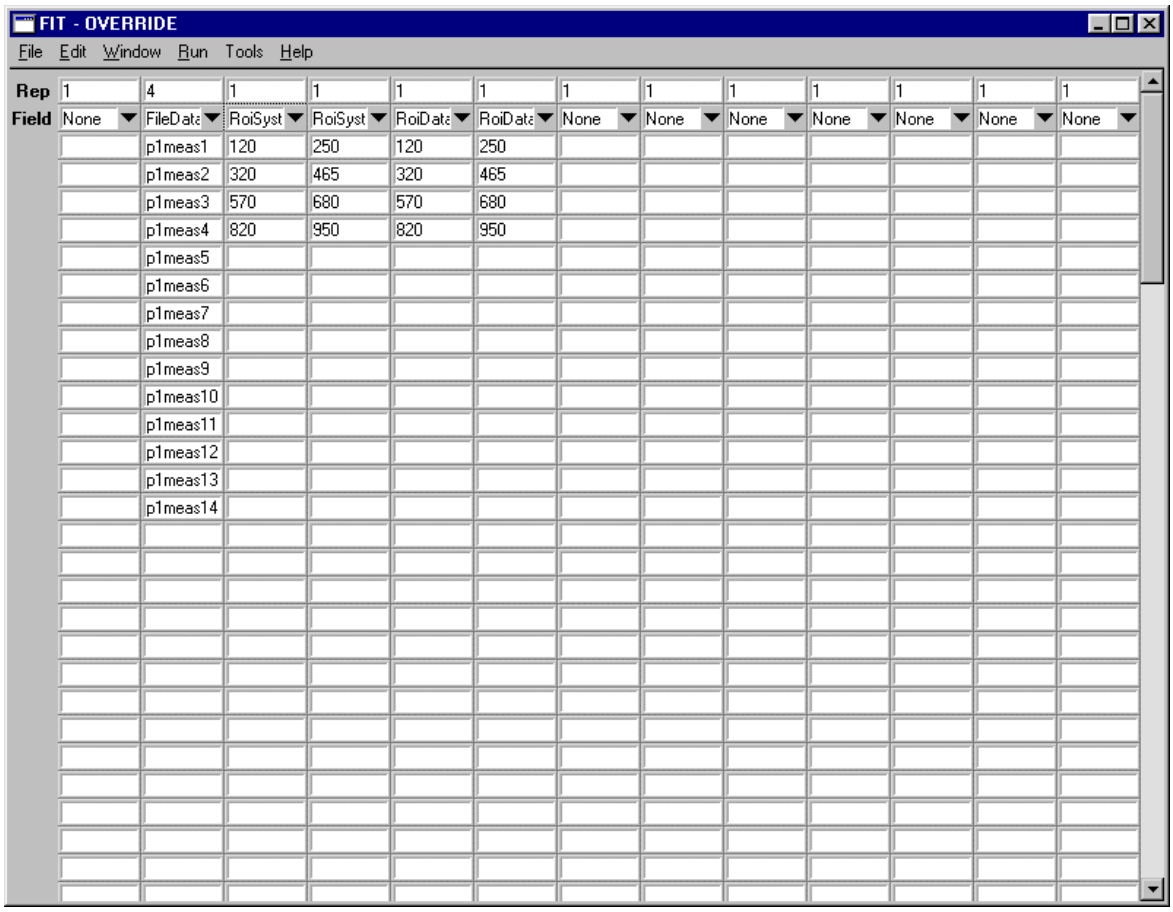

Figure 6. 2 Override window used for a fast processing of the data.

Using the option **Run-Monitor** the data could be visualized on the plot window in order to specify easily the regions of interest and the values for FractFirst and FractLast.

In the following figure, the resulting plot from the fitting of a data curve can be observed.

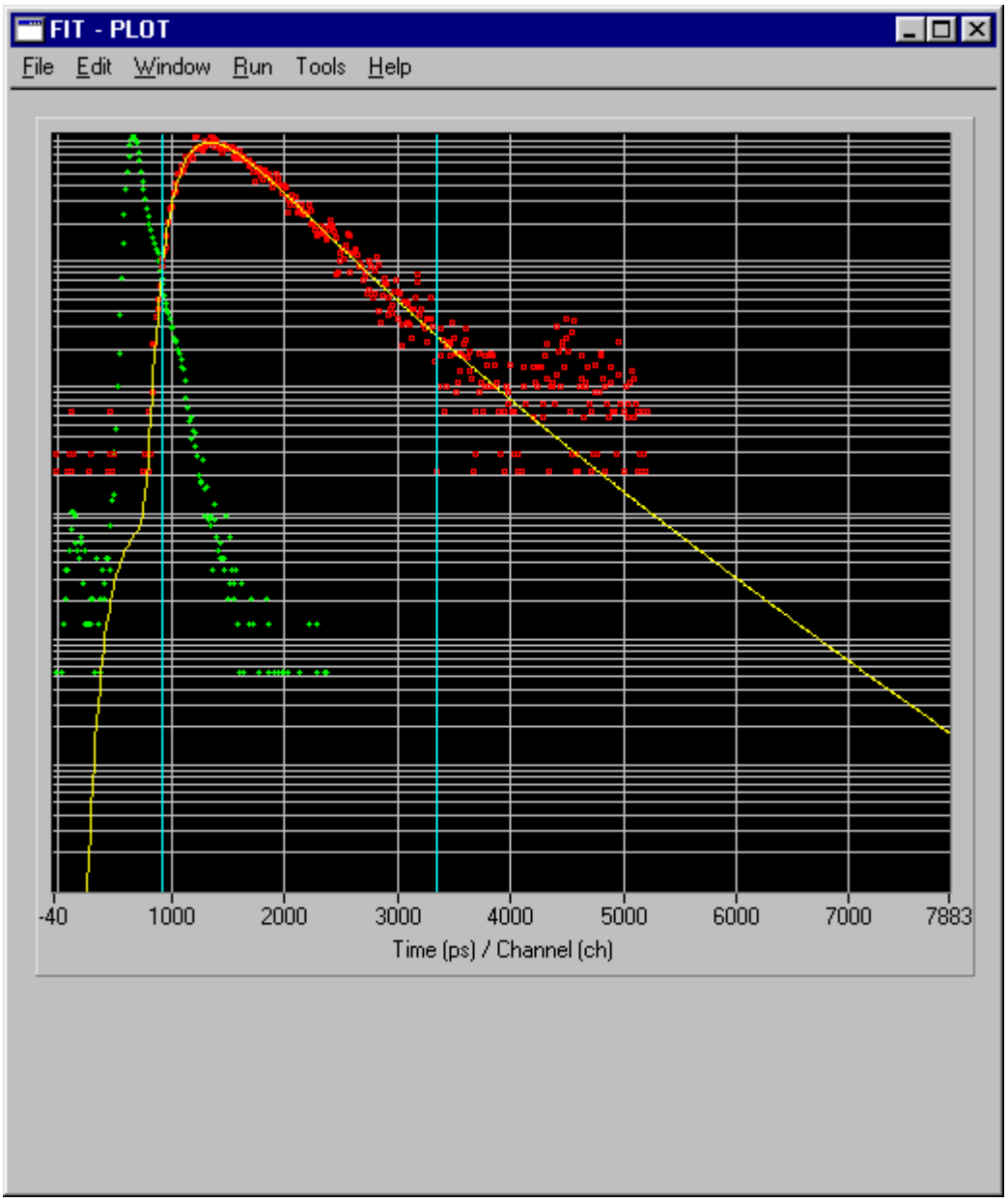

Figure 7. 3 Example of the fitting of a data set TPSF. The data measured and the instrumental function are represented by dots, while the fitted curve is represented by a continuous line. The ROI is determined by two vertical lines approximately between the x values 990 ps/ch and 3300 ps/ch. The instrumental function can be seen to be much narrower than the measured TPSF.

8 Results

From all of the plots obtained from measuring on the 30 volunteers, the ones which were most representative of the usual trend both for 15 mm and 20 mm inter-fibre distance have been chosen to be shown in this report, due to the very large amount of data stored. For each inter-fibre distance, ten volunteers have been chosen. For five out of these ten, the scattering plot (showing μ_s' over μ_a) will be presented, and for the rest μ_s' and μ_a will be plotted in separate graphs showing the position of each measurement on the breast.

Most of the volunteers were nurses working at the same department where the project was advertised in the hospital. A homogeneous group mainly with ages from 30 to 55 was chosen, including also a few younger and older. This group is interesting because most breast tumours are diagnosed within this age range. Other factors such as weight or length were not taken into account when the volunteers were chosen.

The following plots show the total data obtained for all volunteers and for each different wavelength and inter-fibre distance. Here the typical ranges of values obtained both for μ_s' and μ_a can be observed. For each volunteer a total of 14 points is shown, corresponding to the 14 different measurements performed on both breasts. The dimensions used for both μ_s' and $\mu_a$is cm^{-1}.

It can be noted that most of the data measured for μ_a in the wavelengths 660 nm and 785 nm is found in the range from 0.01 to 0.06 cm^{-1}, while for 910 nm and 974 nm the range is from 0.1 to 0.3 cm^{-1}. On the other hand, for μ_s' most of the measurements are found in the range from 5 to 15 cm^{-1} for all wavelengths and for both inter-fibre distances. These ranges of values are approximately the same that have been obtained in similar studies previously[21].

The absolute values obtained for both optical parameters may not be very precise, due to different possible sources of error which will be discussed in the next chapter, but the main aim has been to find a trend between the relative values obtained, while the real absolute values have less interest for this work. On the other hand, human tissue is highly heterogeneous (differences in skin thickness, fat layer thickness, blood perfusion, etc), making it hard to evaluate if the absolute values obtained are more or less accurate. Therefore, there will always be differences between the values obtained in different measurements, which makes a difference from measuring on homogeneous phantoms.

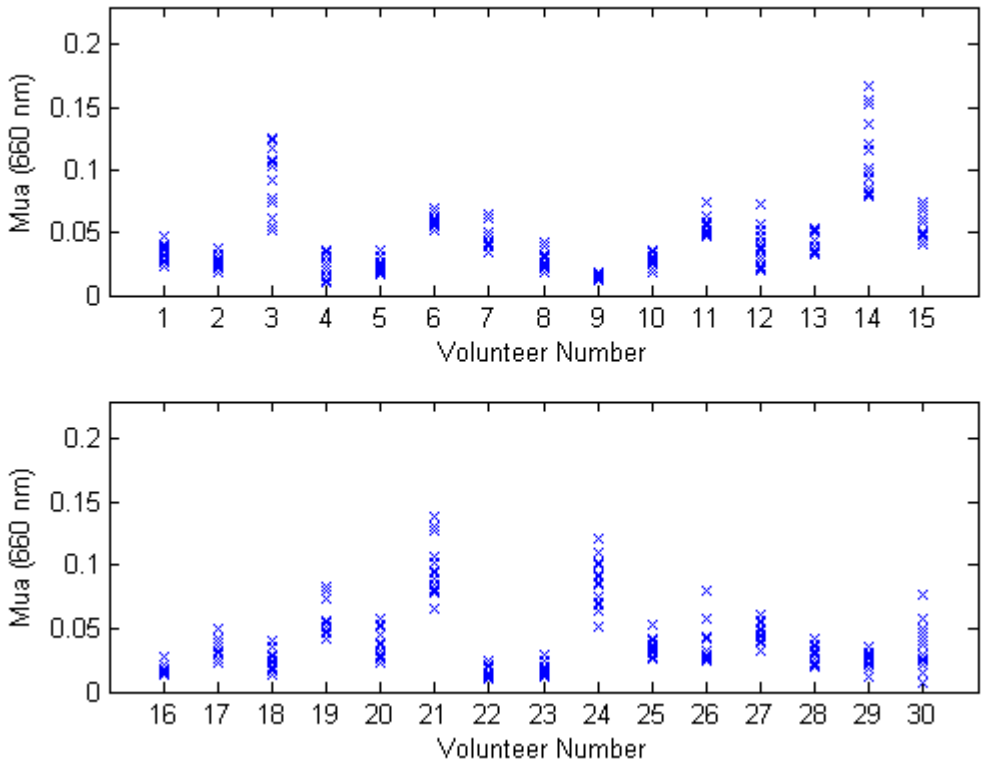

Figure 8.2 Absorption for 660 nm and 15 mm inter-fibre distance.

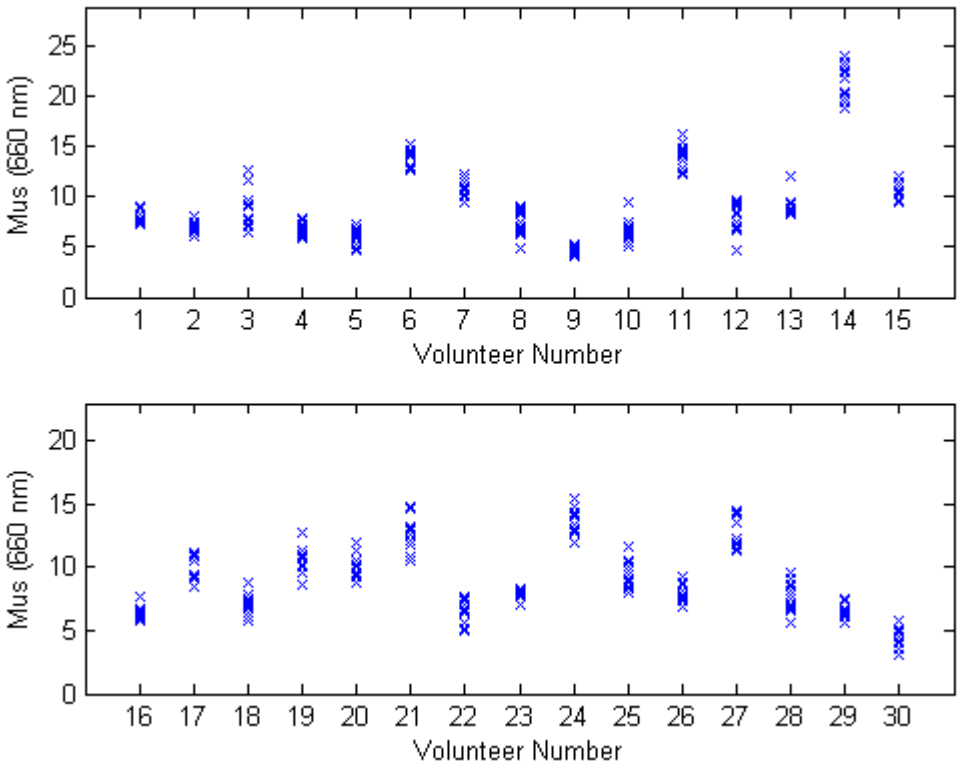

Figure 8.3 Scattering for 660 nm and 15 mm inter-fibre distance.

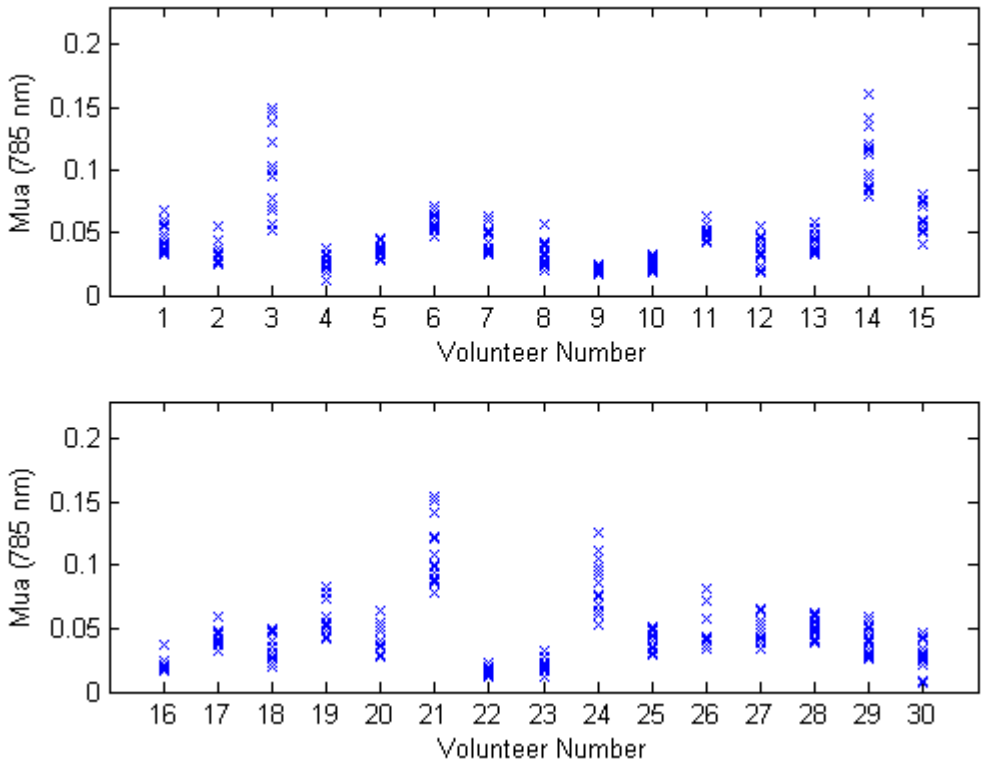

Figure 8.4 Absorption for 785 nm and 15 mm inter-fibre distance.

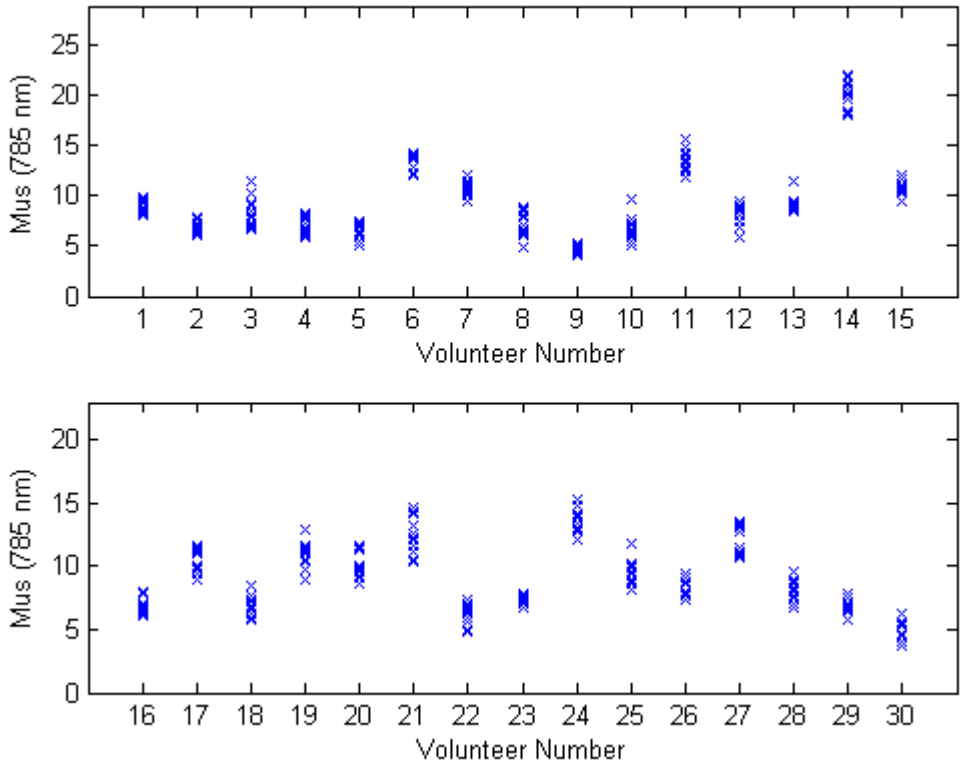

Figure 8.5 Scattering for 785 nm and 15 mm inter-fibre distance.

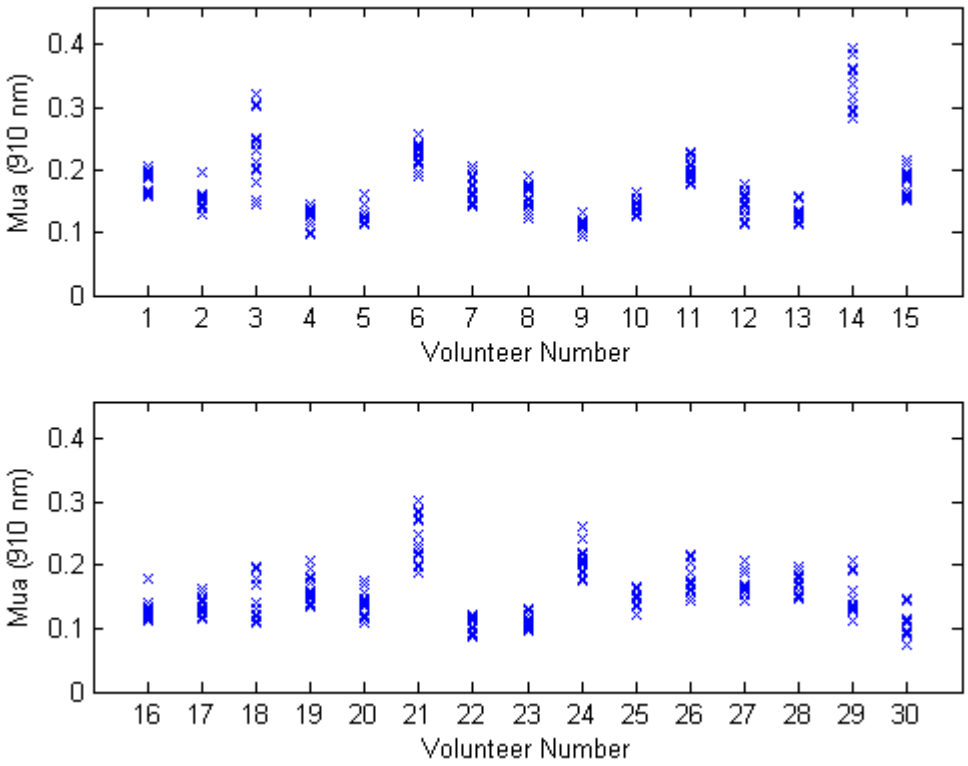

Figure 8.6 Absorption for 910 nm and 15 mm inter-fibre distance.

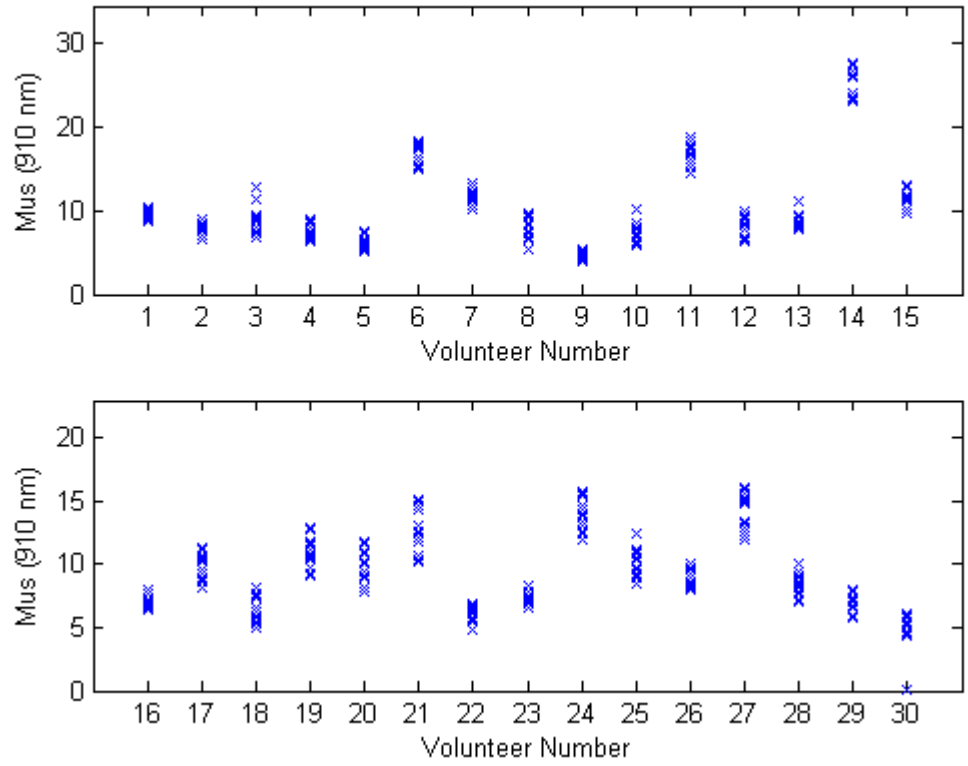

Figure 8.7 Scattering for 910 nm and 15 mm inter-fibre distance.

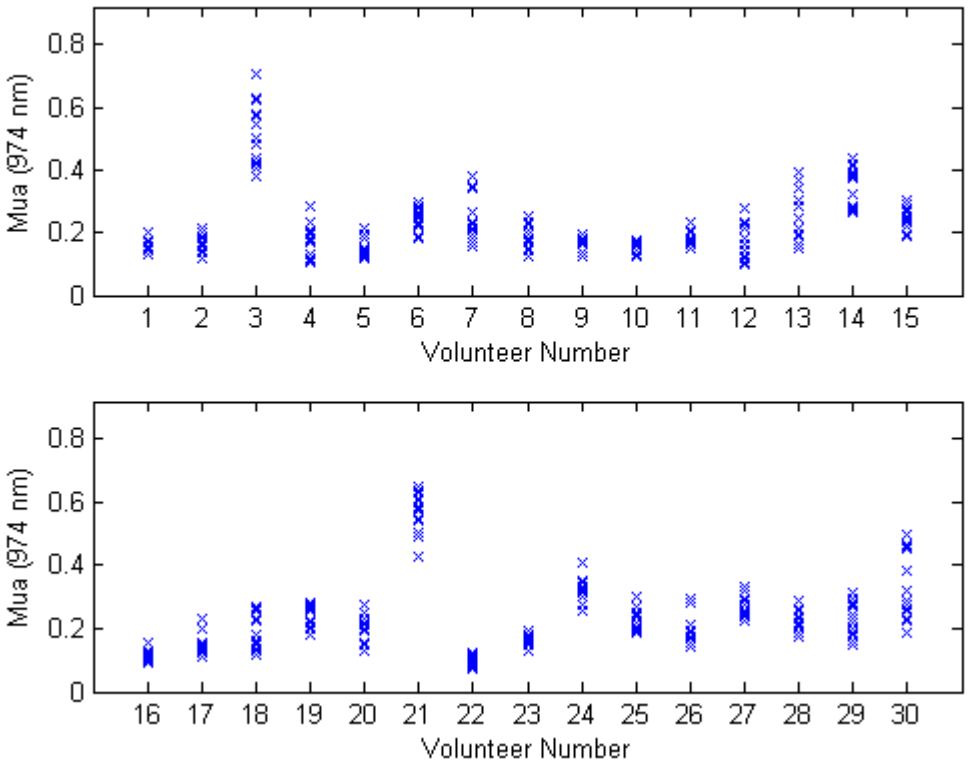

Figure 8.8 Absorption for 974 nm and 15 mm inter-fibre distance.

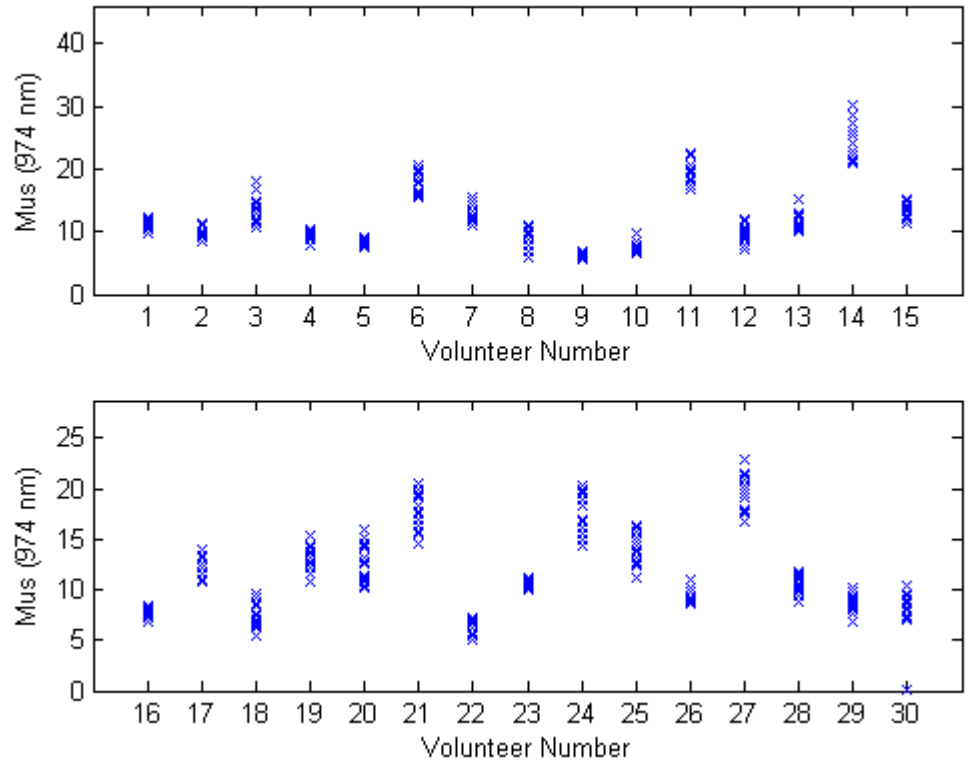

Figure 8.9 Scattering for 974 nm and 15 mm inter-fibre distance.

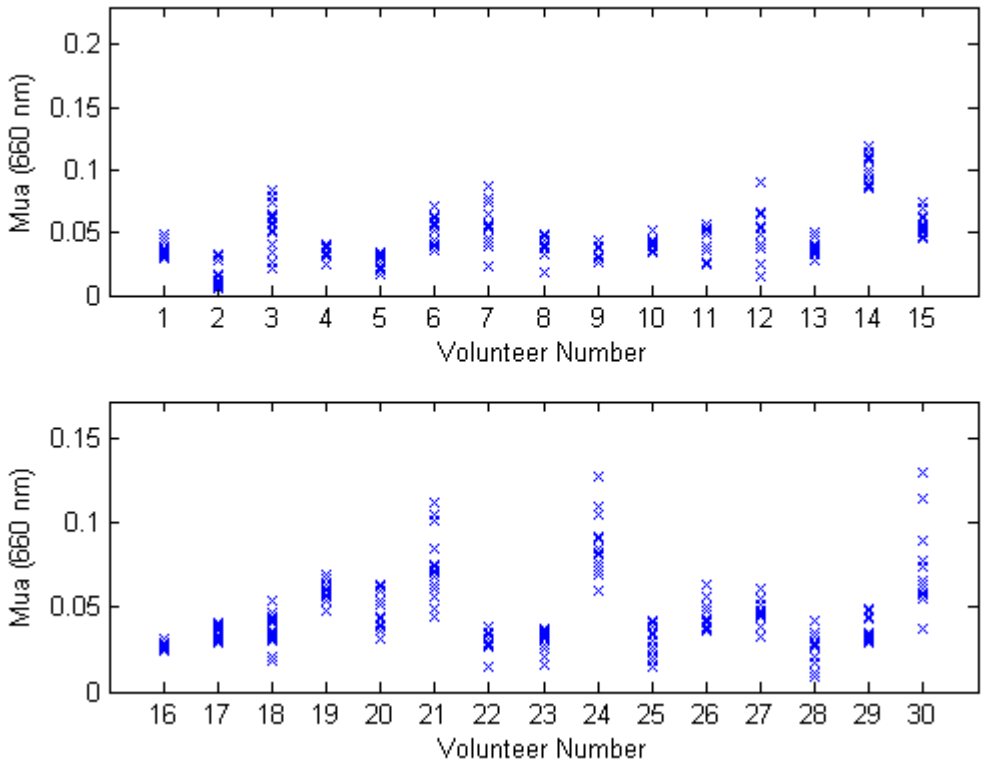

Figure 8.10 Absorption for 660 nm and 20 mm inter-fibre distance.

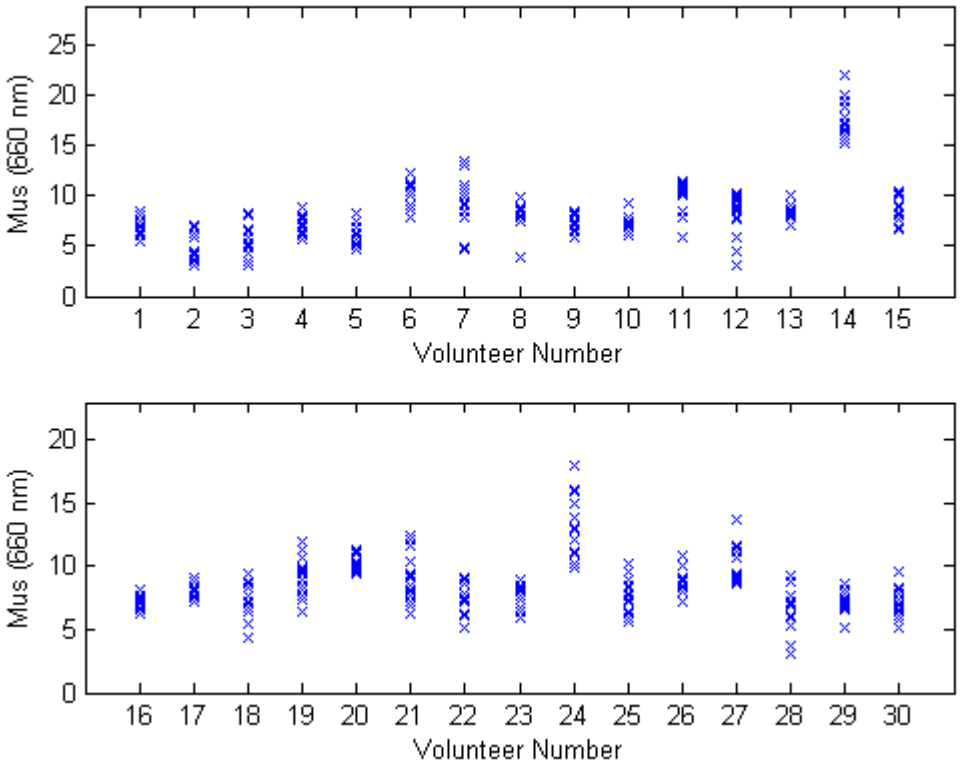

Figure 8.11 Scattering for 660 nm and 20 mm inter-fibre distance.

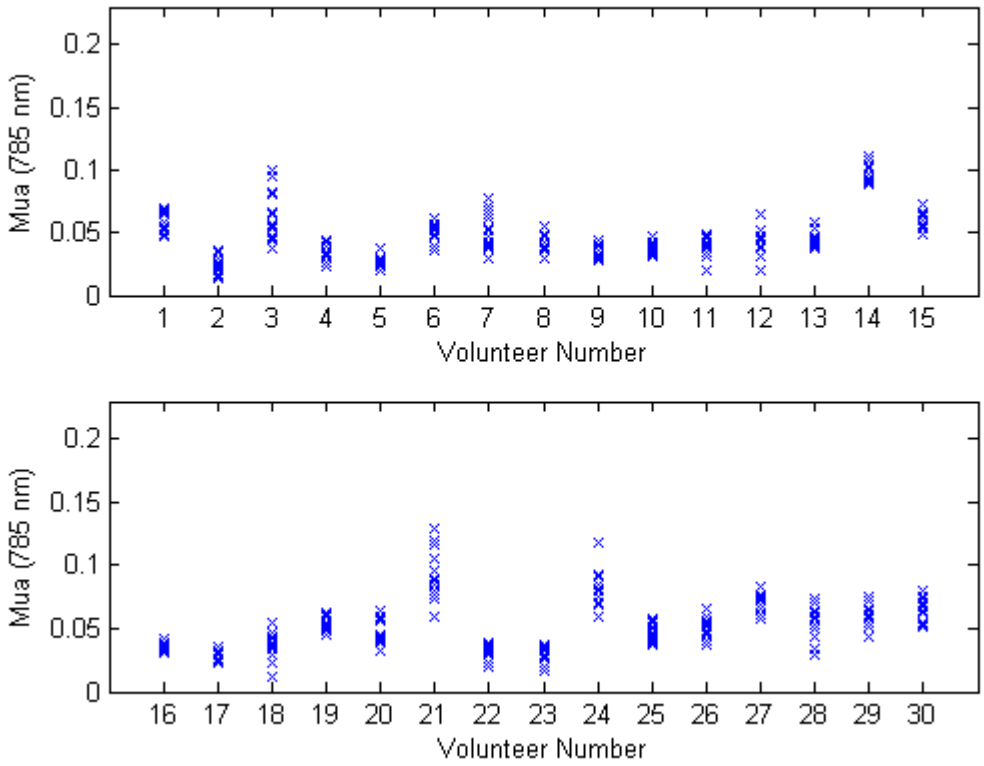

Figure 8.12 Absorption for 785 nm and 20 mm inter-fibre distance.

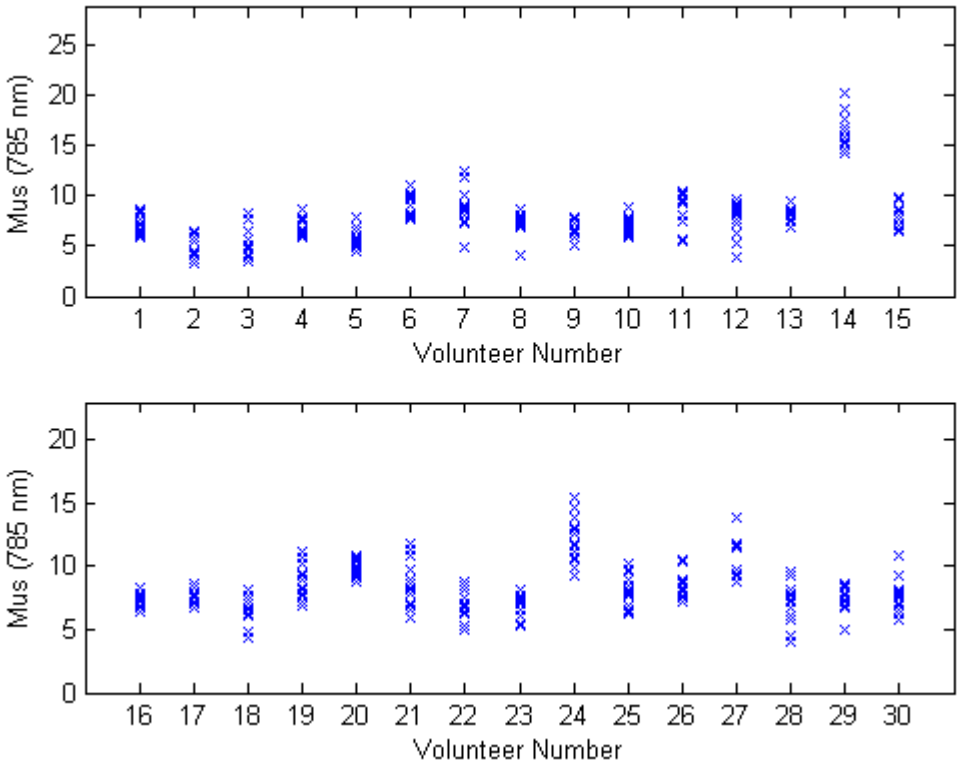

Figure 8.13 Scattering for 785 nm and 20 mm inter-fibre distance.

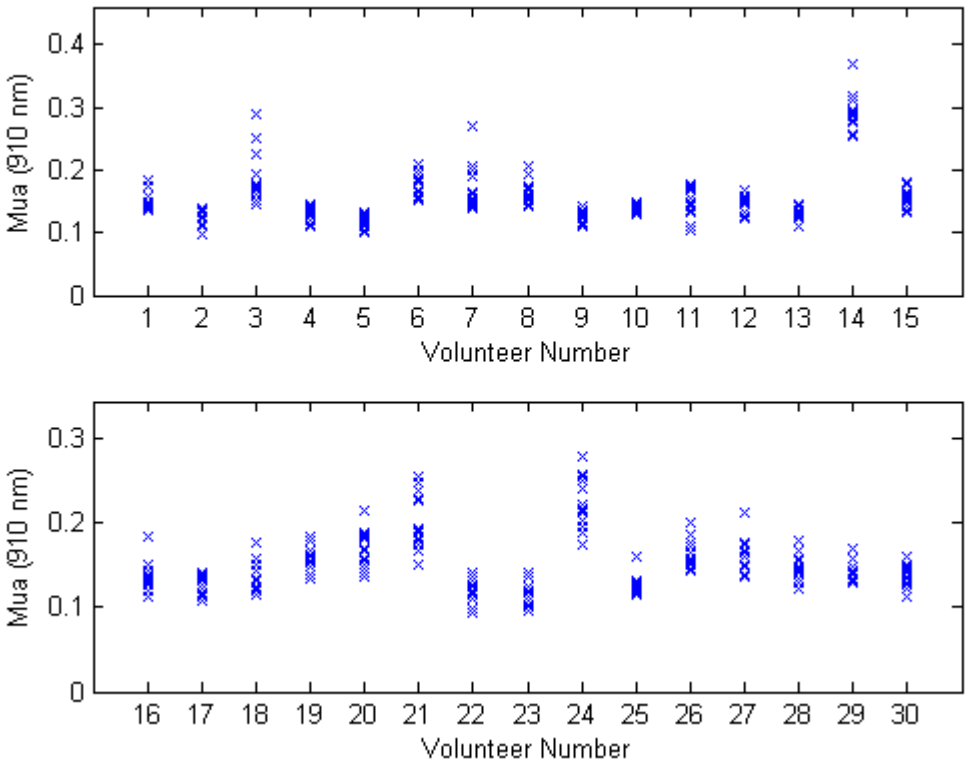

Figure 8.14 Absorption for 910 nm and 20 mm inter-fibre distance.

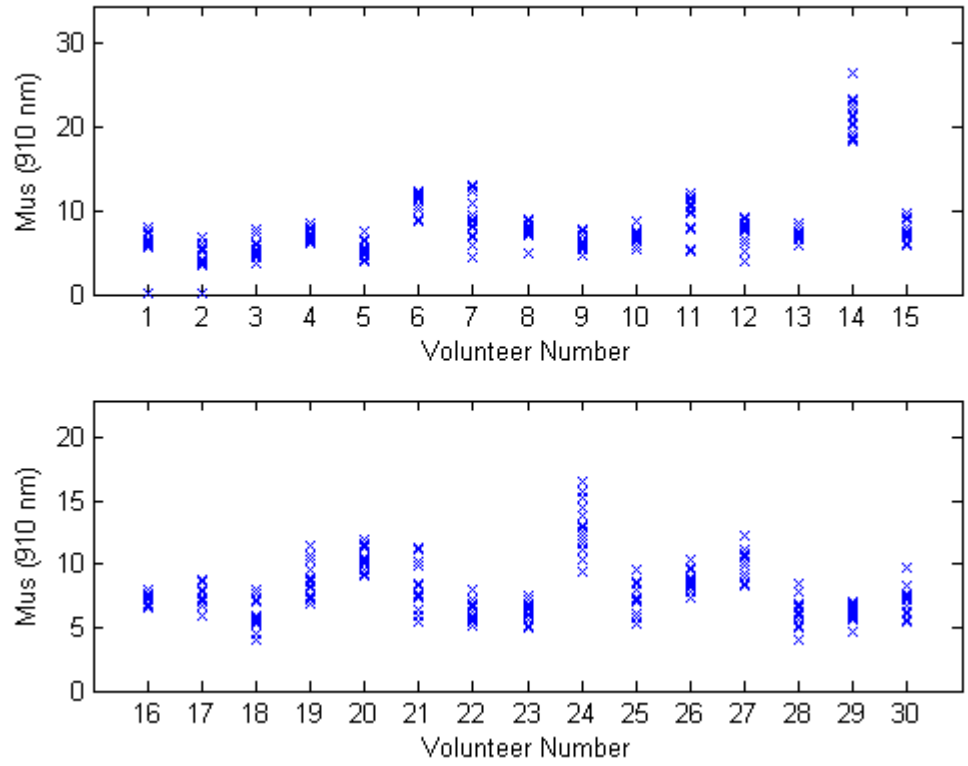

Figure 8.15 Scattering for 910 nm and 20 mm inter-fibre distance.

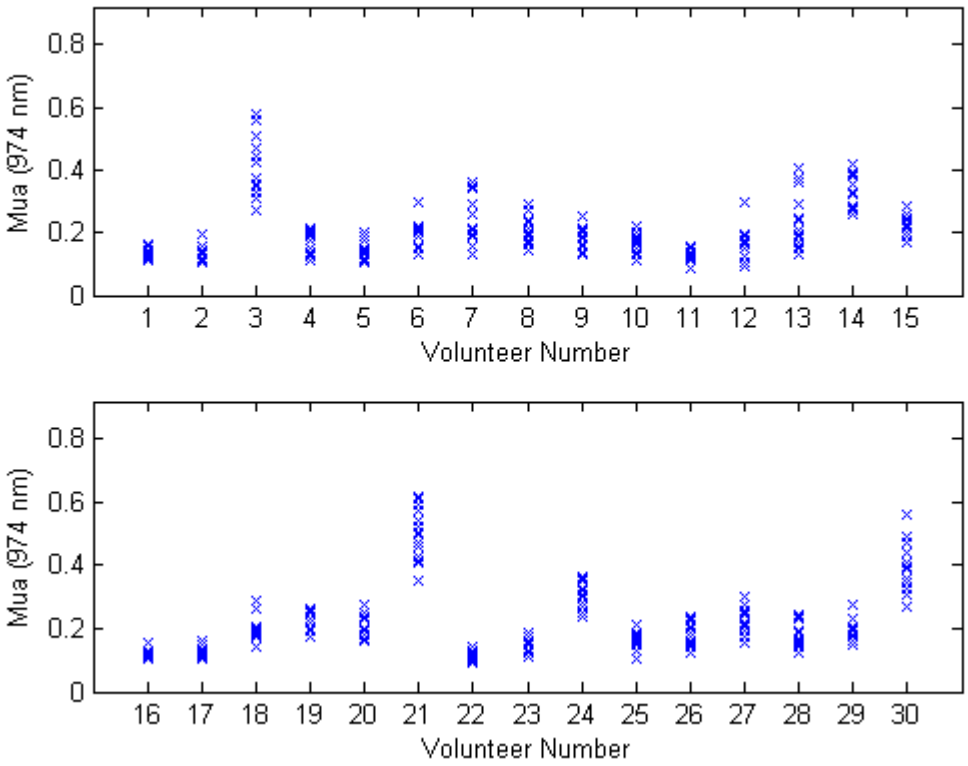

Figure 8.16 Absorption for 974 nm and 20 mm inter-fibre distance.

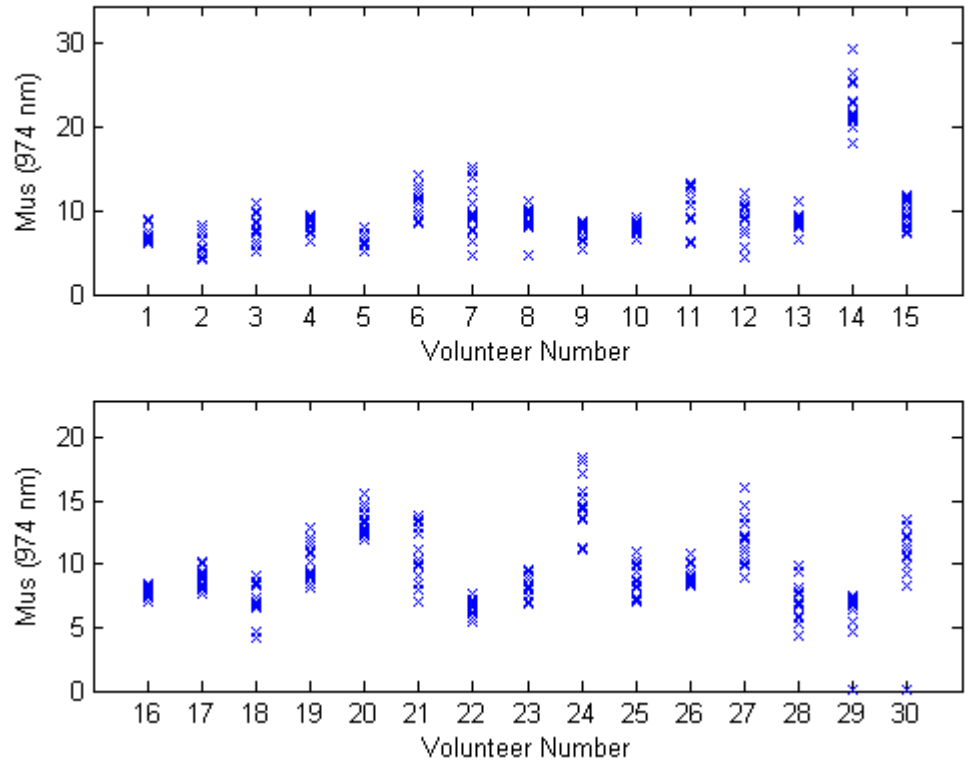

Figure 8.17 Scattering for 910 nm and 20 mm inter-fibre distance.

8.1 Results of individual measurements

The most representative data together with some relevant information about the corresponding volunteer is shown in the following figures.

In some cases, the data both for 15 and 20 mm distances has been included, but in others only one of them has been chosen. This is because for some volunteers only the values obtained for one of the distances was representative of the typical case. A possible reason can be that they could be tired for the second group of measurements and holding the probe less steadily, which could have induced some errors.

To understand the figures, the following has to be taken into account.

In the scattering plots (μ_s' over μ_a):

- Upper Outer (Positions 1 to 3)
- Upper Outer (Positions 8 to 10)
- Upper Inner (Positions 4 and 11)
- Lower Inner (Positions 5 and 12)
- Lower Outer (Positions 6 and 13)
- Centre (Positions 7 and 14)

In the plots showing μ_s' or μ_a as a function of position on the breast:

Number 1 in the x-axis represents the measurements 8 to 10 (fixed position on right breast, upper outer).
Number 2 in the x-axis represents the measurements 1 to 3 (small variations on left breast, upper outer).
Number 3 in the x-axis represents the remaining measurements on the right breast (4,5,6 and 7). Different symbols for each of the points have been used according to the legend shown above.
Number 4 in the x-axis represents the remaining measurements on the left breast (11,12,13 and 14). Different symbols for each of the points have been used according to the legend shown above.

Again, the absorption and scattering coefficients are represented in cm^{-1}.

8.1.1 Results for volunteer number 4

Relevant information:

Age: 49
Bra size: D/E
Weight: 88 Kg
Length: 179 cm

Number of children: 2

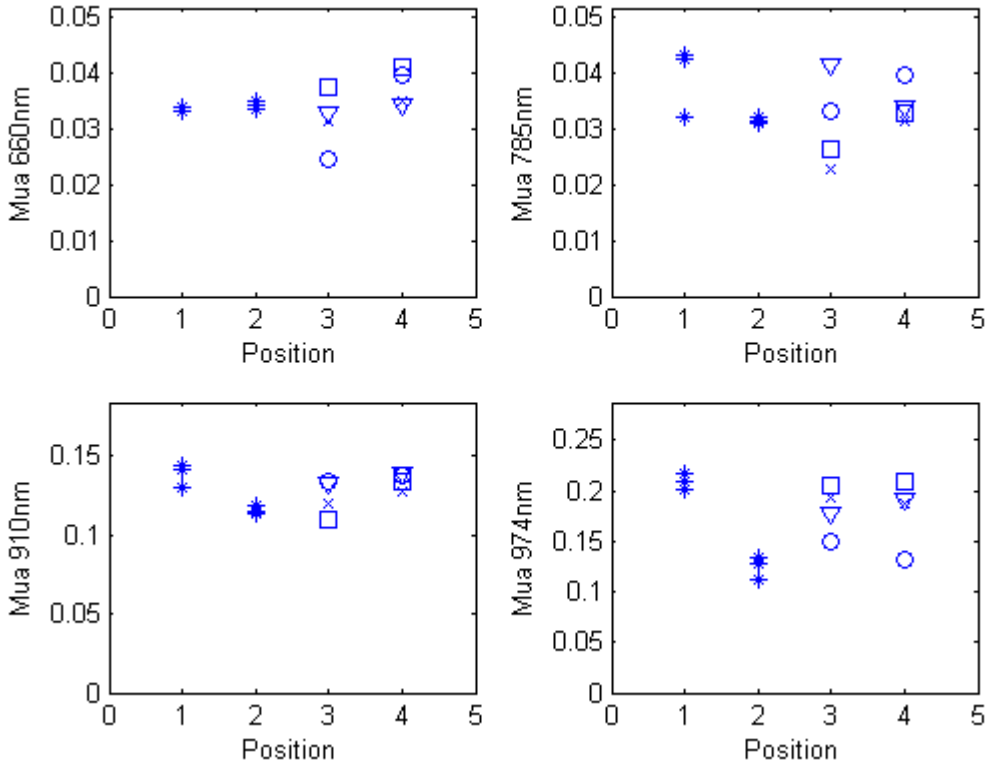

Figure 8.18 Measurements for 20 mm.

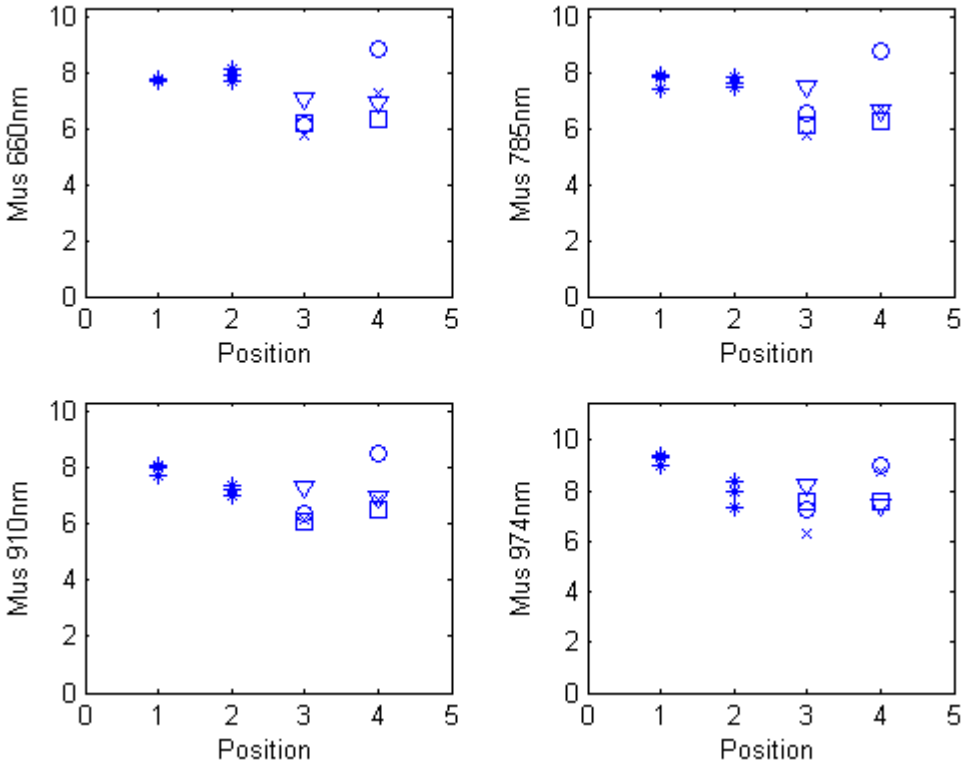

Figure 8.19 Measurements for 20 mm.

It can be noted that in the absorption measured on points 8 to 10 at 785 nm, one of the points presents a deviant value, quite different from the other two. This could be due to the fact that the Temporal Point Spread Function at 785 nm presents a change in its slope that can influence on the fitting procedure. By looking at the fit results, the two higher points (corresponding to positions 9 and 10) seem to be those with imprecision in the fitting.

8.1.2 Results for volunteer number 5

Relevant information:

Age: 50
Bra size: B
Weight: 76 Kg
Length: 174 cm
Number of children: 3

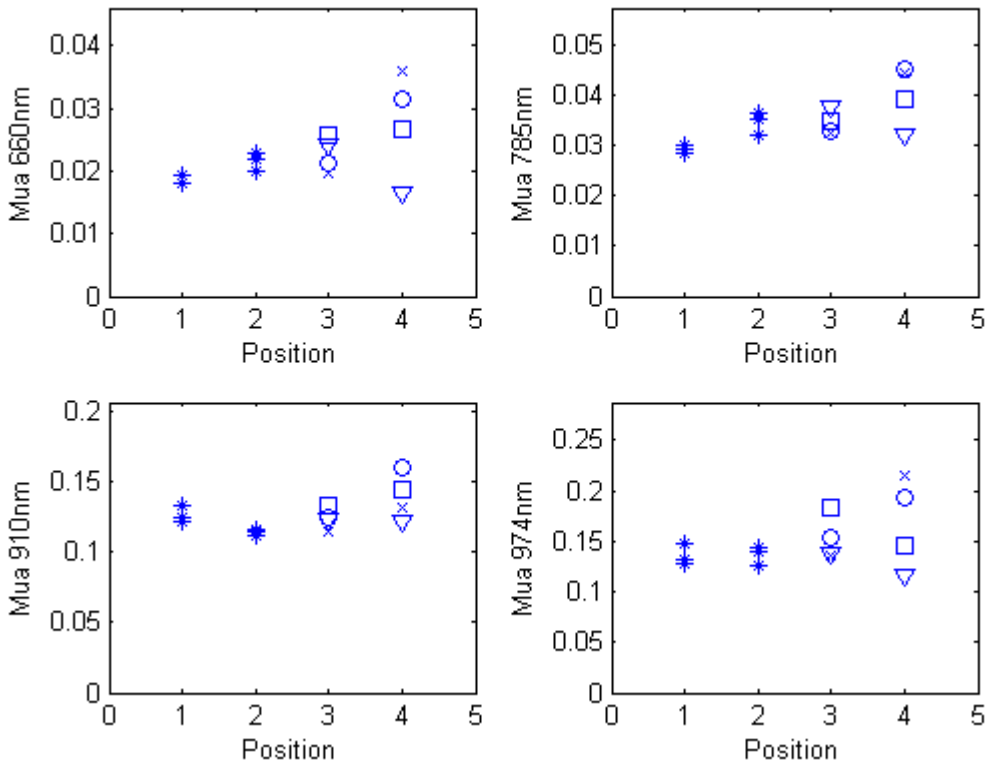

Figure 8.20 Measurements for 15 mm.

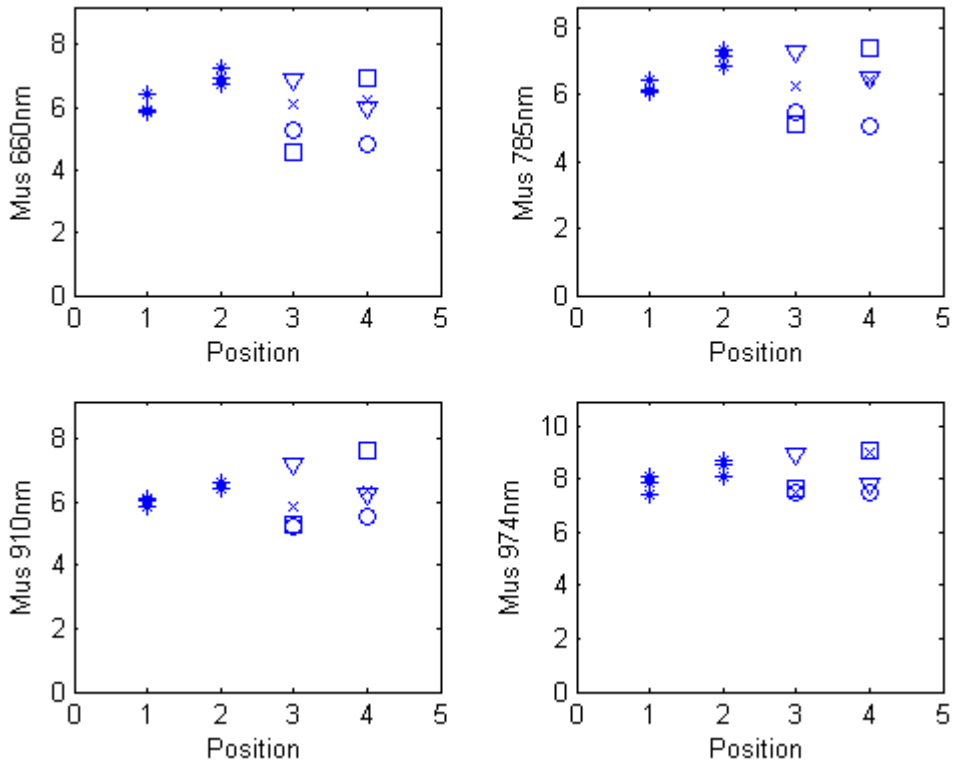

Figure 8.21 Measurements for 15 mm.

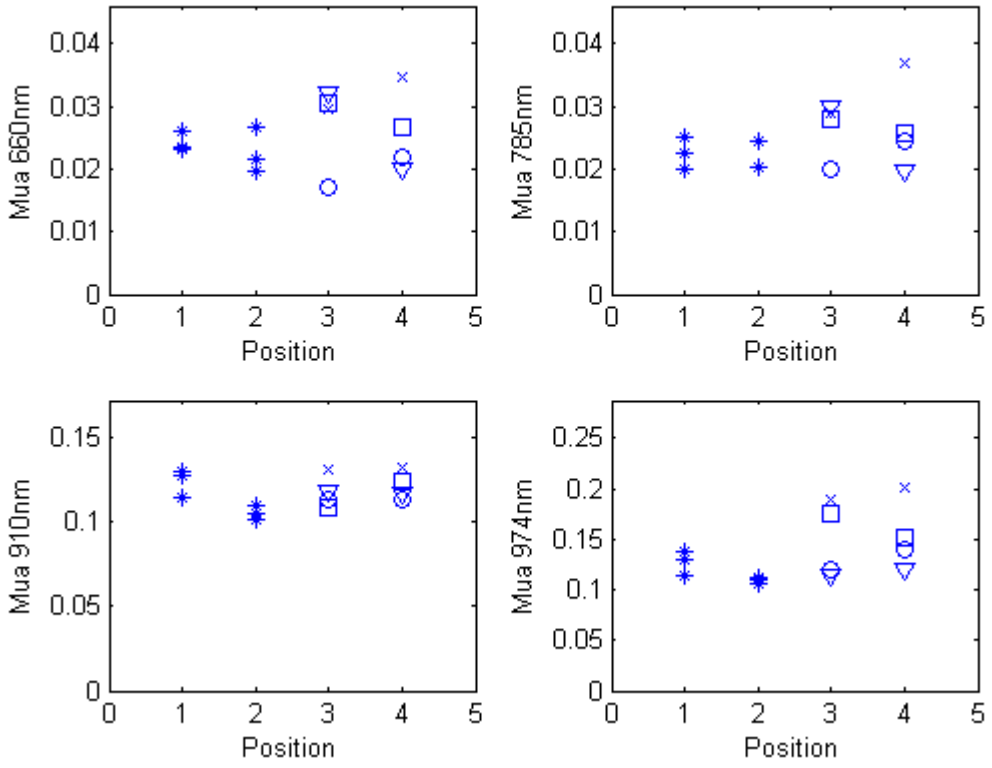

Figure 8.22 Measurements for 20 mm.

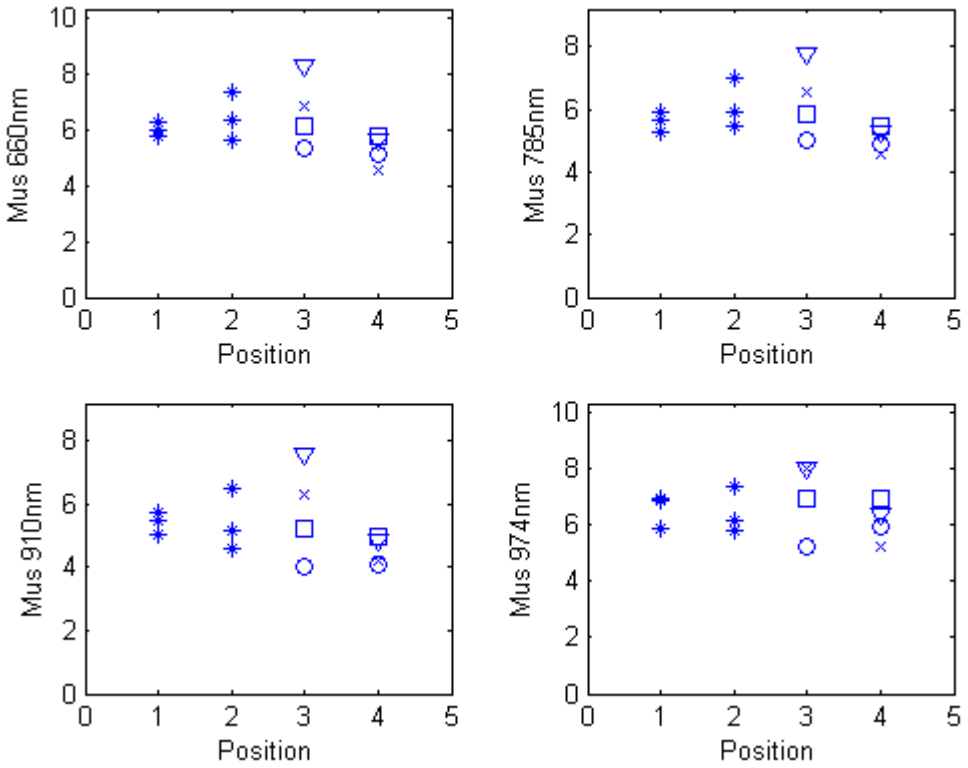

Figure 8.23 Measurements for 20 mm.

It can be noted that in the case of 15 mm, the measurements performed on the same spot give very similar values, and the same happens to the ones performed with small variation in position. For the remaining measurements there is more variation between the values obtained, but it is quite small. In the 20 mm case in most of the points, a bigger variation can be found between the values obtained for different positions.

8.1.3 Results for volunteer number 10

Relevant information:

Age: 45
Bra size: B
Weight: 71 Kg
Length: 165 cm
Number of children: 2

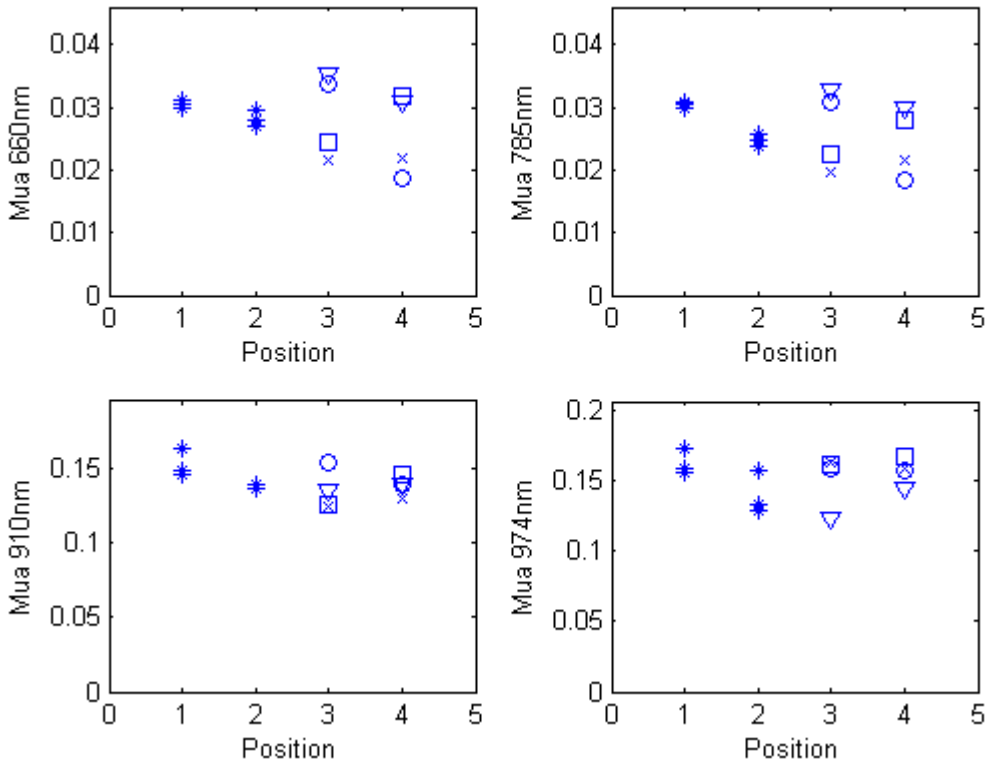

Figure 8.24 Measurements for 15 mm.

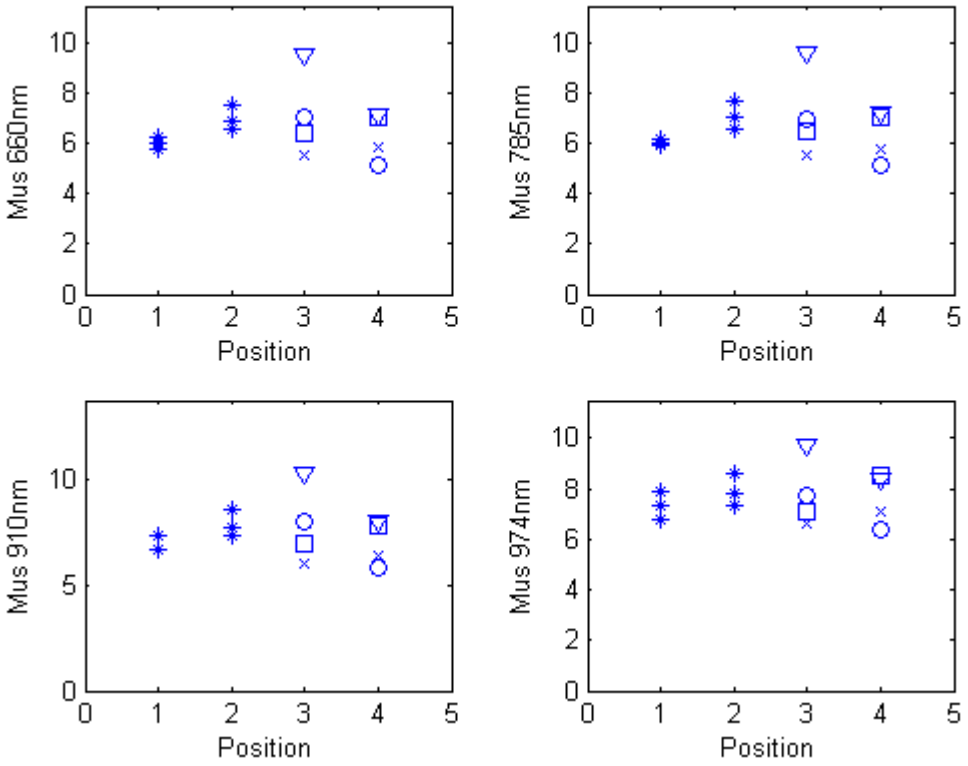

Figure 8.25 Measurements for 15 mm.

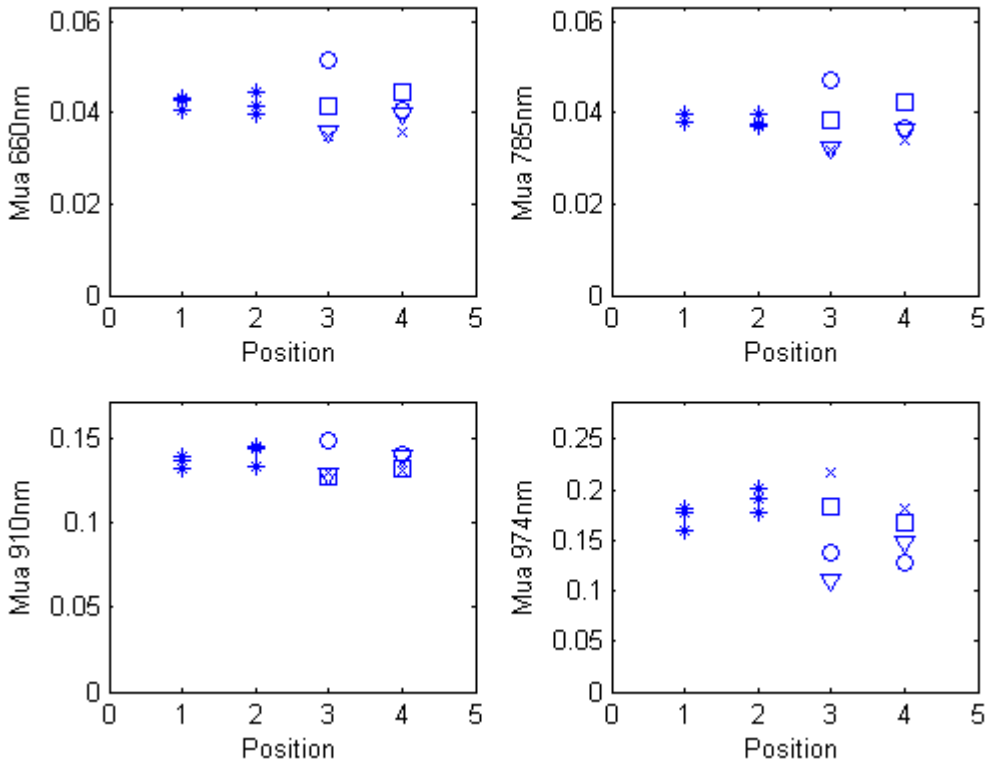

Figure 8.26 Measurements for 20 mm.

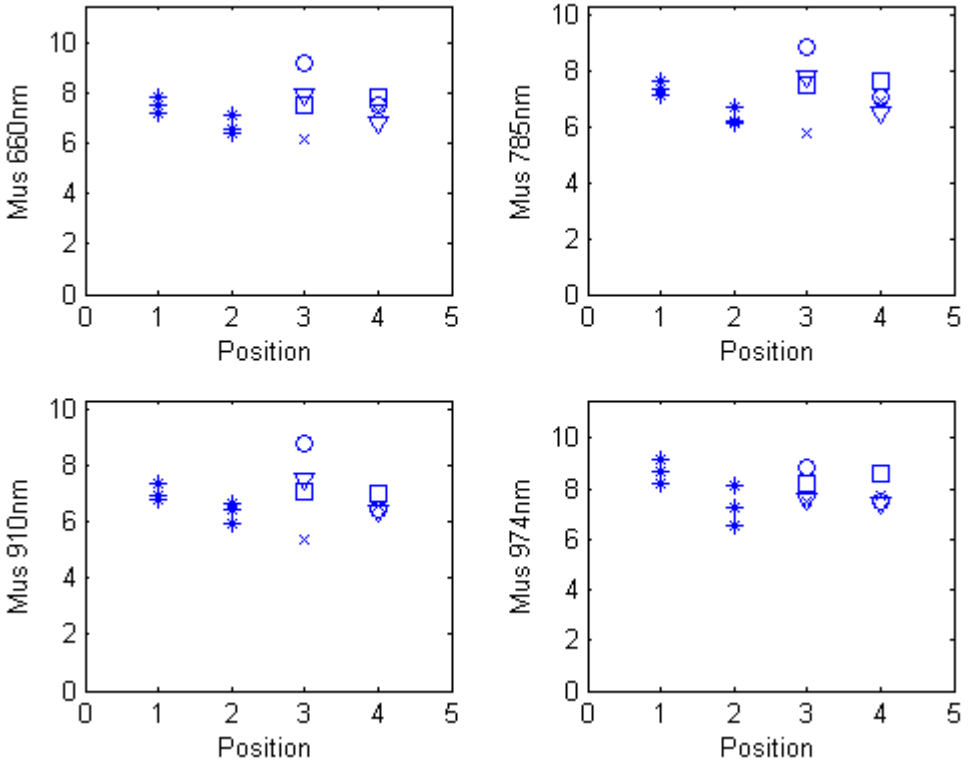

Figure 8.27 Measurements for 20 mm.

It may be noted that the values obtained for the absorption coefficient using 15 mm inter-fibre distance are slightly lower than the corresponding for 20 mm, which can be due to the fact that with 20 mm the probing is deeper into the tissue.

8.1.4 Results for volunteer number 15

Relevant information:

Age: 49
Bra size: D
Weight: 64 Kg
Length: 174 cm
Number of children: 3

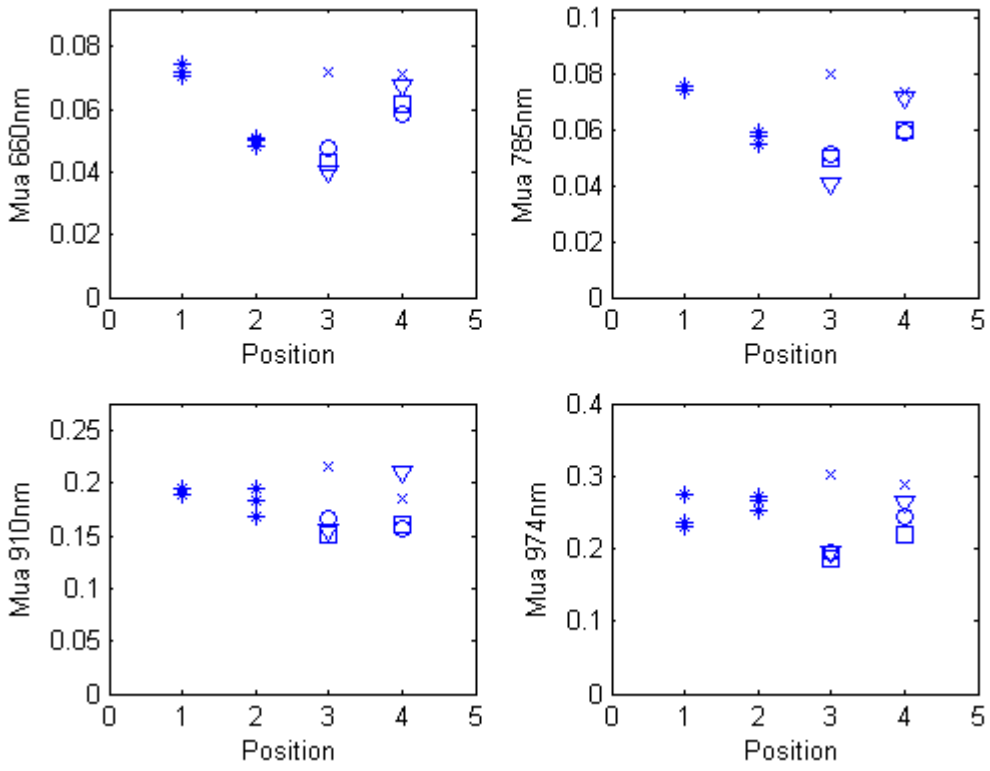

Figure 8.28 Measurements for 15 mm.

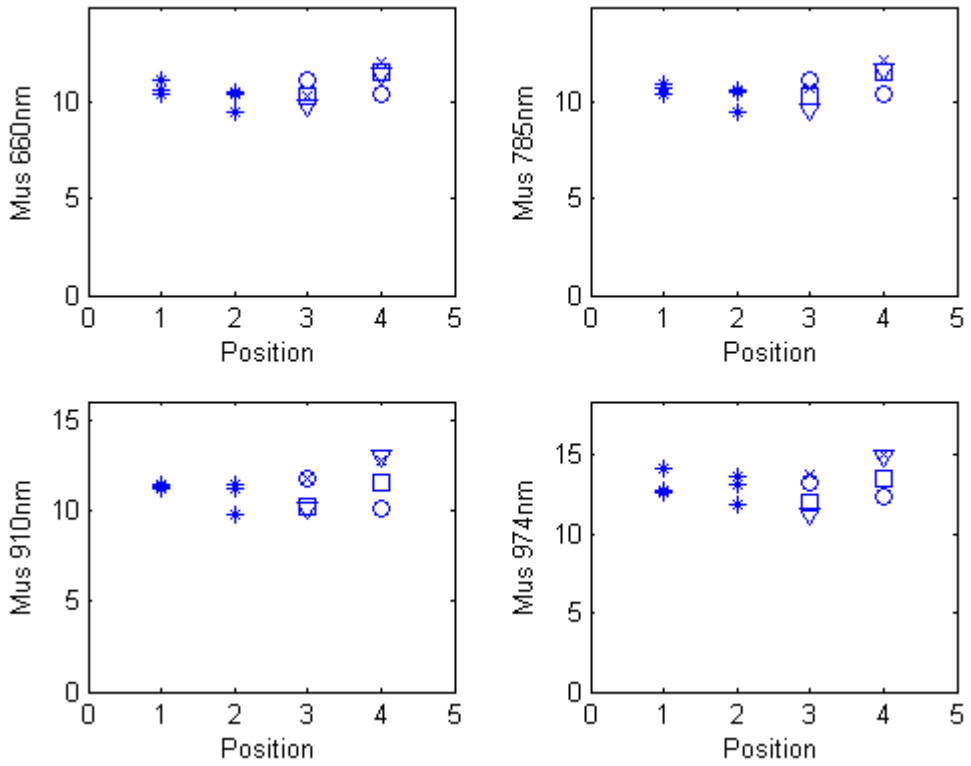

Figure 8.29 Measurements for 15 mm.

For this volunteer, the measurement number 11 (marked as 11 in the graphs) was performed on point 13, number 12 was performed on point 11, and number 13 on point 12, by mistake. The graphs for 20 mm were not chosen for this volunteer because the probe was lifted between measurements 8 and 9, by mistake.

8.1.5 Results for volunteer number 16

Relevant information:

Age: 51
Bra size: B
Weight: 86 Kg
Length: 175 cm
Number of children: 2
Uterus had been extracted.

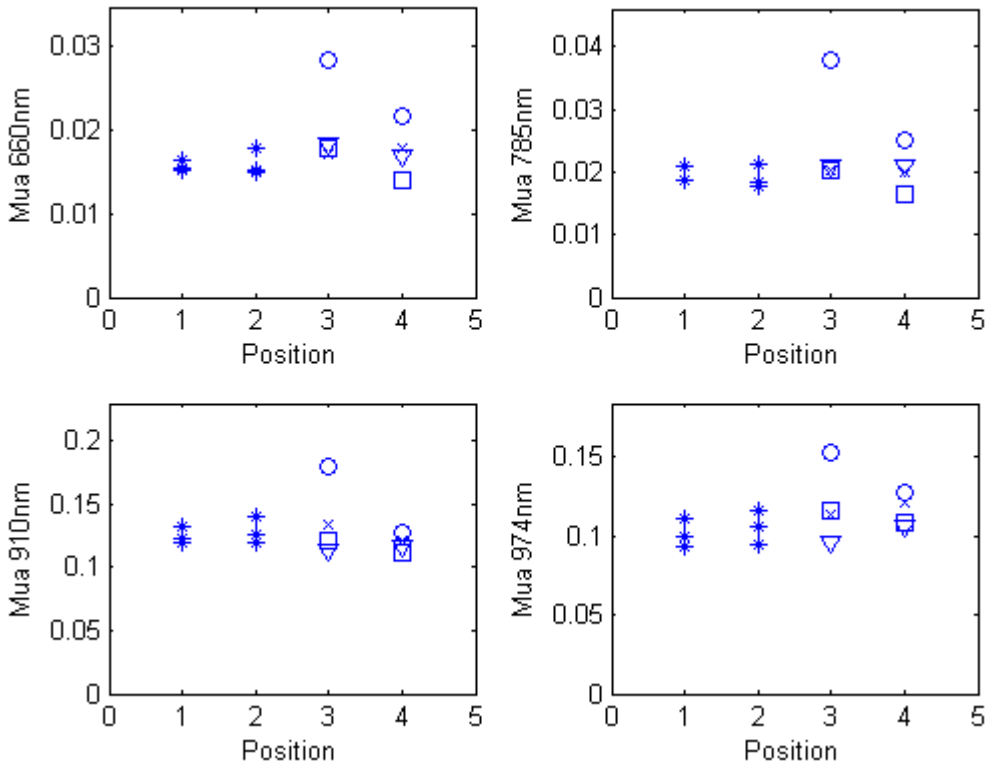

Figure 8.30 Measurements for 15 mm.

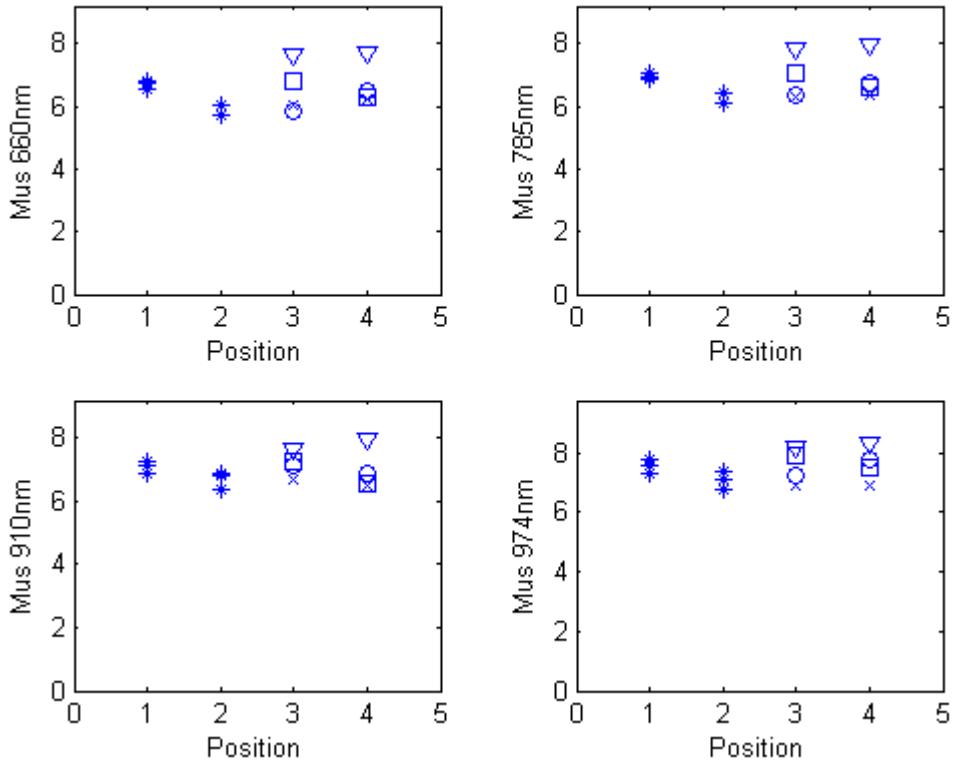

Figure 8.31 Measurements for 15 mm.

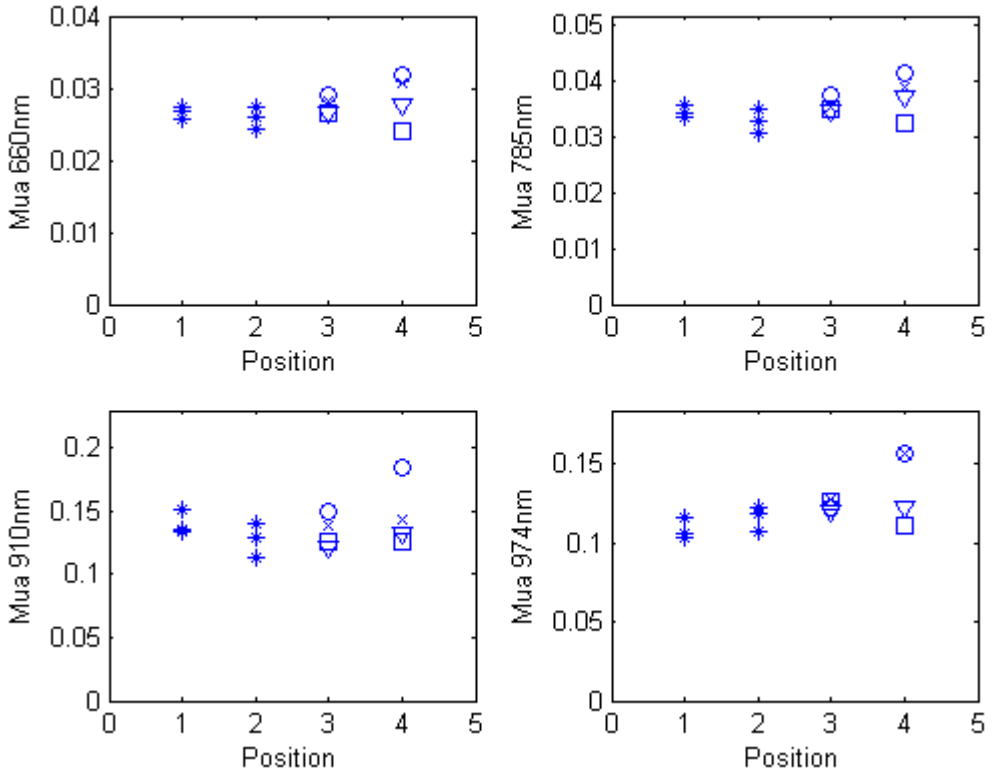

Figure 8.32 Measurements for 20 mm.

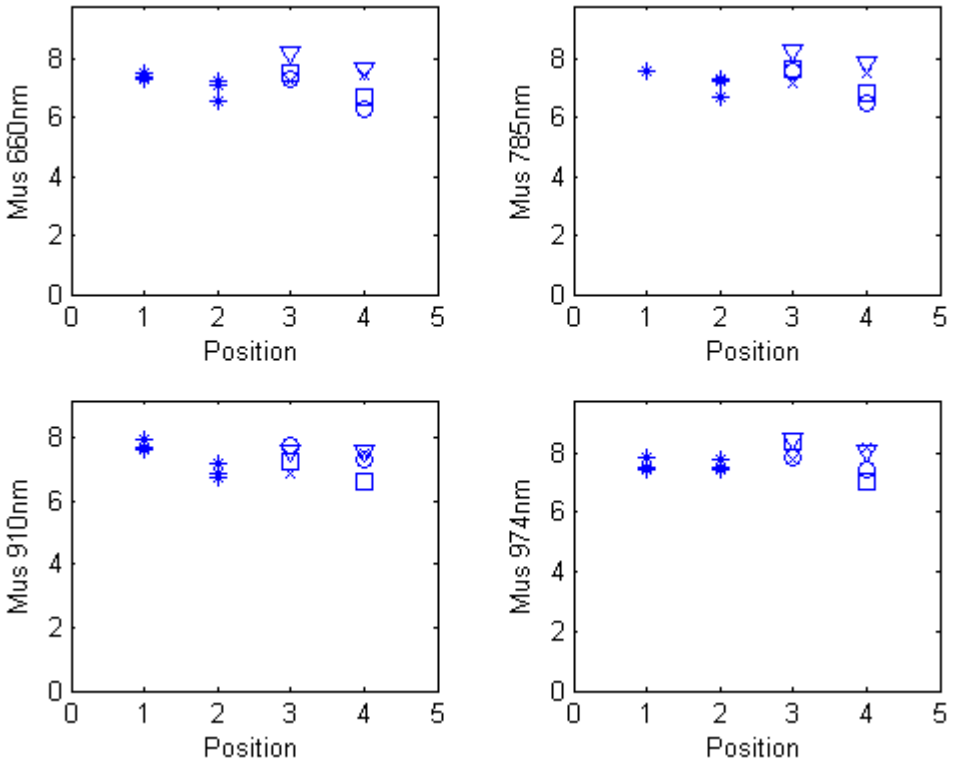

Figure 8.33 Measurements for 20 mm.

It can be observed that the scattering coefficient is slightly higher for the measurements performed on points 5 and 12 both for 15 and 20 mm, while the absorption is higher for points 4 and 11 on both breasts.

8.1.6 Results for volunteer number 17

Relevant information:

Age: 43
Bra size: A
Weight: 70 Kg
Length: 162 cm
Number of children: 3
Uterus had been extracted.

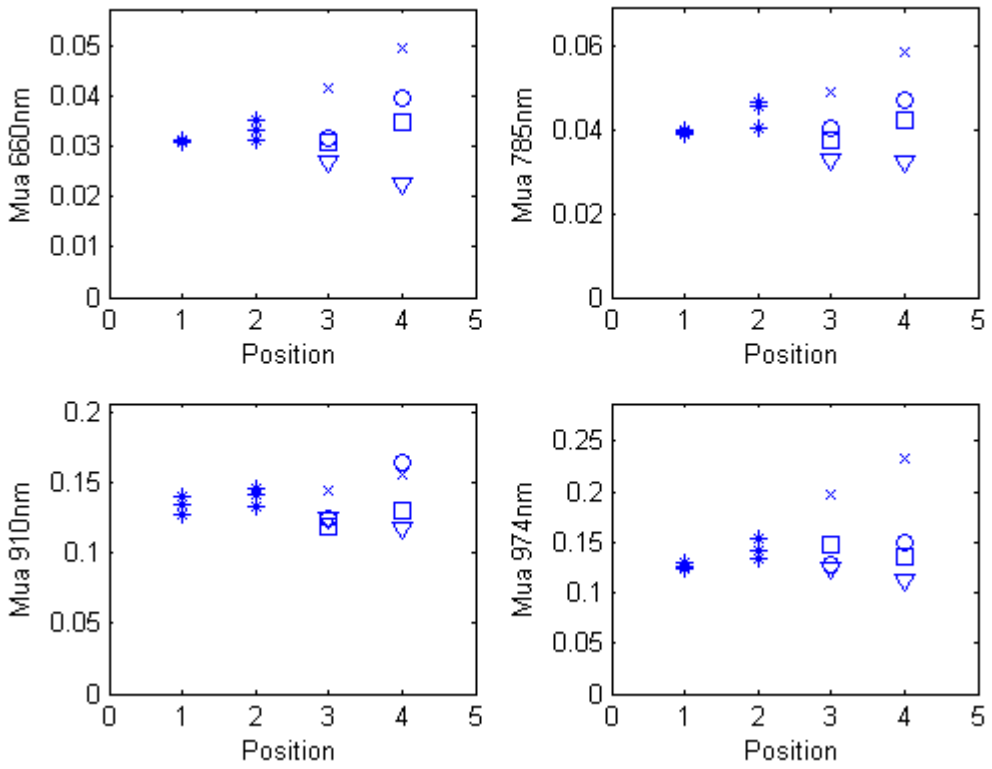

Figure 8.34 Measurements for 15 mm.

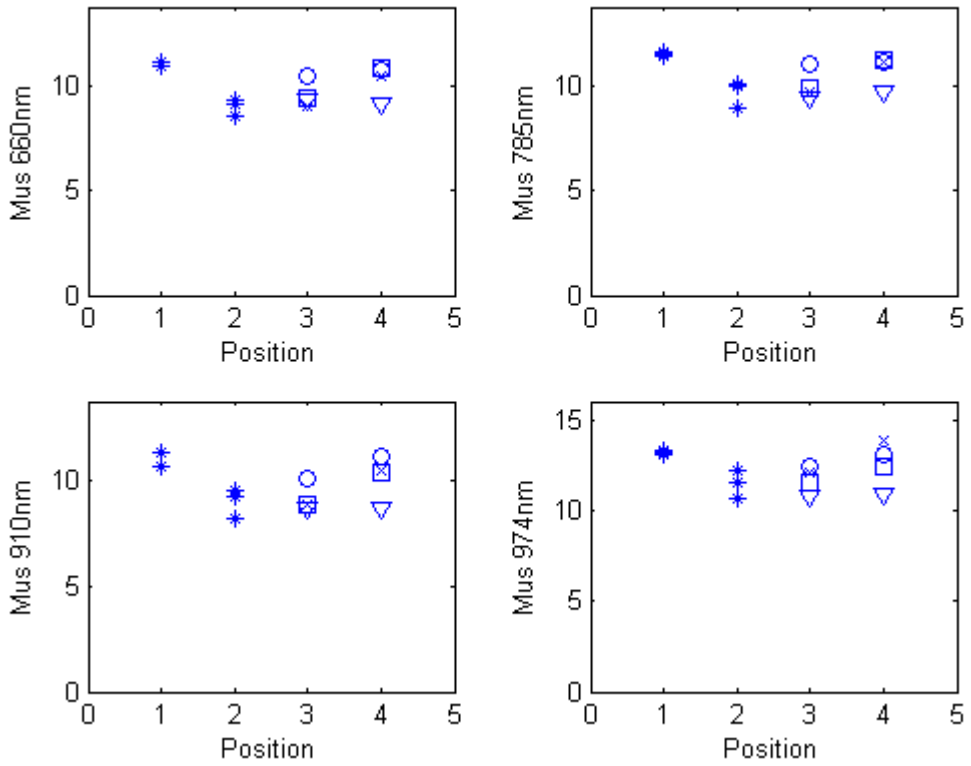

Figure 8.35 Measurements for 15 mm.

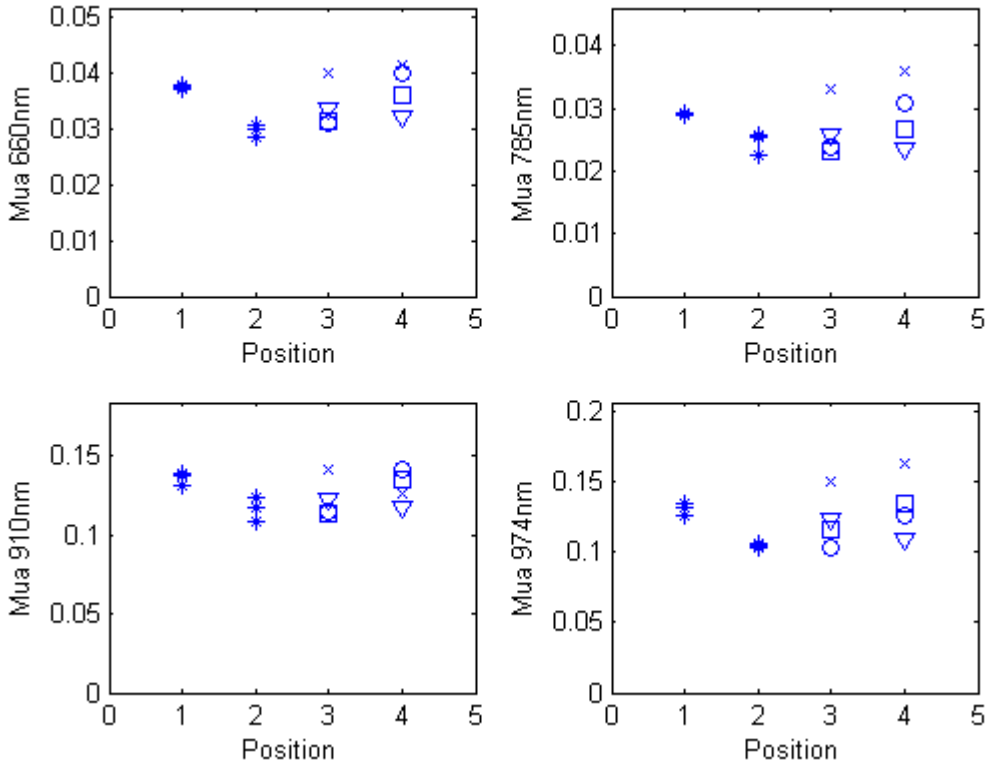

Figure 8.36 Measurements for 20 mm.

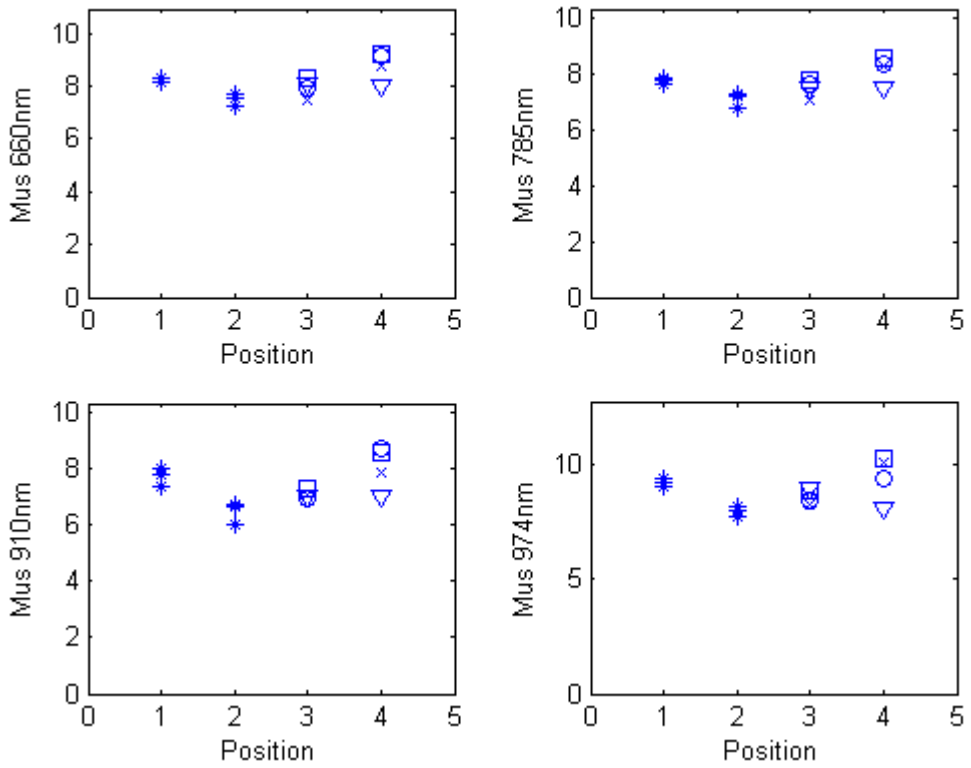

Figure 8.37 Measurements for 20 mm.

It can be noted that both for 15 and 20 mm, the absorption is higher for the points 7 and 14, which can be due to the probe having been held very near the nipple, inside the areola. In this area the absorption is higher, as the skin is darker.

8.1.7 Results for volunteer number 2

Relevant information:

Age: 47
Bra size: B
Weight: 63 Kg
Length: 165 cm
Number of children: 2

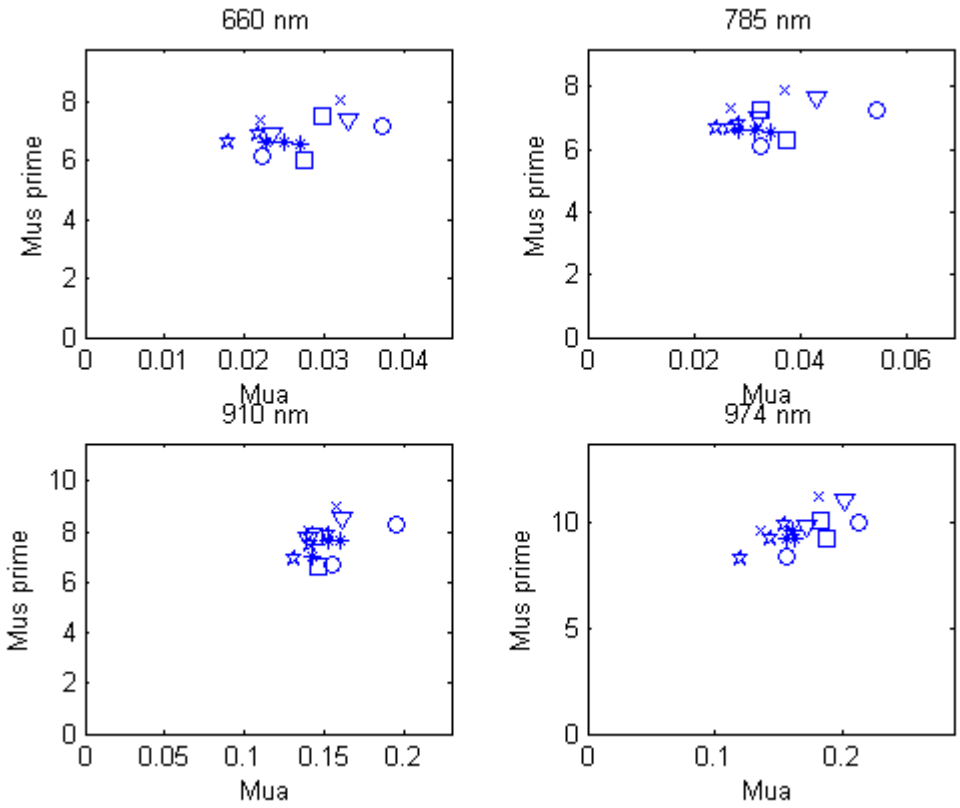

Figure 8.38 Measurements for 15 mm.

It can be seen that the values are clustered together. The points which deviate are situated on the left breast.

8.1.8 Results for volunteer number 6

Relevant information:

Age: 42
Bra size: C/D
Weight: 60 Kg
Length: 157 cm
Number of children: 3

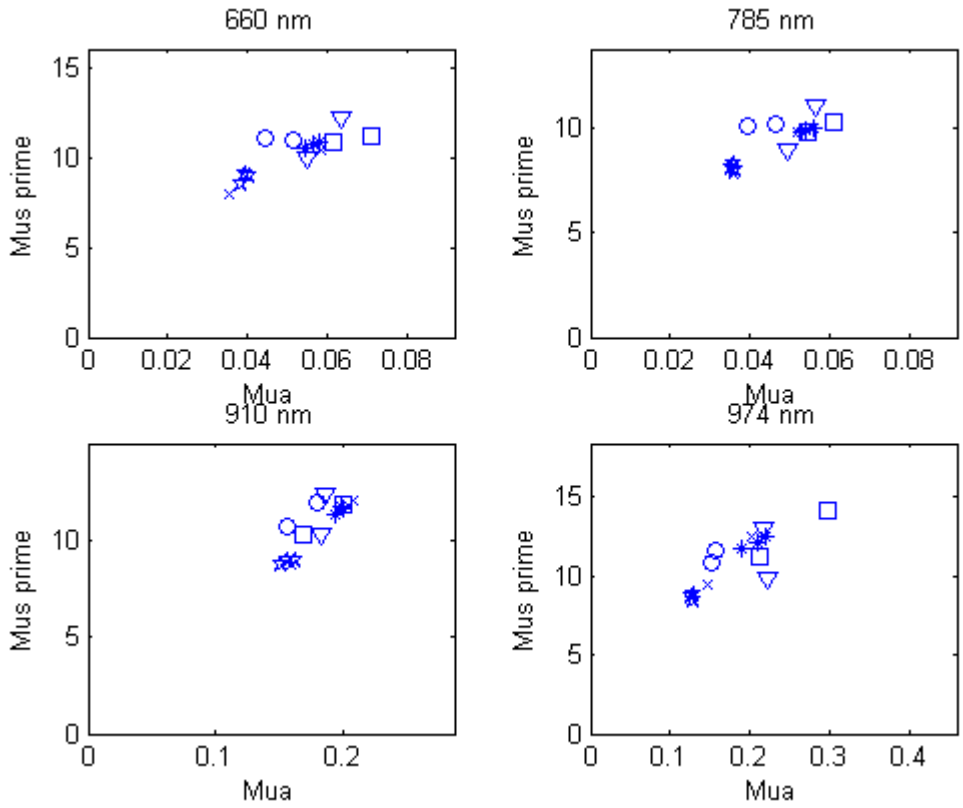

Figure 8.39 Measurements for 20 mm.

Again, the values obtained are quite close together.

8.1.9 Results for volunteer number 8

Relevant information:

Age: 55
Bra size: B
Weight: 70 Kg
Length: 170 cm
Number of children: 1

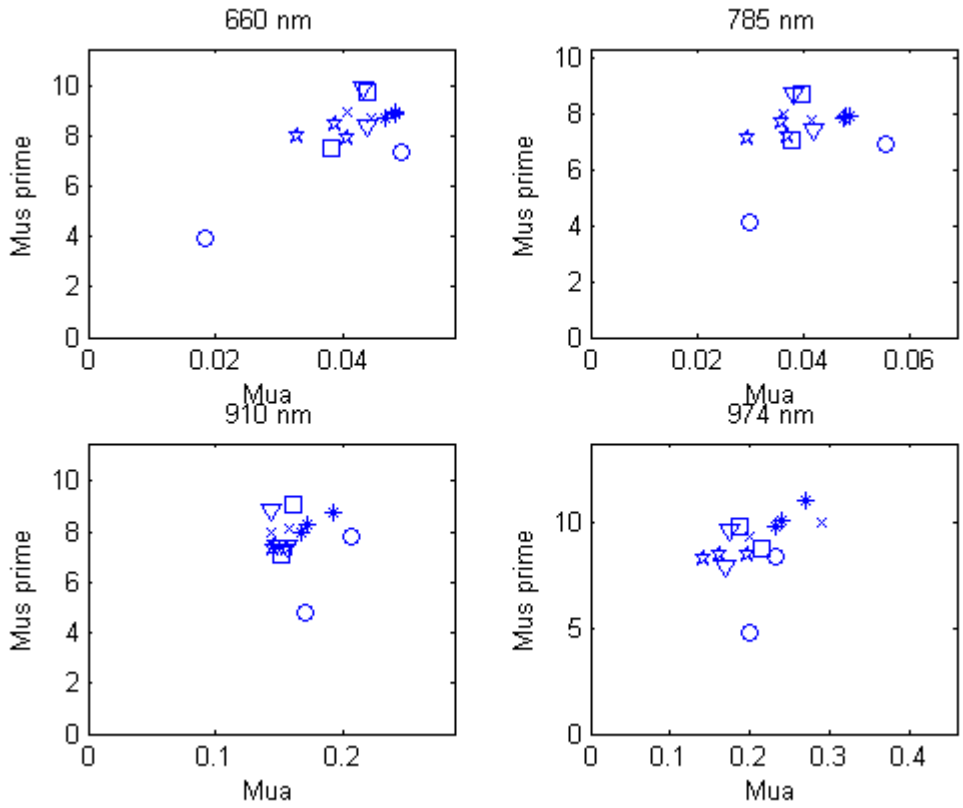

Figure 8.40 Measurements for 20 mm.

It can be noted that one of the values is lower than the rest, both for absorption and scattering, the one measured in position 4.

8.1.10 Results for volunteer number 9

Relevant information:

Age: 22
Bra size: C
Weight: 60 Kg
Length: 165 cm
Number of children: 0

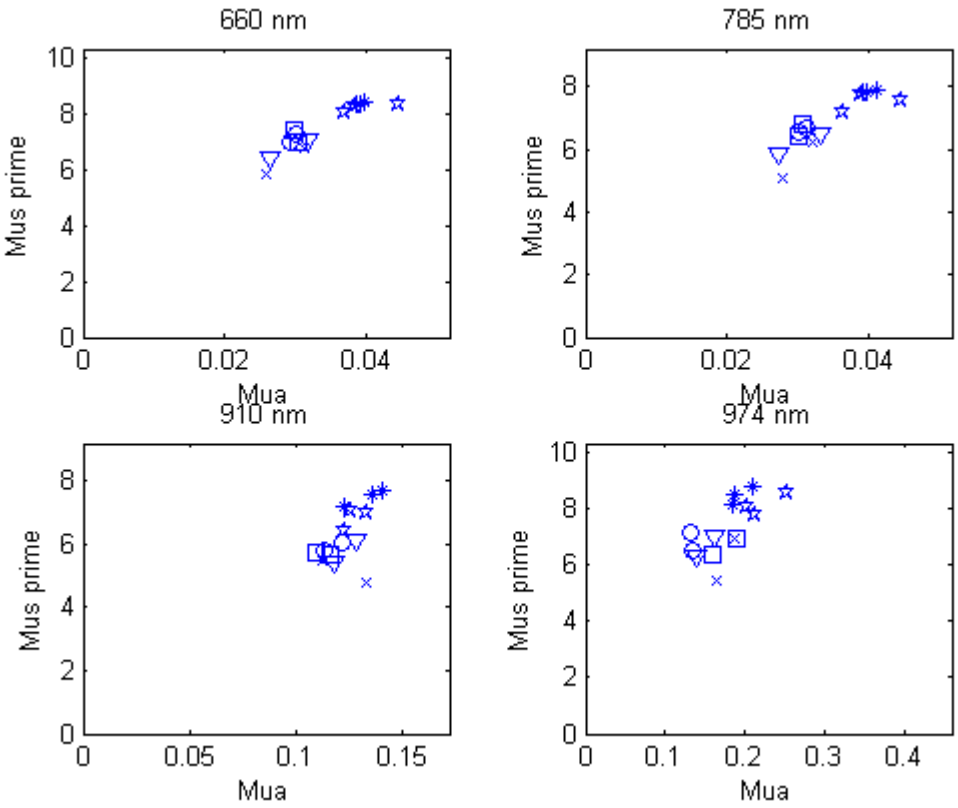

Figure 8.41 Measurements for 20 mm.

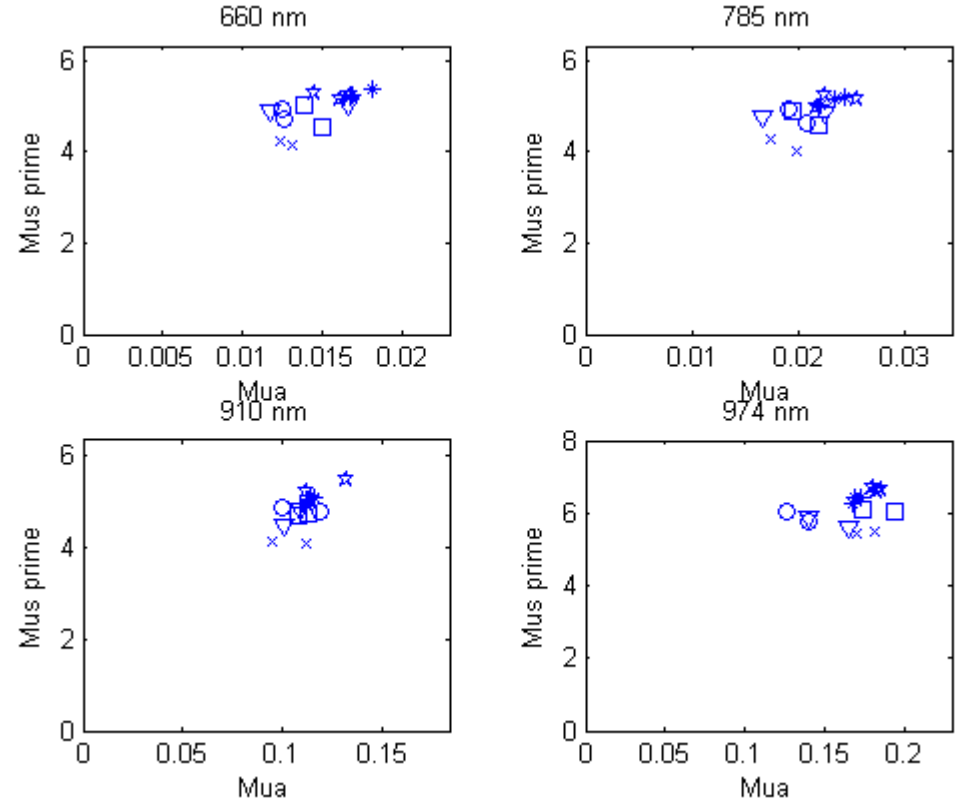

Figure 8.42 Measurements for 15 mm.

It can be observed that the values for the scattering from 15 mm measurements are quite lower than the ones measured for the rest of the volunteers for the same distance.

8.1.11 Results for volunteer number 13

Relevant information:

Age: 33
Bra size: B
Weight: 65 Kg
Length: 163 cm
Number of children: 2

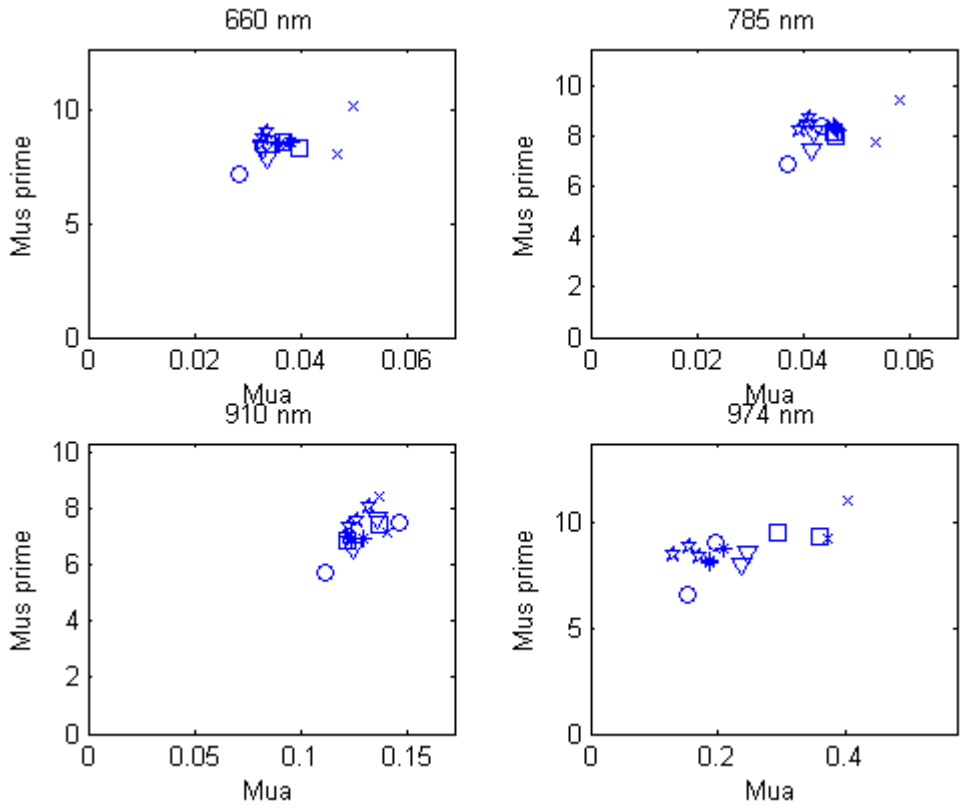

Figure 8.43 Measurements for 20 mm.

The absorption is slightly higher for points 7 and 14 than for the rest, except for 910 nm. Measurement number 4 presents a slightly lower absorption than the rest. The scattering is more or less uniform for all of the points. In 974 nm it can be seen that the values are more spread out.

8.1.12 Results for volunteer number 23

Relevant information:

Age: 41
Bra size: C
Weight: 78 Kg
Length: 172 cm
Number of children: 3

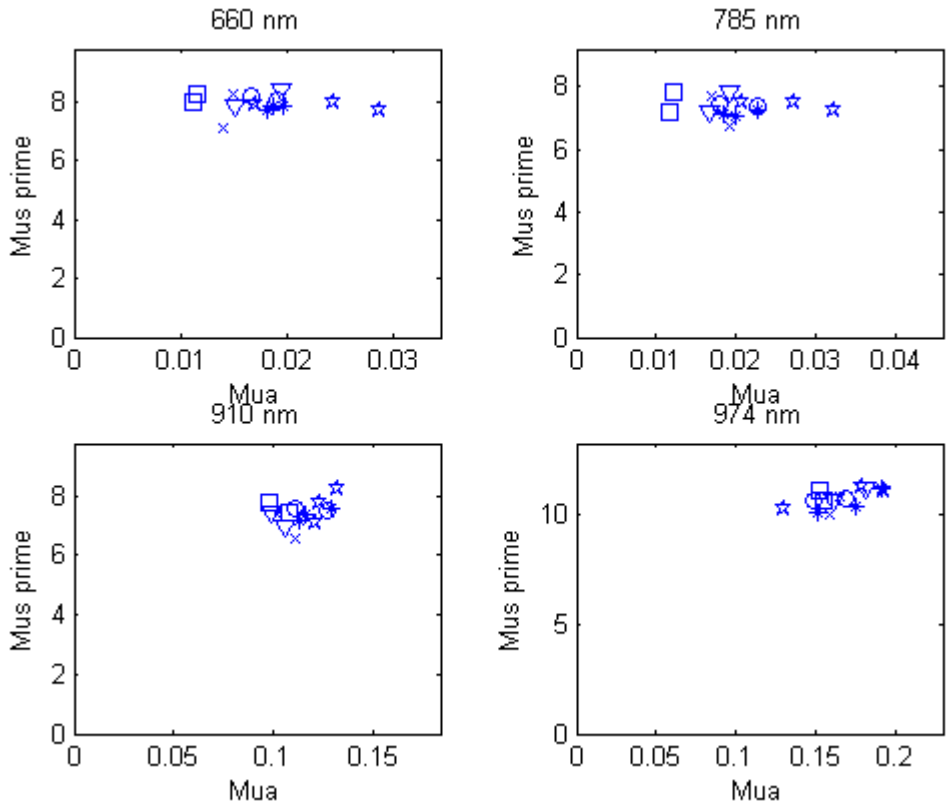

Figure 8.44 Measurements for 15 mm.

In this case, the probe was moved quite a lot between measurements 1, 2 and 3, and this may have caused the separation between these values in the graphs.

8.1.13 Results for volunteer number 25

Relevant information:

Age: 33
Bra size: C
Weight: 68 Kg

Length: 158 cm
Number of children: 0

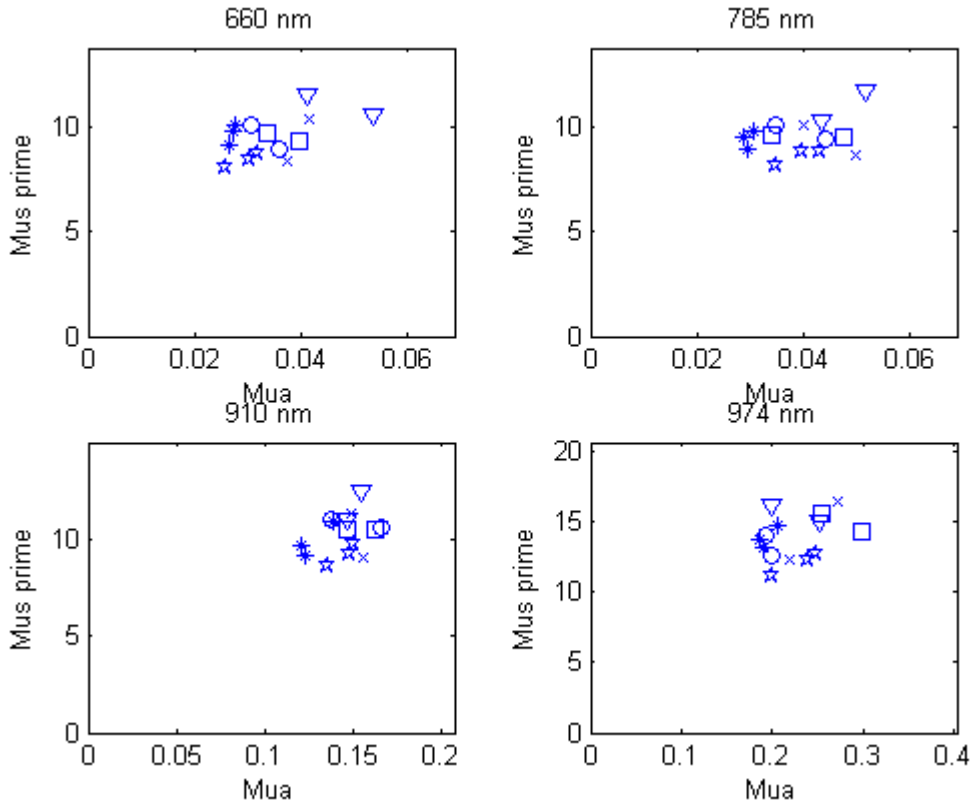

Figure 8.45 Measurements for 15 mm.

There are no measuring points which show great differences in values from the rest. All of them are quite clustered together.

8.1.14 Results for volunteer number 26

Relevant information:

Age: 50
Bra size: B
Weight: 72 Kg
Length: 175 cm
Number of children: 0

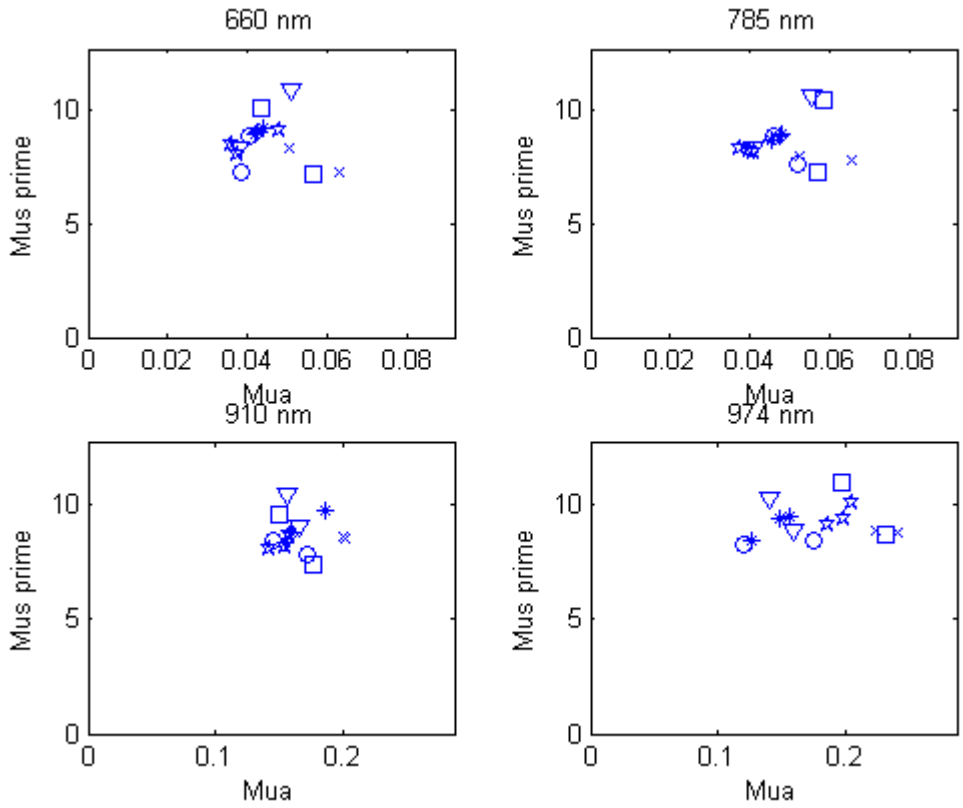

Figure 8.46 Measurements for 20 mm.

It can be noted that the values for 974 nm are more spread out than for the rest of the wavelengths.

8.1.15 Results for volunteer number 29

Relevant information:

Age: 27
Bra size: C
Weight: 63 Kg
Length: 175 cm
Number of children: 0

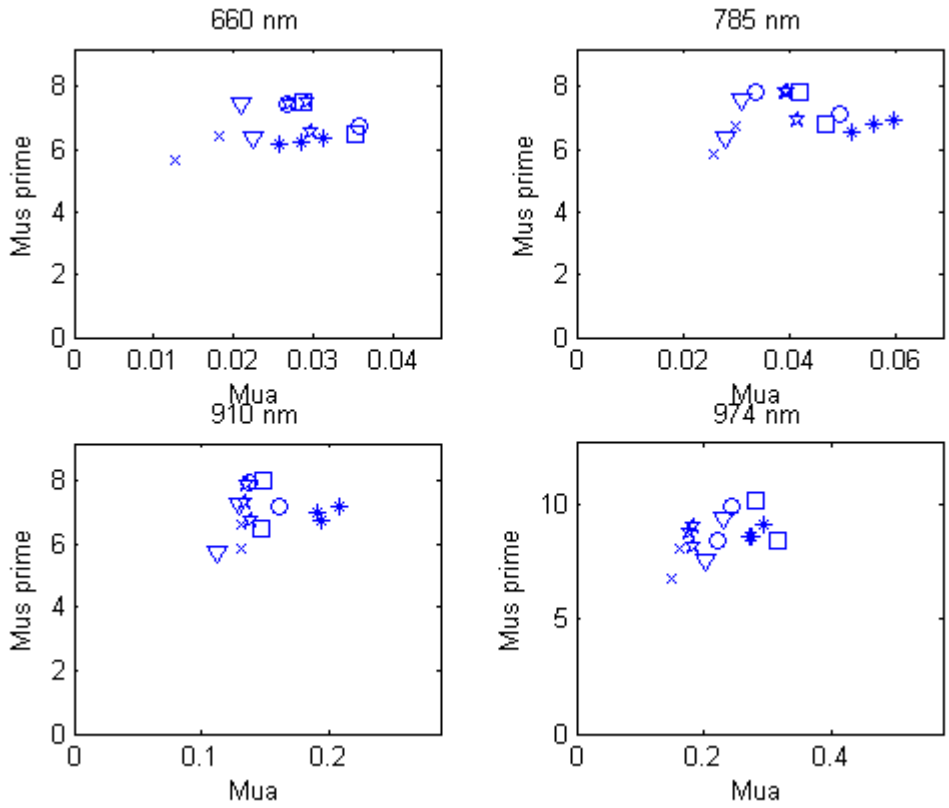

Figure 8.47 Measurements for 15 mm.

8.2 Analysis of the data

Looking at the data obtained from all of the volunteers and the corresponding plots, the volunteer´s attributes (age, weight, bra size, hormone treatments, etc) cannot be concluded from a set of measurements. The range of variation between the values obtained for a specific volunteer can be due to the factors described in chapter 5. It cannot be said by looking at a set of measurements from a volunteer in which point on the breast a specific measurement was performed.

The values obtained from measurements from the left breast are usually higher than the ones from the right breast. On the other hand, only looking at the values obtained for one breast, either right or left, no conclusion can be extracted about which point a specific value was measured at.

In what concerns the difference between the values obtained for 15 mm and 20 mm, the absorption seems to be higher in the case of 20 mm, except in the 910 nm case. This behaviour could be expected, since with 20 mm inter fibre distance light penetrates deeper into the tissue.

The statistical parameters mean and standard deviation have been calculated in order to extract a more accurate conclusion on the similarity of all recorded data. See following figures:

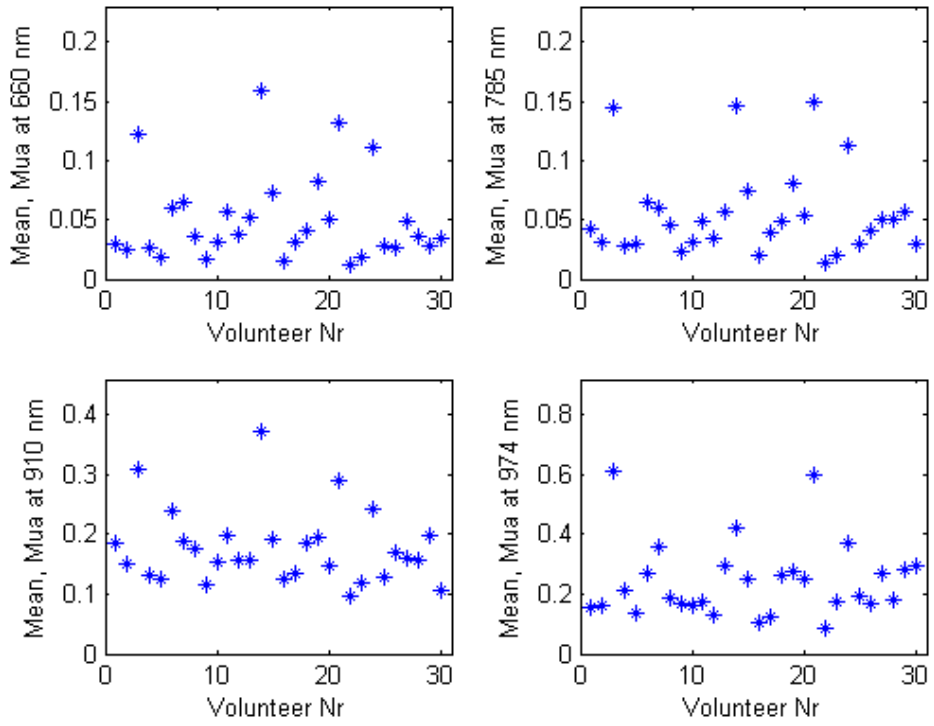

Figure 8.48Mean values for μ_a in measurements 8 to 10 for 15 mm.

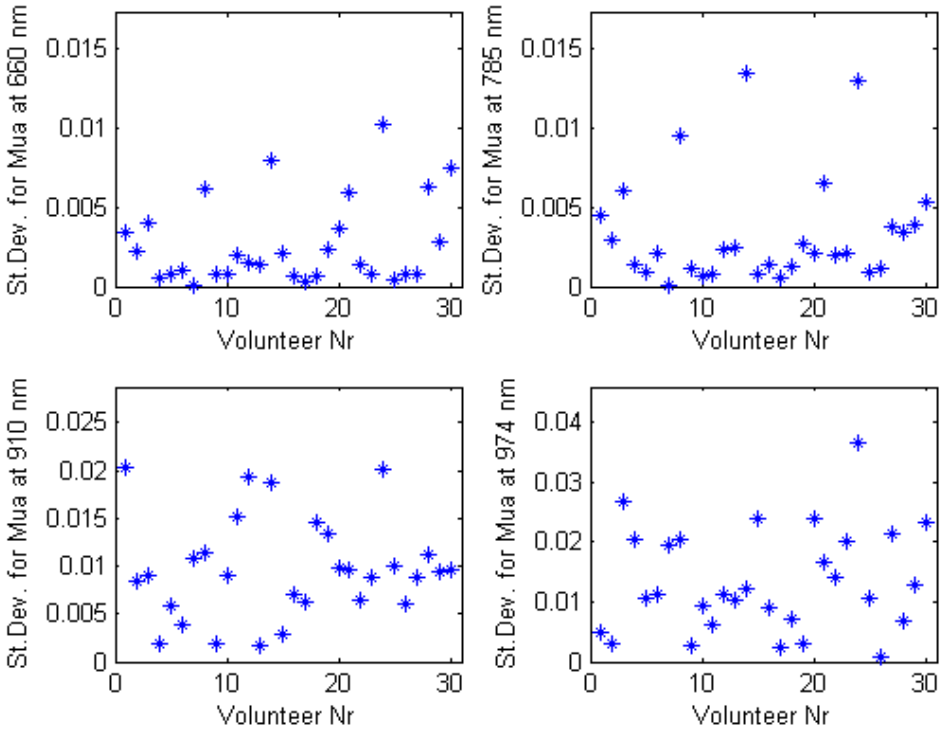

Figure 8.49 Standard deviation for μ_a in measurements 8 to 10 for 15 mm.

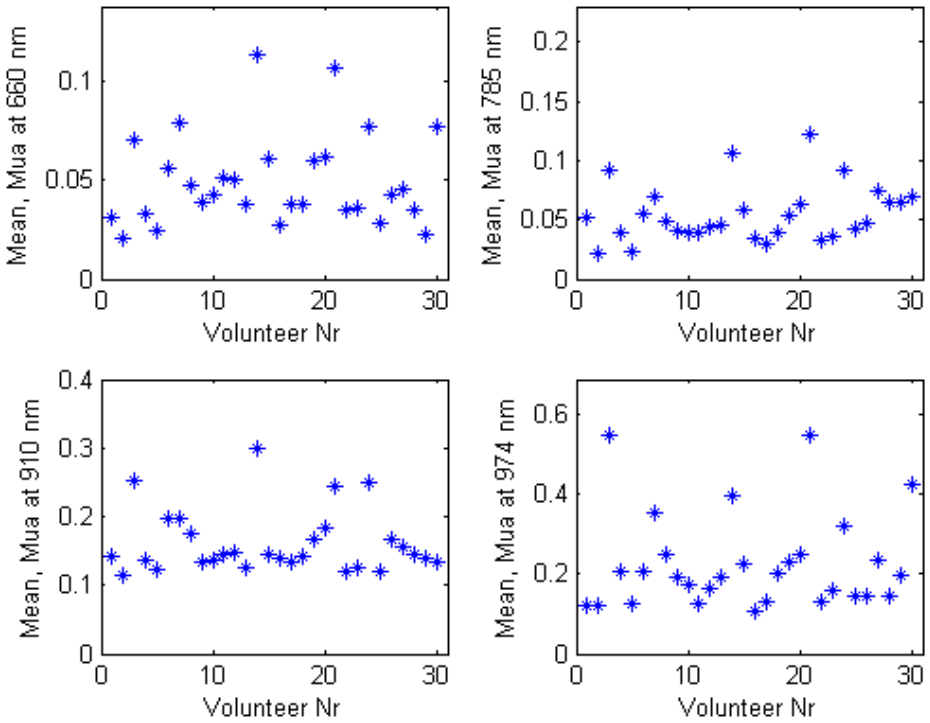

Figure 8.50 Mean values for μ_a in measurements 8 to 10 for 20 mm.

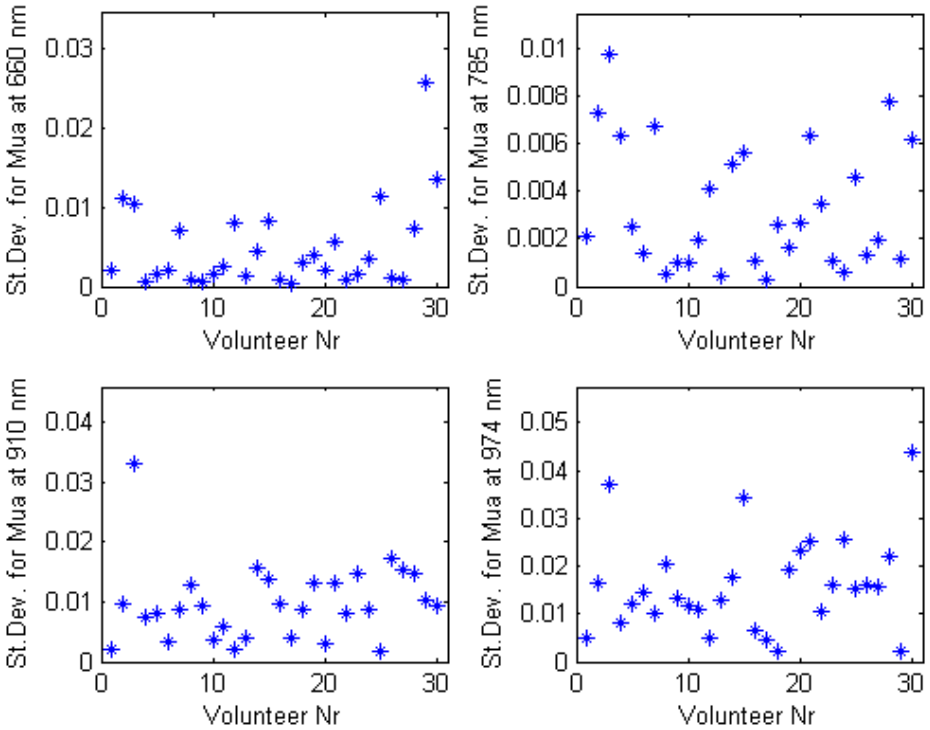

Figure 8.51 Standard deviation for μ_a in measurements 8 to 10 for 20 mm.

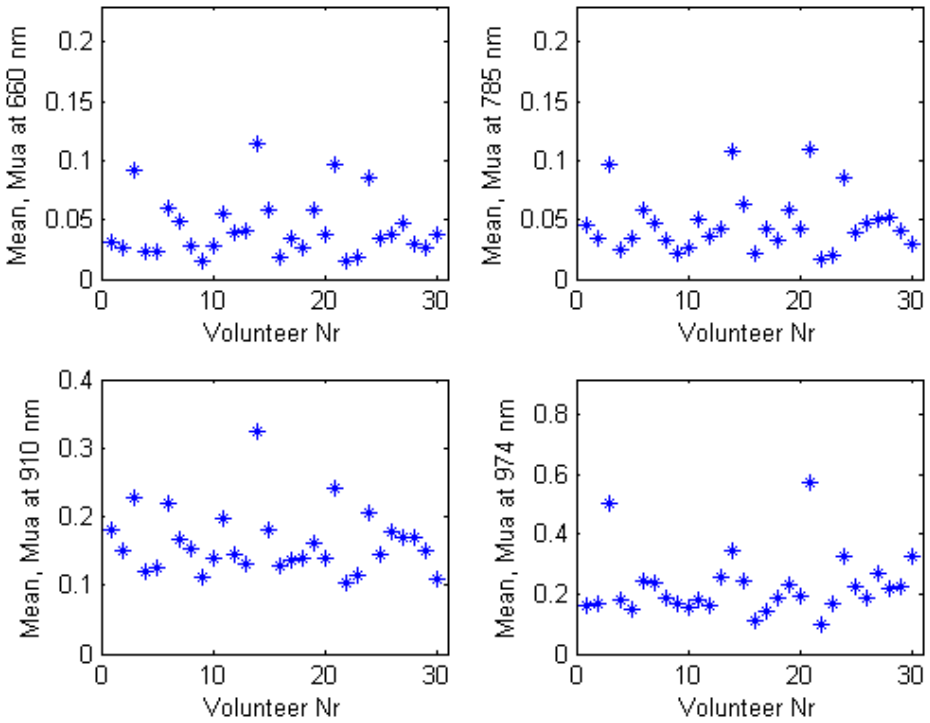

Figure 8.52 Mean values for μ_a in all measurements for 15 mm.

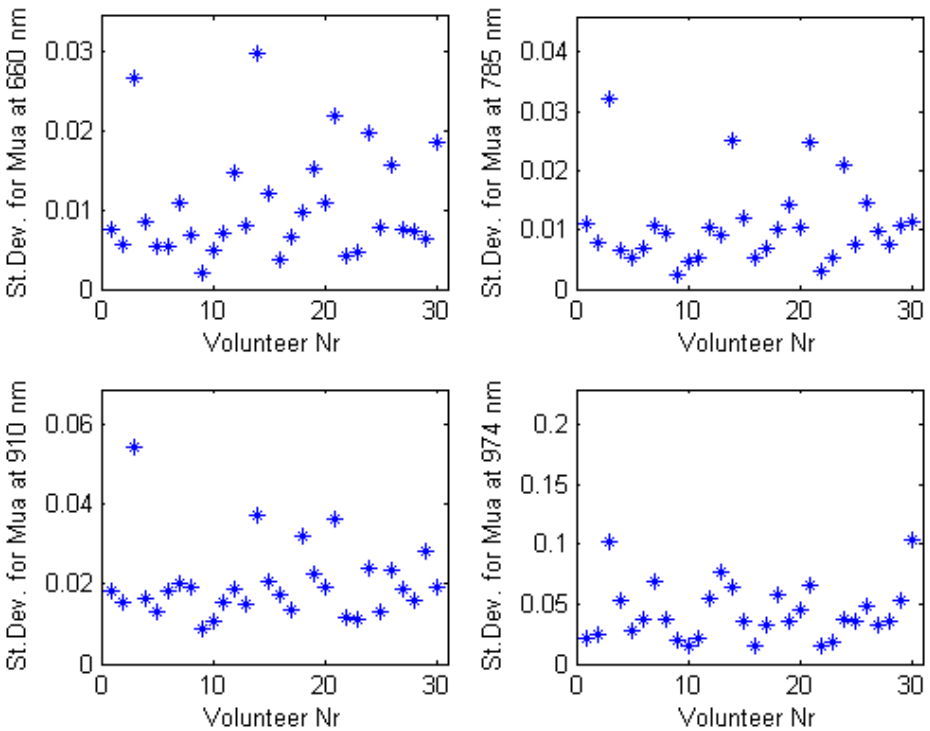

Figure 8.53 Standard deviation for μ_a in all measurements for 15 mm.

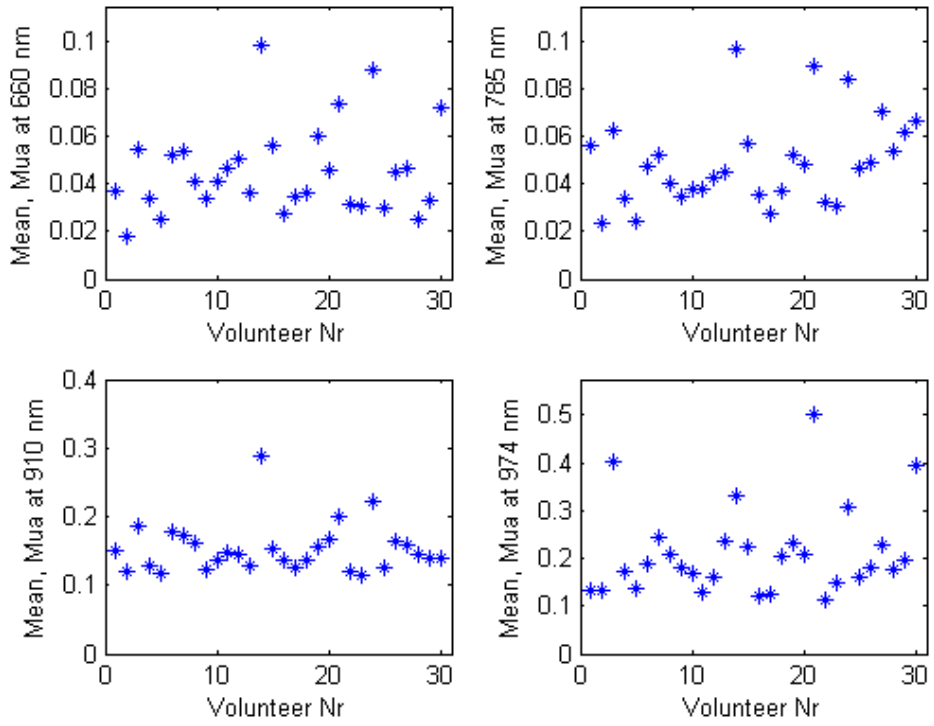

Figure 8.54 Mean values for μ_a in all measurements for 20 mm.

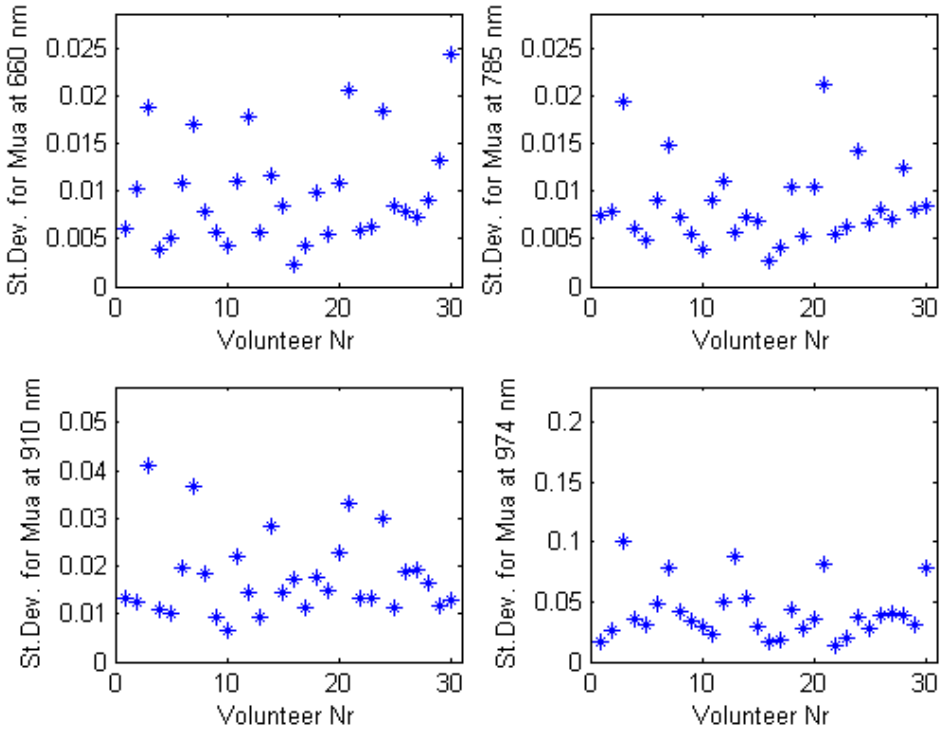

Figure 8.55 Standard deviation for μ_a in all measurements for 20 mm.

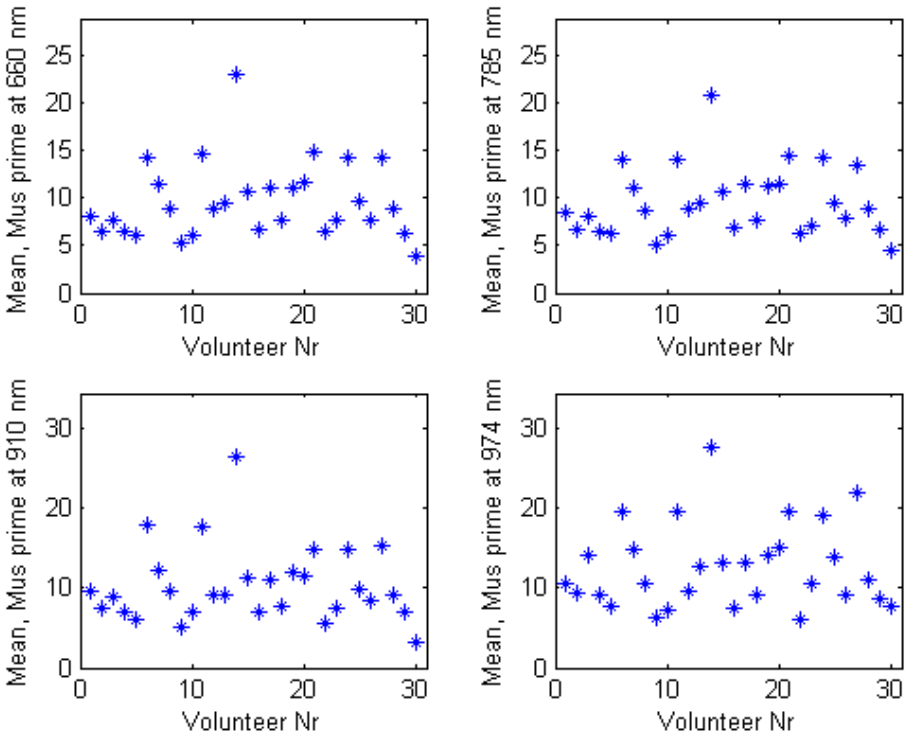

Figure 8.56 Mean values for μ_s' in measurements 8 to 10 for 15 mm.

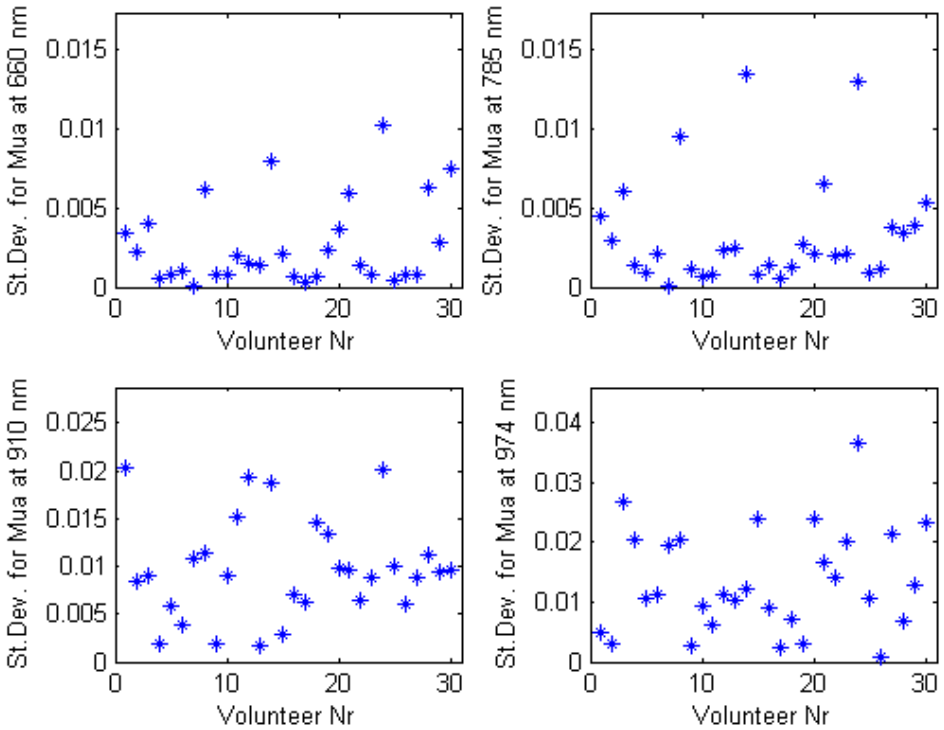

Figure 8.57 Standard deviation for μ_s' in measurements 8 to 10 for 15 mm.

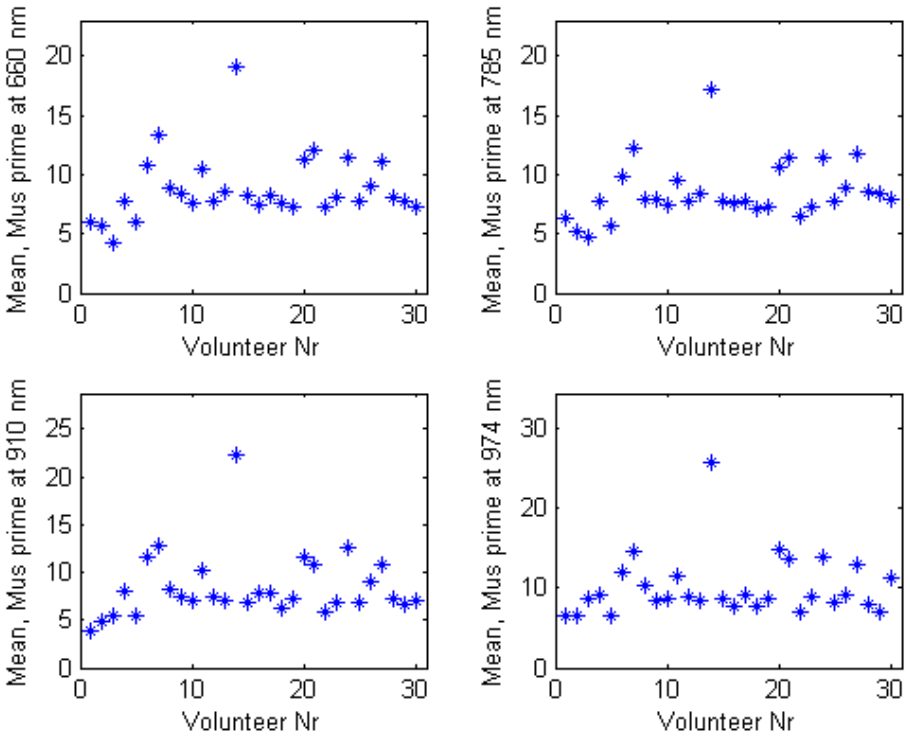

Figure 8.58 Mean values for μ_s' in measurements 8 to 10 for 20 mm.

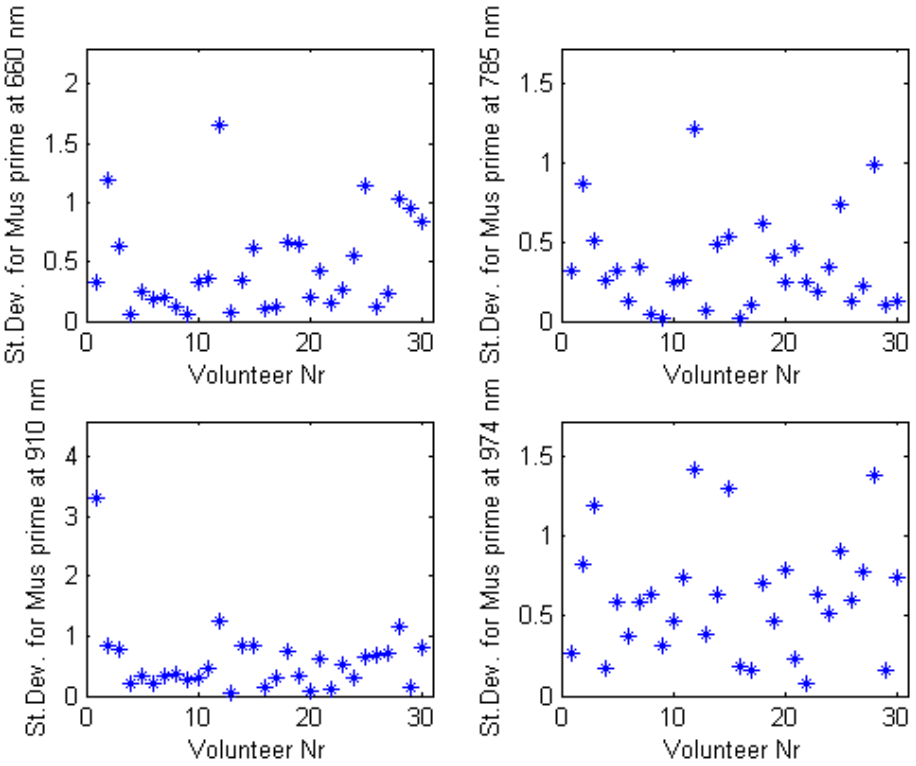

Figure 8.59 Standard deviation for μ_s' in measurements 8 to 10 for 20 mm.

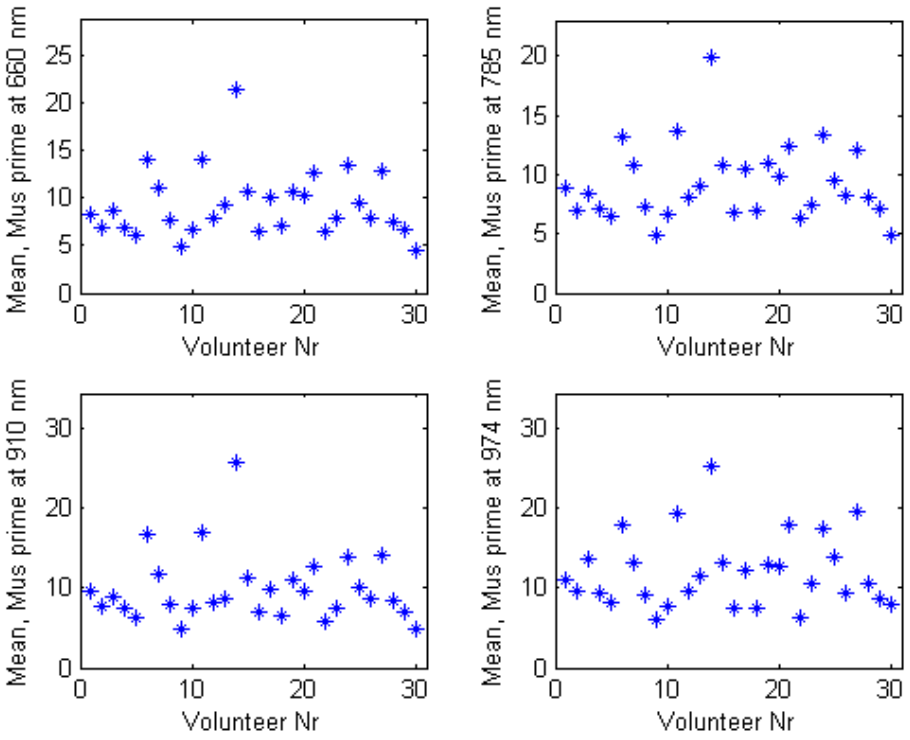

Figure 8.60 Mean values for μ_s' in all measurements for 15 mm.

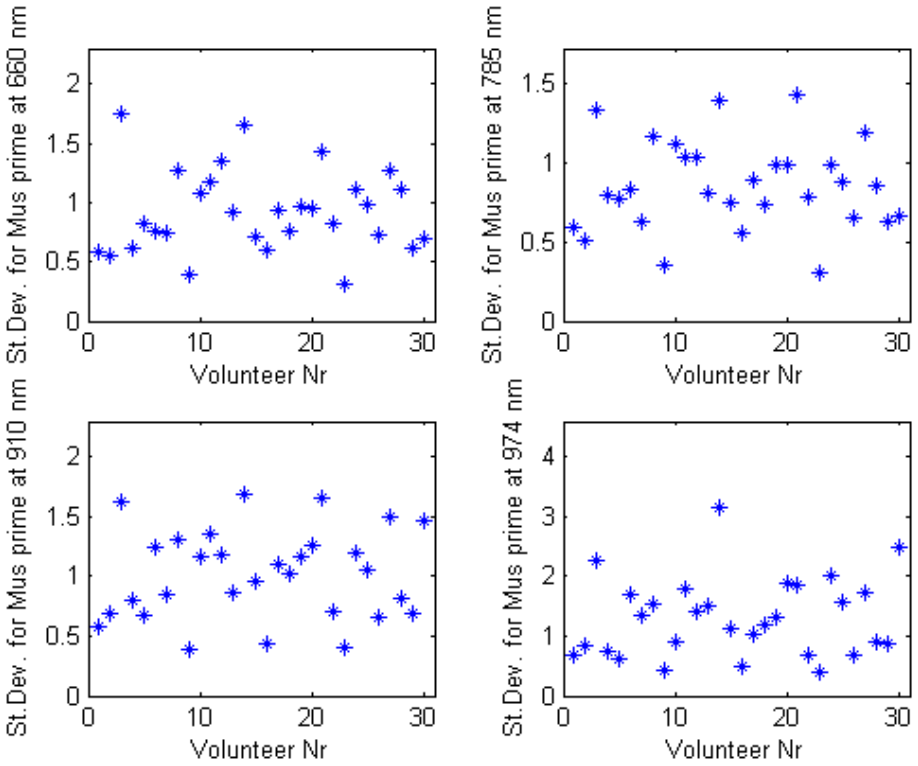

Figure 8.61 Standard deviation for μ_s' in all measurements for 15 mm.

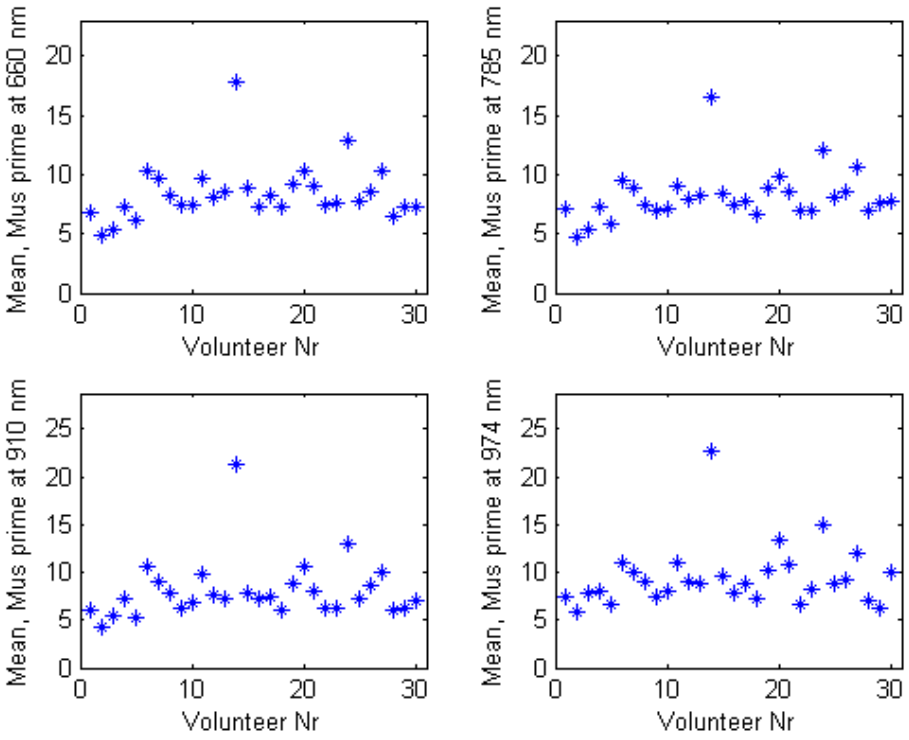

Figure 8.62 Mean values for μ_s' in all measurements for 20 mm.

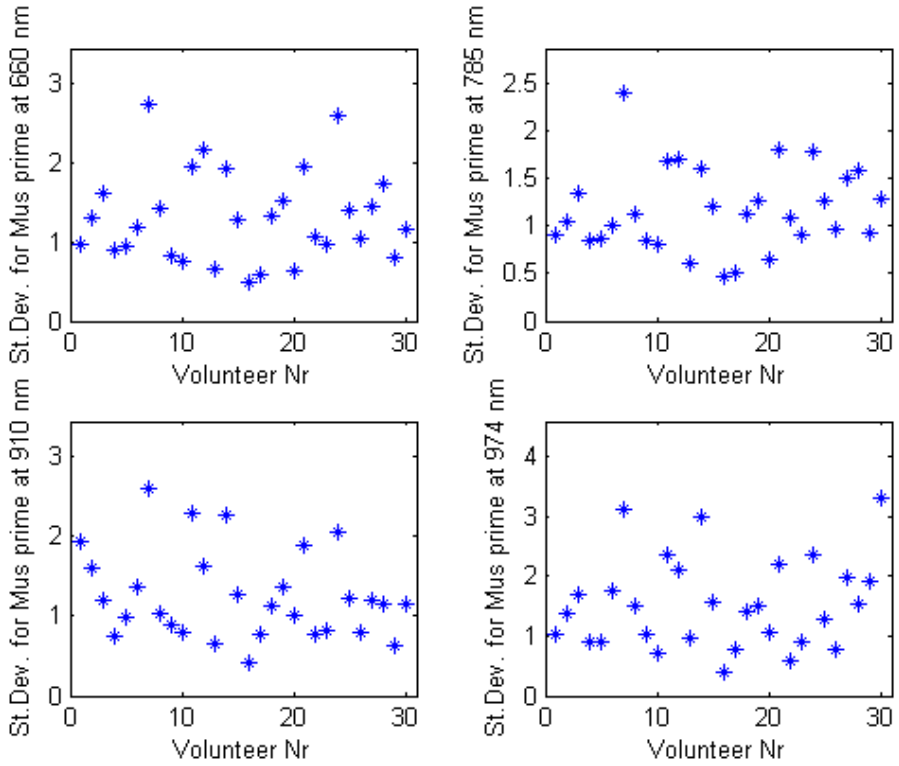

Figure 8.63 Standard deviation for μ_s' in all measurements for 20 mm.

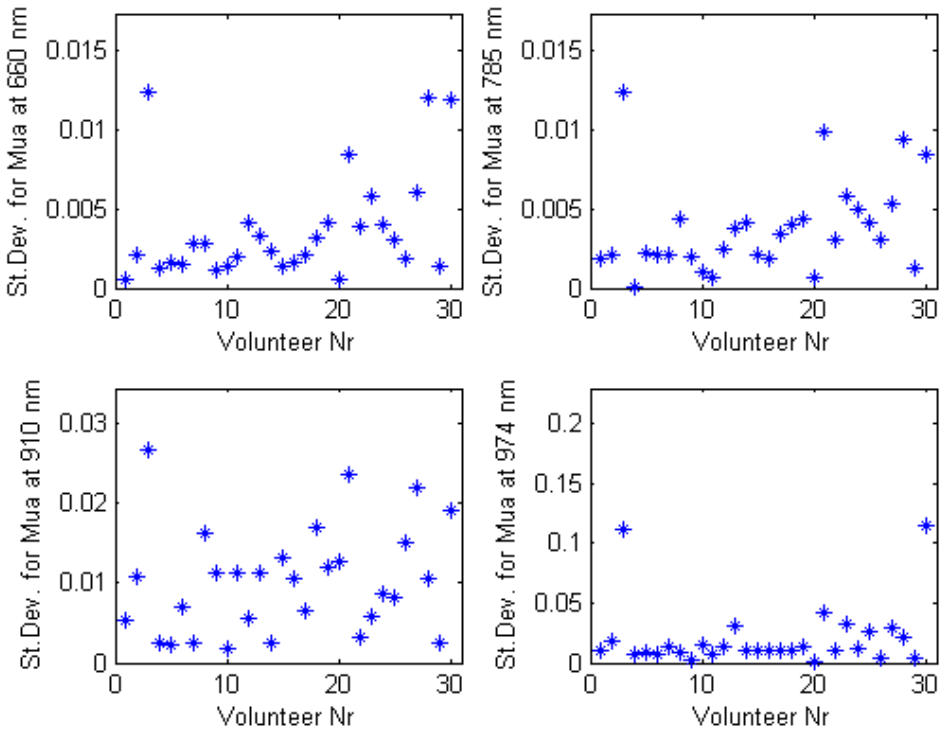

Figure 8.64 Standard deviation for μ_a' in measurements 1 to 3 for 15 mm.

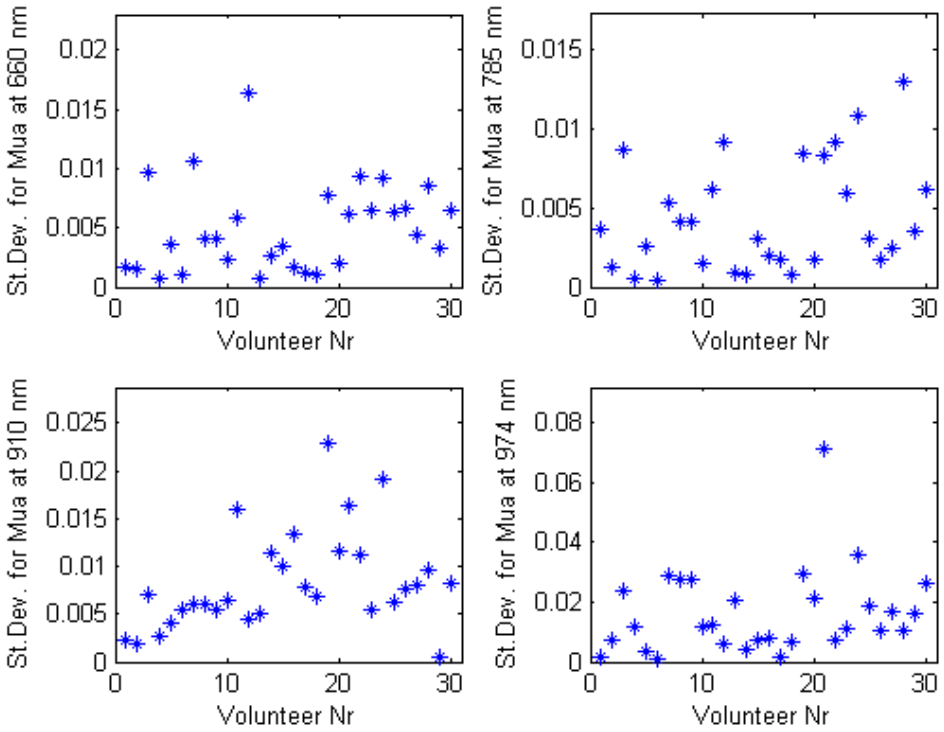

Figure 8.65 Standard deviation for μ_a' in measurements 1 to 3 for 20 mm.

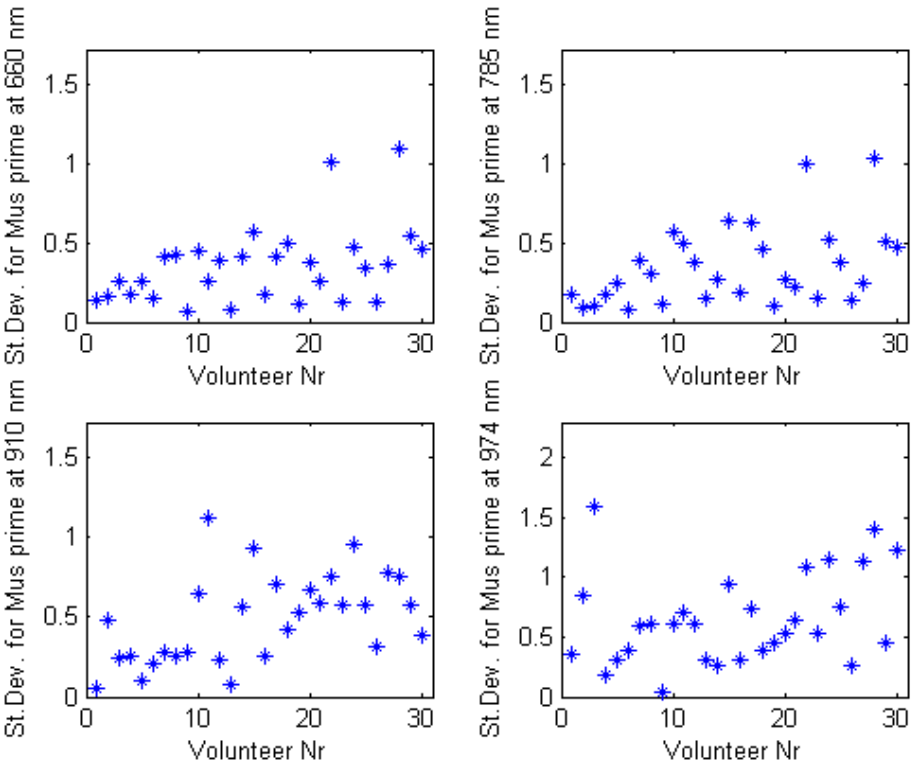

Figure 8.66 Standard deviation for μs' in measurements 1 to 3 for 15 mm.

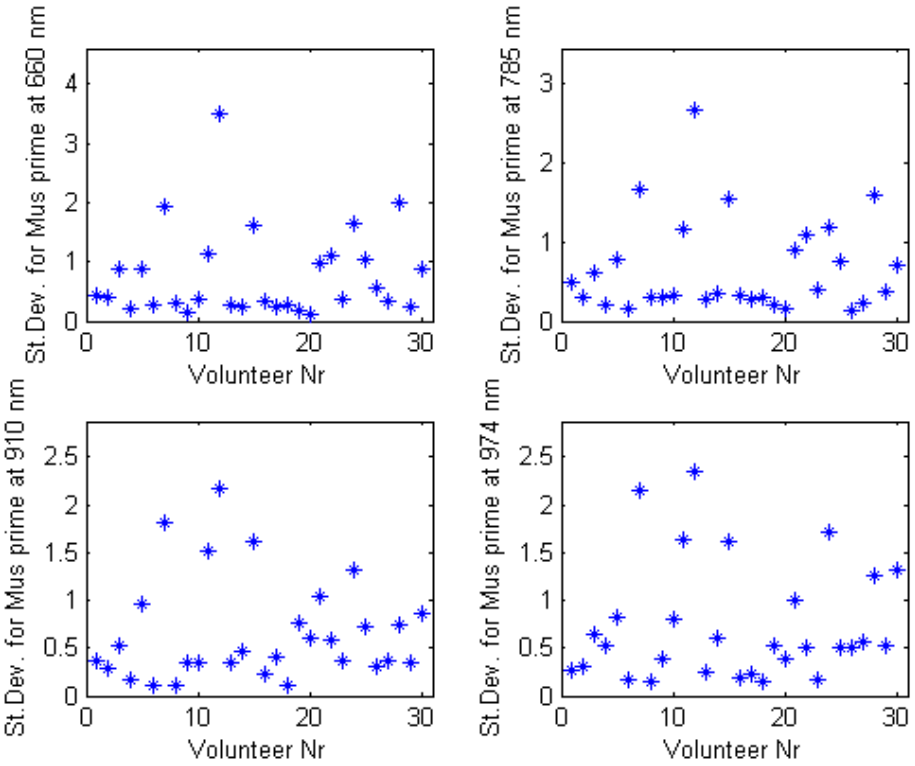

Figure 8.67 Standard deviation for μs' in measurements 1 to 3 for 20 mm.

From the mean and standard deviation graphs and the previous plots (taking into account the ones which are not included in the report), it can be concluded that there are significant differences for μ_s'and μ_a from one volunteer to another (which was suggested by J. Swartling *et al*[21]), or from one breast to the other in the same volunteer. As was expected, the standard deviation calculated for measurements 8 to 10 takes lower values than it takes for all measurements. It can be concluded that the majority of values obtained from the measurements are stable and found within a fixed range. In the cases where the standard deviation for a specific volunteer is higher than the common trend it can be due to the factors discussed in chapter 9.

The fact that the standard deviation is low does not contradict the statement that the measured absolute values may not be totally realistic; if there would have been the same or a similar repetitive error throughout the measurements, it would not have affected the value of the standard deviation.

In some cases, one of the points measured on one of the breasts shows a significantly different value from the rest on that same breast. It is usually the value that corresponds to point 4, both for scattering and absorption. This may be due to some of the factors discussed in chapter 9.

In addition, the difference in value between the points measured on the same breast is low except for the few cases mentioned above, and this can be concluded from the low values the standard deviation takes and by observing the μ_a and μ_s' plots.

It can also be observed that the standard deviation calculated for points 1-3 is very low, which leads to believe that there is not an abrupt change in the optical properties of the breast tissue within a small area.

9 Accuracy Of The Measurements

In general, the results obtained show that measurements are quite reliable seen as relative values. This is assured by observing that the measurements performed in the same spot (8, 9 and 10) or with small variations in the position (1, 2 and 3) give very similar values both for absorption and scattering coefficients. All of the measurements have been performed under the same conditions, both referring to the system and to the environment surrounding it. In addition, the posterior treatment of the curves obtained has been done in the exact same way.

9.1 Inaccuracy due to the performance procedure

It is very likely that some factors in the measurement procedure may have affected the results of the measurements, although no rigorous proof of this is included in this work, because of lack of time. The main factors to take into account are the following:

Some of the volunteers were not holding the probe in a steady and stable way, since the time during which the data was collected was long, especially in measurements number 8, 9 and 10 (three minutes holding the probe on the same spot) or when the stage of collection of data had to be restarted because of an overload signal. In addition, the shape of the probe makes it quite uncomfortable to be holding it against the soft tissue in the breast. There could also be a difference in the way the light enters the tissue depending on the more or less perpendicularity of the probe against the tissue and on the strength with which it was pressed against the tissue, difficult to control because of the particular geometry of the breast. Sometimes, one of the fibres was pressed much harder than the other, due to the shape of the breast.

It can be observed that the values measured on the left breast usually present a higher variation than those on the right. A possible reason for this is that it was more difficult to control the positioning of the probe on the left breast due to the place in which the bunk was situated. The short length of the fibres from the system to the probe and the stiffness of these also made it more difficult to handle the probe on the left breast. The difference in values from the 8 to 10 measurements and the 1 to 3 ones may be caused by a different positioning of the probe in the upper outer part of the left breast, where there was less visibility from the part of the personnel performing the measurements. It could be that in some cases the point measured was nearer the muscle and cartilage below the armpit than the breast in the upper outer. In the case of the upper inner quadrant, it could be that the measuring point was more on the chest than on the actual breast because of the way the volunteer was holding the probe. These might be the reasons why some of the values for these points are differing so much from the rest in some cases. These variations may have been avoided if the personnel

controlling the measurements would have been positioned in front of the volunteer instead of by her side.

9.2 Stability of the apparatus

A critical factor in the measurement which affects decisively the fitting procedure is the time shift between the instrument function and the corresponding data, as it should be constant throughout the measurements in order to obtain reasonable results. Even a small shift of two or more channels can make it almost impossible to obtain a good fitting of the data. This is why it is so important to assure the stability over time of the system.

The system was stable during the measurements. The lasers were turned on approximately one and a half hours before starting the measurements, to make sure that they were stable, as it was known that at the beginning when they were started they shifted in time while they warmed up. It was proved in Milan that the lasers were really stable after the stated time, when the measurements on each volunteer were started (see figure 9.1).

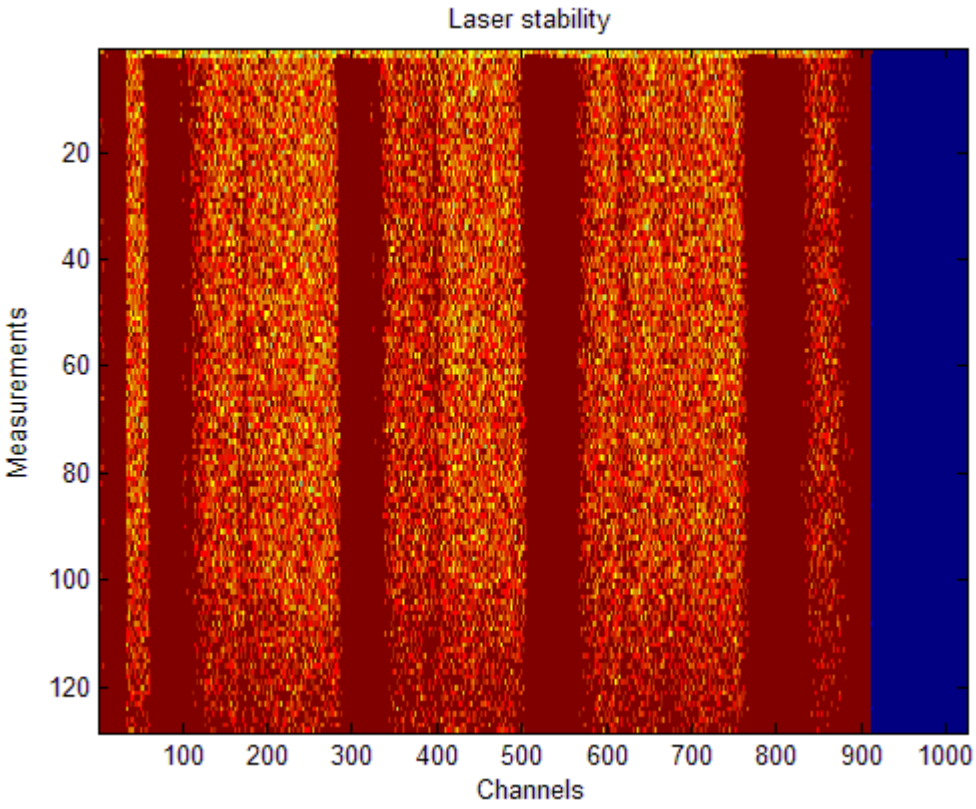

Figure 9.1 Performance of the lasers during 128 short measurements. Each horizontal line represents a different measurement, where the darker areas represent higher intensity than the lighter ones.

It can not be assured that a small shift was not produced during the whole measurement procedure in a day, as it was noticed that the power of each of the 910 and 974 nm lasers decreased during the day (see table 9.1), but this possible shift would have been corrected by the continuous recording of the instrumental function previous to each volunteer.

Laser Power Measurements. 5/27-03. System started at 0800.			
Laser setting	**0900**	**1200**	**1700**
660 nm	4.80 mW	4.40 mW	4.05 mW
785 nm	2.55 mW	2.30 mW	2.15 mW
910 nm	4.60 mW	4.30 mW	4.00mW
974 nm	5.90 mW	5.60 mW	5.20 mW

Table 9.1 Changes of the laser power during the day. The power was measured with all the lasers on and selecting different wavelength calibration in the power meter.

The detector was not affecting the measurements after the high voltage having been turned on and stepped up until 3200 Volts (see figure 9.2).

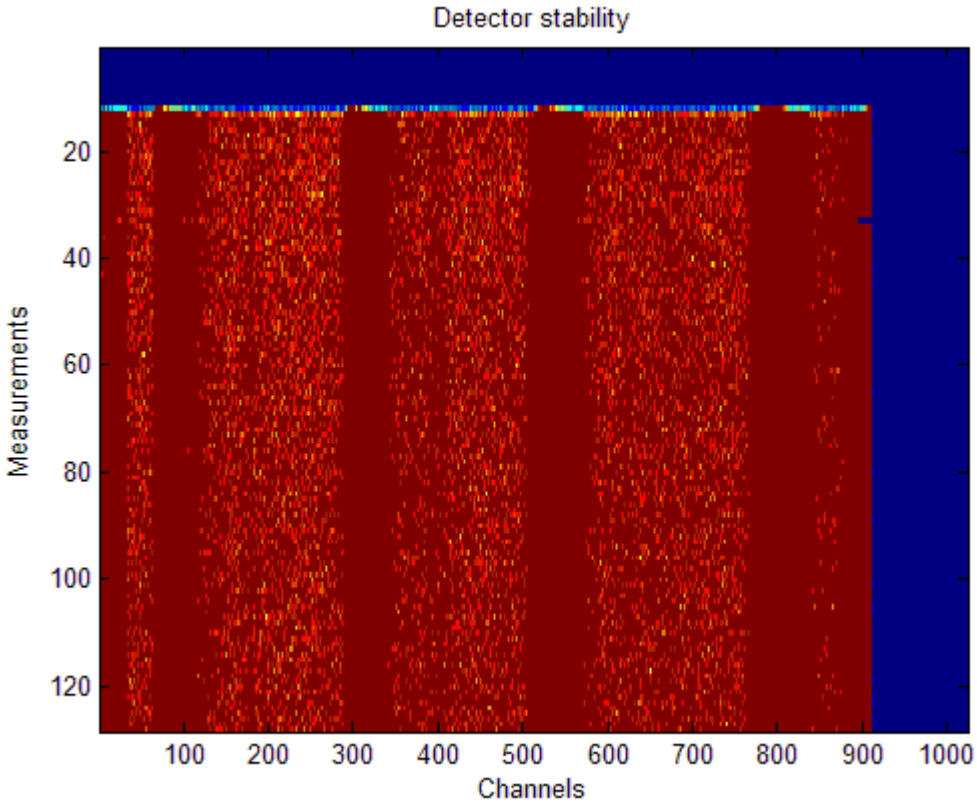

Figure 9.2 Analogous test to the one for the lasers stability.

A stability test was also performed for the SPC card. It showed that during approximately the first four to five minutes since the SPC program is started there is a time shift (see figure 9.3). This is due to the fact that it is an old version of the card. According to Wolfgang Becker, from the manufacturing company, this time shift is of about 10 or 20 ps. The effect comes from the leackage currents in the TAC-range switches.

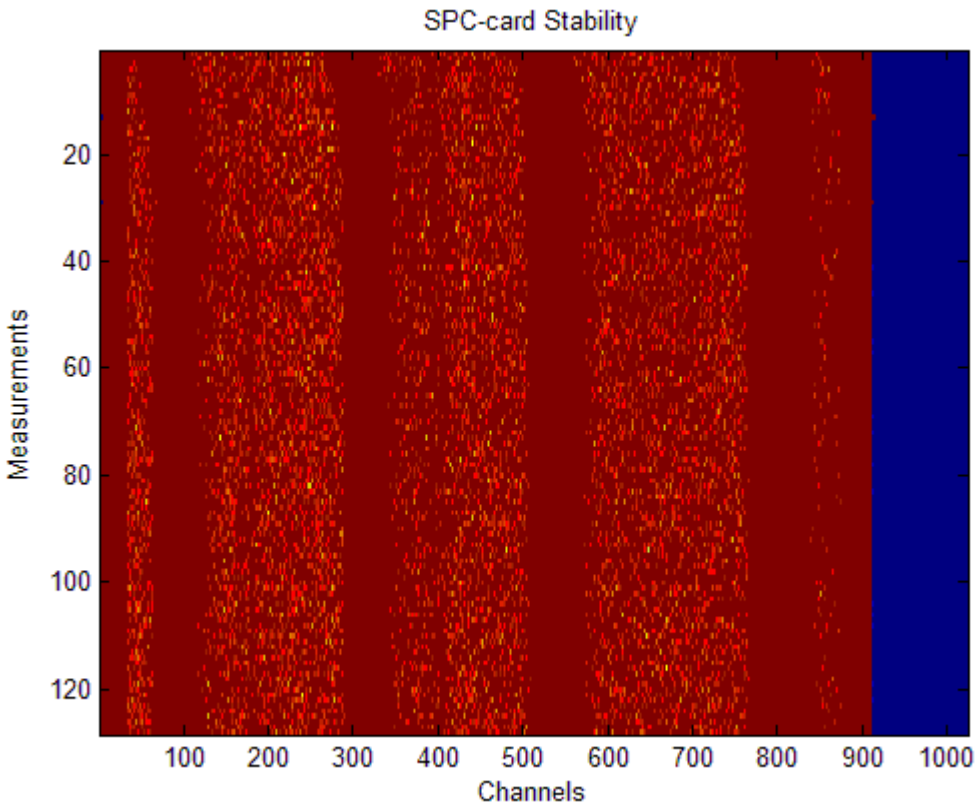

Figure 9.3 Analogous test to the one for the lasers stability.

This has not affected the measurements because the SPC program was always started enough time before the measurements began.

It can be observed in figure 9.3, although it is hard to see, that some glitches can appear which shift the signal a few channels. When this was observed during the measurements, the corresponding measurement was restarted to be sure of having a static time shift. It could be that in some cases the glitch was so small that it was not observable on the screen. In this case, it would have affected the measurement only of the present point.

In what concerns the signal obtained in the measurements at the hospital, there was a reflection situated just after the 660 nm TPSF, both in the instrument function and the data. This reflection was never before observed during experiments in the laboratory and it varied in intensity from volunteer to volunteer

and from day to day. The problem this reflection posed for some of the volunteers was that its positive slope was added to the negative slope of the 660 nm TPSF (see figure 9.4), altering its value, so that the fitting had to be performed using the unaltered part of the tail.

Another phenomenon observed in the data signal was the existence of two different slopes on the 785 nm TPSF's negative tail (see figure 9.4). This might be due to fluorescence originated in the skin. This had to be taken into account in the same way as the reflection for 660 nm explained before, during the fitting procedure.

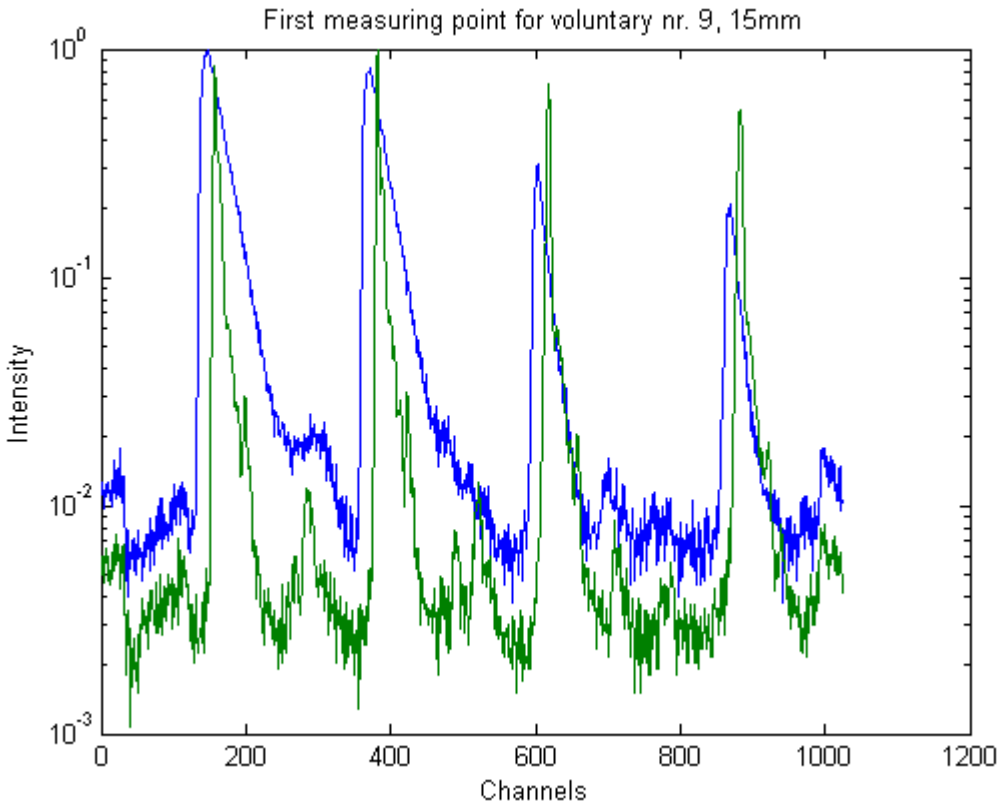

Figure 9.4 This curve shows both the instrument and the data function. Here the reflection tops and the two slopes can be seen.

During the measurements, the total number of counts for all the channels (1024) was approximately 300 000 in 60 seconds. Because of the high absorption that human tissue presents at 910 and 974 nm, it sometimes occurred that the peaks at these two wavelengths had very low number of counts, which may have affected the fitting for these two peaks.

Now with the changes in the system that were performed in Milan, the signal is much higher, approximately 600 000 counts in 4 sec. Therefore, this may no

longer be a problem. It will affect the data collecting time and therefore the time the volunteer has to be holding the probe.

9.3 Fitting procedure

No acceptable results could be obtained from the measurements by using the FIT program before help from its developers, Antonio Pifferi *et al.*, at the Politecnico di Milano was received.

In a further stage, it has been realised that by changing some of the critical parameters in the fitting, namely the values of FractFirst and FractLast, a change in the values obtained for the optical parameters is achieved. A change in the range of 0.5 to 1 cm^{-1} when it comes to the scattering coefficient has been observed so far. In the case of the absorption coefficient, the change can be approximately of 0.01 cm^{-1} for 660 and 785 nm, and of 0.05 to 0.1 cm^{-1} for 910 and 974 nm. It has also been noticed that in some cases where the values obtained are significantly high a much bigger change in μ_s' and μ_a can be achieved by varying the mentioned parameters. This matter requires further study.

The curves obtained from the measurements performed on the same volunteer did not present significant differences between each other in the regions of interest, as can be observed in the figure below.

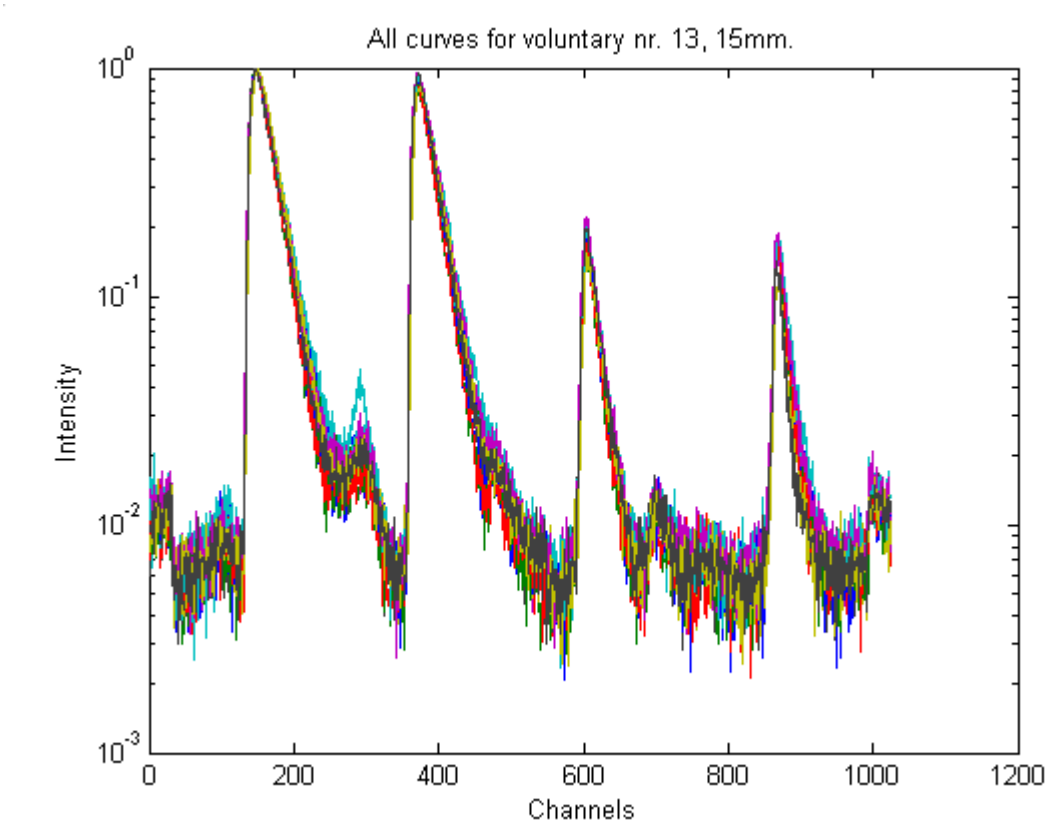

Figure 9.5 This plot is showing all curves that were obtained for voluntary nr.13 for 15mm.

In order to save time and perform the maximum number of fittings under the same conditions, the region of interest and the values for FractFirst and FractLast have been kept unaltered in most cases (see figure 9.6).

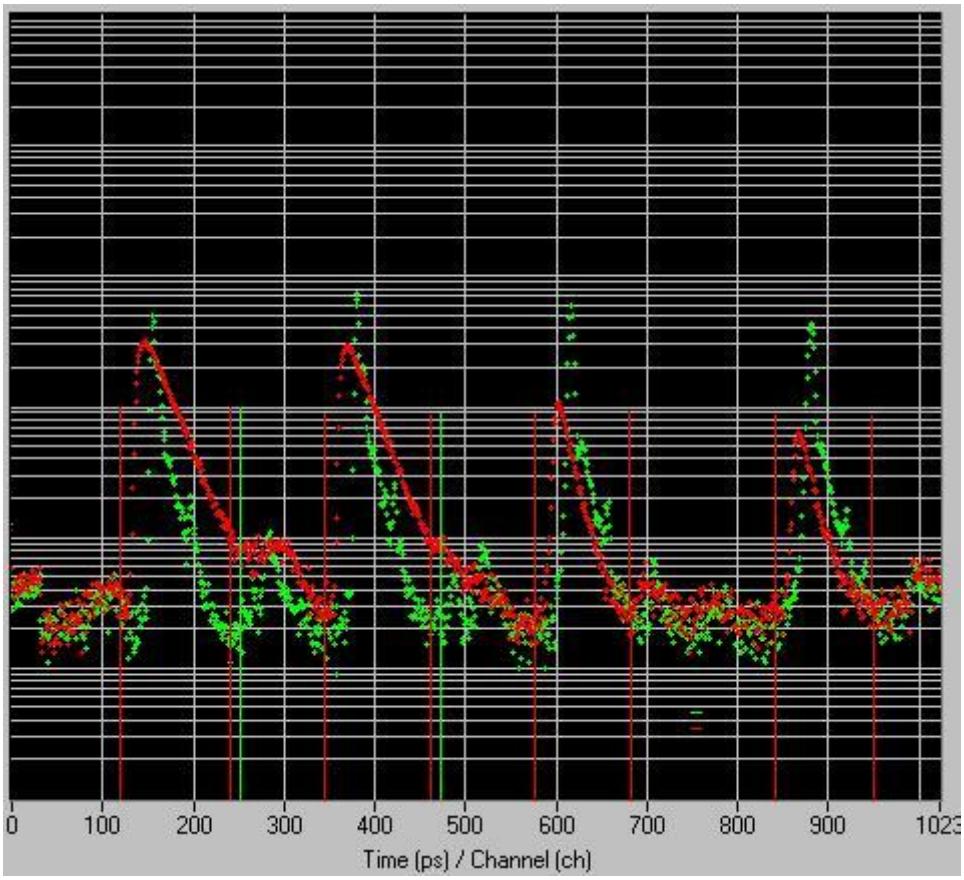

Figure 9.6 Regions of interest for both instrument function and data recorded for volunteer nr. 8, 15 mm, measured on point 1.

In some cases, the regions of interest for 660 nm and 785 nm have been adjusted due to the reflection situated in the TPSF for 660 nm and the variations of the second slope present in the TPSF for 785 nm. This adjustment does not exceed ± 10 channels in any case.

FractFirst and FractLast have been kept constant with fixed values of –10 % and 5% respectively, in order to keep as many counts as possible within the region defined by both parameters, but still get a good fitting.

The optimisation of the fitting based on the χ^2 value implied sometimes choosing as region to be fitted a very small part of the TPSF, which may bring as a result a less reliable value for the optical coefficients. In most of the measurements for all wavelengths the χ^2 value is found in the range from 1 to 15, sometimes higher than 15. Within this range, the highest χ^2 values are obtained for 660 and 785 nm. Modifying FractFirst and FractLast to obtain a decrease in the χ^2 value does not

result on a significant change of the values obtained for μ_s' and μ_a; this change is kept in the range mentioned above. The figure 9.7 shows that the fitting is good even for a high χ^2 value.

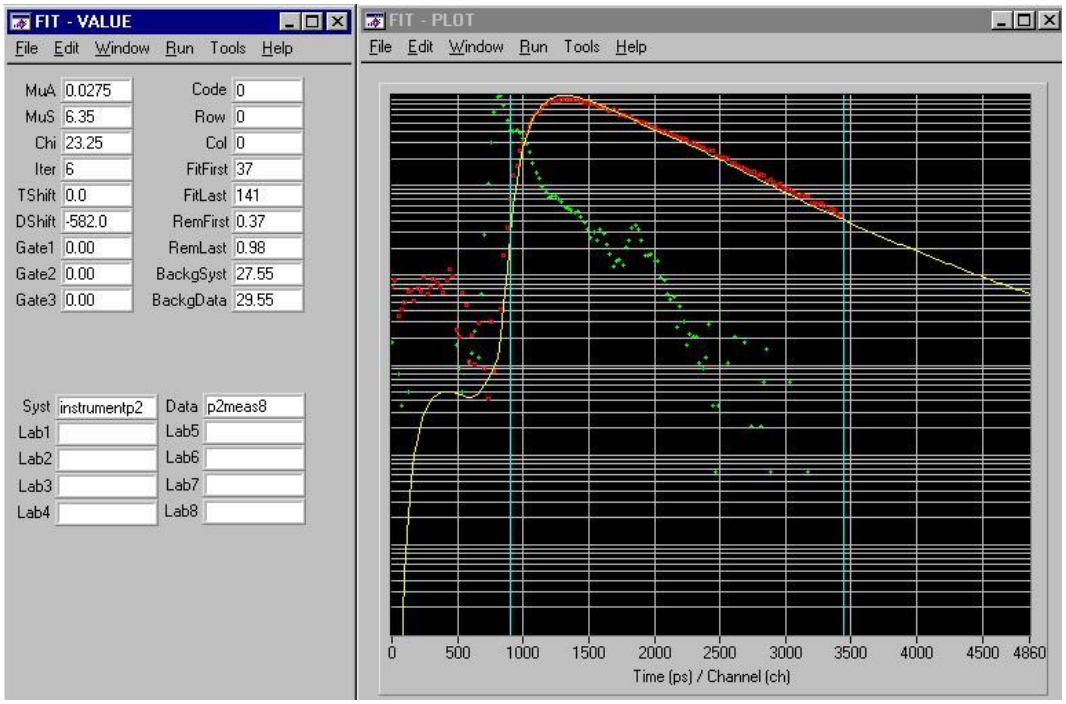

Figure 9.7 Fitting plot for volunteer nr. 2, measuring point 8 for 20mm, 660 nm.

9.4 Measurements on phantoms

An attempt on measuring on phantoms was made before the measurements at the hospital were started. No useful results could be obtained from these measurements because of the problems with the FIT program and different circumstances that were not taken into account during these measurements (e g no blockage was situated between the source and the detector fibre tips). The lack of time also prevented the correct analysis of the data and the acquisition of further measurements on phantoms.

After the Milan trip and the changes performed there on the system, some measurements were performed on phantoms, and these produced accurate and repetitive results, as can be seen in the figure below:

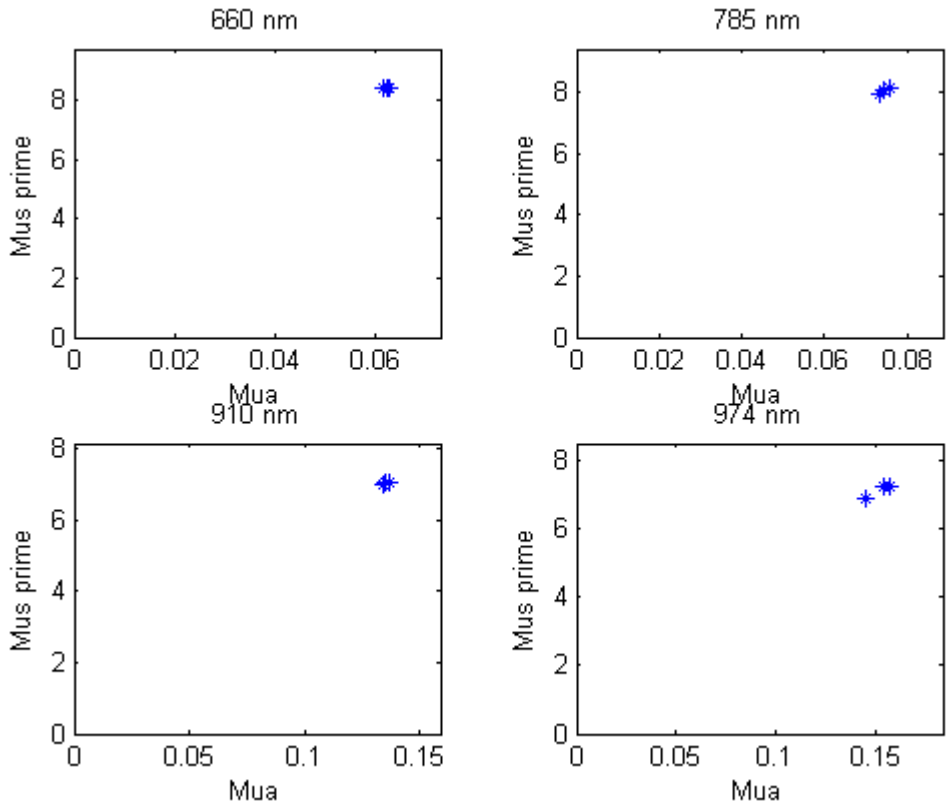

Figure 9. 8 Measurements on phantom B2 using 20mm.

Since the changes performed on the system in Milan only affected the intensity of the signal, it can be assumed that the system was stable before these changes were made.

10 Conclusions

The aim of this work was to find if the different points on the breast or different volunteers show different optical properties. From the set of data obtained in this study, it can be concluded that there are differences between the optical properties of the breast from one volunteer to another, though these differences cannot in principle be attached to the specific attributes of the individual under study.

There are small differences between values obtained from different points on the same breast, but these differences might be due to external factors affecting the measurements, and it is hard to quantify how much these factors affect. In order to extract a clearer conclusion in this respect, it would be necessary to increase the number of measuring points on the same breast, to obtain more data. The fact that the standard deviation calculated for points 1-3 is very low supports the idea that there is not an abrupt change in the optical properties of the breast tissue within a small area.

It would be necessary to revise and optimise the fitting procedure in what concerns FractFirst and FractLast parameters, in order to obtain more accurate results. Due to the lack of time after the knowledge about the correct way of using the FIT program was achieved and the data was recorded, the effect this optimisation would have had on the results could not be evaluated.

In what concerns the comparison between the values obtained for 15 mm with the ones obtained for 20 mm, the differences are small, being the standard deviation the parameter which better shows these differences. It is slightly higher in the case of 20 mm than 15mm, therefore it would be of higher interest to focus further studies on the 20 mm case or longer inter-fibre distances.

The difference in values observed between the right and left breasts could be better acquainted for if information about which of the breasts was bigger for each of the volunteers or if they were right-handed or left-handed would have been collected.

A very important goal was to improve the system and have it working in a stable and reliable way for *in vivo* measurements. This has been successfully achieved.